CANADIAN THESES ON MICROFICHE

I.S.B.N.

THESES CANADIENNES SUR MICROFICHE

National Library of Canada
Collections Development Branch

Canadian Theses on
Microfiche Service

Ottawa, Canada
K1A 0N4

Bibliothèque nationale du Canada
Direction du développement des collections

Service des thèses canadiennes
sur microfiche

NOTICE

The quality of this microfiche is heavily dependent upon the quality of the original thesis submitted for microfilming. Every effort has been made to ensure the highest quality of reproduction possible.

If pages are missing, contact the university which granted the degree.

Some pages may have indistinct print especially if the original pages were typed with a poor typewriter ribbon or if the university sent us a poor photocopy.

Previously copyrighted materials (journal articles, published tests, etc.) are not filmed.

Reproduction in full or in part of this film is governed by the Canadian Copyright Act, R.S.C. 1970, c. C-30. Please read the authorization forms which accompany this thesis.

AVIS

La qualité de cette microfiche dépend grandement de la qualité de la thèse soumise au microfilmage. Nous avons tout fait pour assurer une qualité supérieure de reproduction.

S'il manque des pages, veuillez communiquer avec l'université qui a conféré le grade.

La qualité d'impression de certaines pages peut laisser à désirer, surtout si les pages originales ont été dactylographiées à l'aide d'un ruban usé ou si l'université nous a fait parvenir une photocopie de mauvaise qualité.

Les documents qui font déjà l'objet d'un droit d'auteur (articles de revue, examens publiés, etc.) ne sont pas microfilmés.

La reproduction, même partielle, de ce microfilm est soumise à la Loi canadienne sur le droit d'auteur, SRC 1970, c. C-30. Veuillez prendre connaissance des formules d'autorisation qui accompagnent cette thèse.

THIS DISSERTATION HAS BEEN MICROFILMED EXACTLY AS RECEIVED

LA THÈSE A ÉTÉ MICROFILMÉE TELLE QUE NOUS L'AVONS REÇUE

NL-339 (r. 82/08)

Canadä

34

0-315-12349-4

National Library of Canada **Bibliothèque nationale du Canada**

Canadian Theses Division · Division des thèses canadiennes

Ottawa, Canada
K1A 0N4   60260

PERMISSION TO MICROFILM — AUTORISATION DE MICROFILMER

• Please print or type — Écrire en lettres moulées ou dactylographier

Full Name of Author — Nom complet de l'auteur

KELAMIS   PANAYOTIS   GEORGE

Date of Birth — Date de naissance	Country of Birth — Lieu de naissance
10 - 10 - 58	GREECE

Permanent Address — Résidence fixe

c/o Physics Dept. U of A.
T6G 2J1   Edmonton - Alta

Title of Thesis — Titre de la thèse

Attenuation of seismic waves and Generalized
& Ray Theory

University — Université

Univ. of Alberta - Edmonton - Alta

Degree for which thesis was presented — Grade pour lequel cette thèse fut présentée

Ph. D. in Geophysics

Year this degree conferred — Année d'obtention de ce grade	Name of Supervisor — Nom du directeur de thèse
1982	Prof E.R. Kanasewich

Permission is hereby granted to the NATIONAL LIBRARY OF CANADA to microfilm this thesis and to lend or sell copies of the film.

The author reserves other publication rights, and neither the thesis nor extensive extracts from it may be printed or otherwise reproduced without the author's written permission.

L'autorisation est, par la présente, accordée à la BIBLIOTHÈ-QUE NATIONALE DU CANADA de microfilmer cette thèse et de prêter ou de vendre des exemplaires du film.

L'auteur se réserve les autres droits de publication; ni la thèse ni de longs extraits de celle-ci ne doivent être imprimés ou autrement reproduits sans l'autorisation écrite de l'auteur.

Date	Signature
September 28, 1982	

NL-91 (4/77)

THE UNIVERSITY OF ALBERTA

ATTENUATION OF SEISMIC WAVES AND

GENERALIZED RAY THEORY

by

©   PANAYOTIS G. KELAMIS

A THESIS

SUBMITTED TO THE FACULTY OF GRADUATE STUDIES AND RESEARCH

IN PARTIAL FULFILMENT OF THE REQUIREMENTS FOR THE DEGREE

OF DOCTOR OF PHILOSOPHY

IN

GEOPHYSICS

DEPARTMENT OF PHYSICS

EDMONTON, ALBERTA

FALL, 1982

THE UNIVERSITY OF ALBERTA

RELEASE FORM

NAME OF AUTHOR   PANAYOTIS G. KELAMIS

TITLE OF THESIS   ATTENUATION OF SEISMIC WAVES AND
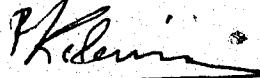
GENERALIZED RAY THEORY

DEGREE FOR WHICH THESIS WAS PRESENTED   PH.D.

YEAR THIS DEGREE GRANTED   1982

(Signed)

PERMANENT ADDRESS:

c/o Department of Physics
University of Alberta
Edmonton, Canada
T6G 2J1

DATED *September 28, 1982*

THE UNIVERSITY OF ALBERTA

FACULTY OF GRADUATE STUDIES AND RESEARCH

The undersigned certify that they have read, and

recommend to the Faculty of Graduate Studies and Research,

for acceptance, a thesis entitled ATTENUATION OF SEISMIC

WAVES AND GENERALIZED RAY THEORY

submitted by   PANAYOTIS G. KELAMIS

in partial fulfilment of the requirements for the degree

of Doctor of Philosophy in Geophysics.

.....E. R. Kanasewich.....
Supervisor

.H.A.K. Cheung........

.Gh. Cumming.........

.A. J. Capen.........

.C. H. Chap.........
External Examiner

Date ...September 20, 1982....

ABSTRACT

The exact solution for a buried source is presented for a layer over a half space. The source is a stress discontinuity on or in the first layer of an elastic medium. The computer algorithm evaluates a solution based on the Cagniard-Pekeris formulation and the complete analytic results are given in terms of generalized rays. The near-field solution is particularly interesting and the results are applicable to exploration problems involving shallow layers. For a vertical or horizontal stress discontinuity the results show effects not predicted by intuition. In addition to the expected shear wave arrivals one has a prominent group of compressional waves whose radial component is substantial at larger distances. The formation of a surface head wave is also of interest. The results for a layer over a half space are decomposed into individual generalized rays which are examined and modified to incorporate the effects of attenuation through a viscoelastic medium and the interface effects. The generalized rays are grouped naturally into families, each family is completely defined by an integer F (F=1,2,...) which indicates the number of interactions of the ray with the two boundaries. Examples are shown for a weathered layer over a half space and for the reflected and head waves from a Mississippian type half space in a simplified "Alberta" foothills model.

ACKNOWLEDGEMENTS

TABLE OF CONTENTS

LIST OF FIGURES

CHAPTER 1

1. Introduction

The propagation of elastic waves in a layered solid, due to point sources, has been studied extensively both theoretically and numerically. The solution, either in exact or in approximate form, has been given for different simple and complex models. My approach to the problem involves generalized ray theory and a Cagniard-Pekeris inversion because the method yields the complete and exact solution.

The problem of an SH-torque situated inside a layer overlying a half space was solved by Pekeris et al. (1963). The axis of the torque was vertical and the displacement due to the source had a triangular shape at large distances. This type of source excites only horizontally polarized (SH) waves and these retain their shear character upon reflection at the two boundaries. Abramovici (1970) presented the solution of a compressional pulse in a layered half space. The vertical and horizontal components of the displacement were given analytically in terms of individual generalized rays. In his paper, he extended the work of Pekeris et al. (1965) by considering the general case for Poisson's ratio σ and not the particular case $\sigma = 0.25$ for the layer. He computed synthetic seismograms for various depths of the source and for different locations of the receiver.

Abramovici and Gal-Ezer (1978) studied the motion of a solid made up of one layer over a half space due to the presence of a vertical point force acting beneath or at the free surface using the generalized ray expansion. Each term in the expansion represented a group of rays reflected the same number of times as P or S. The time dependence of the applied force at the source had a triangular shape. They modelled the vertical force as a stress discontinuity along the vertical z axis and they calculated the vertical and horizontal displacements for a receiver located at the free surface.

In this thesis synthetic seismograms for the general case of an horizontal arbitrary force in the x-y plane are computed using the generalized ray theory. The theoretical development of the problem was solved together with Professor F. Abramovici during his visit on a sabbatical leave in 1979-80. The algorithms for the numerical evaluation were carried out jointly at the University of Alberta and at Tel-Aviv University. The x-component of the force gives rise to vertical and radial displacement while the y-component gives rise to transverse motion. The complete mathematical solution for the case of an horizontal arbitrary point force situated inside a layer overlying a half space is given in Appendix A which is an expanded version of the paper by Abramovici, Kanasewich and Kelamis (1982).

For the sake of completeness and to explore the

solution for particular boundary-value problems the solutions for all three sources (SH-point torque, vertical point force and horizontal point force) were examined in detail. The mathematical solution is exact and is obtained in a closed analytical form as a superposition of individual generalized rays. All the possible rays with surface and head waves are included in the seismogram up to a particular time of interest.

Another innovation of this thesis is the introduction of attenuation and dispersion in the synthetic seismograms obtained using the generalized ray theory. This is done by decomposing the seismogram into individual generalized rays and incorporating the effects of anelasticity in the frequency domain into each ray separately. The linear theory of viscoelasticity along with Futterman's model is used to model the anelasticity and reflection coefficients for anelastic media are calculated to take into account the effect of the viscoelastic interface.

In this chapter a review of the literature about the attenuation of seismic waves is made. Particular emphasis is given to the frequency dependence of attenuation and to the various models of absorption and dispersion. In the second chapter synthetic seismograms for a thin "weathered" layer and for a crustal layer model are presented and discussed. The third chapter includes synthetic seismograms with the effects of attenuation and dispersion. Finally, in the fourth chapter synthetics are computed for an

"Alberta" foothills model as an aid to the interpretation of wide angle seismic reflections and head waves.

1.2 Different definitions of Q

It is common experience that as a wave propagates through real material, wave amplitudes attenuate as a result of a variety of processes, which can be summarized microscopically as internal friction or anelasticity. The magnitude of internal friction is expressed in terms of the dimensionless parameter Q which is given by

$$\frac{1}{Q} = \frac{\Delta E}{2\pi E}$$
(1.1)

where ΔE is the amount of energy dissipated per cycle for a harmonic wave and E is the peak strain energy in a cycle of the harmonic wave. Physically, Q is a measure of the imperfections in the elasticity of the materials.

The applicability of the above definition is rather limited; more commonly one observes either (i) the temporal decay of amplitude in a standing wave at a fixed wave-number or (ii) the spatial decay in a propagating wave at a fixed frequency. Assuming that Q >> 1 and for media with linear stress-strain relation we get that the wave amplitude A is proportional to $E^{\frac{1}{2}}$. Thus, equation (1.1) can be written as

$$\frac{1}{Q} = \frac{\Delta A}{\pi A}$$
(1.2)

In case (i) one wants to determine $A = A(t)$, given that $A = A_o$ at $t = 0$. Clearly, A decreases a fraction π/Q at successive times $\frac{2\pi}{\omega}$, $\frac{4\pi}{\omega}$, ..., $\frac{2n\pi}{\omega}$ ... thus we get

$$A(\frac{n2\pi}{\omega}) = A_o (1- \frac{\pi}{Q})^n . \qquad (1.3)$$

ω is the angular frequency. The quantity π/Q is also referred to as the logarithmic decrement δ. Equation (1.3) can also be written as

$$A(t) = A_o(1 - \frac{\omega t}{2nQ})^n \rightarrow A_o e^{-\frac{\omega t}{2Q}} \quad \text{(for large n)}. \qquad (1.4)$$

The Q defined using Eq. (1.4) is called temporal Q.

In case (ii) one follows a particular wave peak along a distance dx and observes the gradual spatial decay of amplitude. Assuming that the direction of propagation is also the direction of attenuation we get

$$\Delta A = \frac{dA}{dx} \lambda \qquad (1.5)$$

where λ is the wavelength. Using the relation between the wavelength λ, the angular frequency ω and the phase velocity c

$$\lambda = \frac{2\pi c}{\omega} \qquad (1.6)$$

equation (1.2) becomes

$$\frac{dA}{dx} = \frac{\omega}{2cQ} A \tag{1.7}$$

with the obvious solution

$$A(x) = A_o e^{-\frac{\omega x}{2cQ}} \tag{1.8}$$

where A_o is the amplitude at $x = 0$. Equation (1.8) defines the value of the spatial Q.

The absorption coefficient α is defined as

$$\alpha = \frac{\omega}{2cQ} \tag{1.9}$$

thus, equation (1.8) can be written as

$$A(x) = A_o e^{-\alpha x}. \tag{1.10}$$

Equation (1.10) describes the attenuation model that will be used in this thesis, i.e., an exponential decay of amplitude with distance. The above definition of the absorption coefficient implies that α is a linear function of frequency; a more detailed discussion of this topic will occur in later sections of this chapter.

For two different positions, x_1 and x_2 ($x_2 > x_1$) with respective amplitudes $A(x_1)$ and $A(x_2)$ using equation (1.10), one gets

$$\frac{A(x_1)}{A(x_2)} = e^{-\alpha(x_1-x_2)} \tag{1.11}$$

or
$$\ln\left[\frac{A(x_1)}{A(x_2)}\right] = -\alpha(x_1-x_2) \qquad (1.12)$$

from which the value of α can be obtained

$$\alpha = \frac{1}{x_2-x_1} \ln\left[\frac{A(x_1)}{A(x_2)}\right] \qquad (1.13)$$

in nepers per unit length or

$$\alpha = \frac{1}{x_2-x_1} 0.20 \log\left[\frac{A(x_1)}{A(x_2)}\right] \qquad (1.14)$$

in dB per unit length.

The definition of Q given in equation (1.1) is equivalent to the Q of an oscillatory electrical circuit. This provides an alternative definition for Q which refers to the forced vibration of a specimen with resonance frequency f. If the frequency of the vibration is varied and its amplitude held constant, then the amplitude of vibration of the specimen traces out a resonance curve. By measuring the width Δf of the resonance curve when the amplitude of vibration equals $1/\sqrt{2}$ of the amplitude at the peak frequency f, Q is expressed as

$$\frac{1}{Q} = \frac{\Delta f}{f} . \qquad (1.15)$$

All these different definitions for Q may be applied when Q >> 1 and they imply that the direction of propagation is

the same as the direction of attenuation (Zener, 1948). For
strongly attenuating media, these definitions will disagree
and thus we have to define Q differently. O'Connell and
Budiansky (1978) proposed the following definition for Q,
which is probably the best of several different definitions
that scientists have used for Q.

$$\frac{1}{Q} = \frac{Im[M]}{Re[M]}$$
(1.16)

where, $M = \lambda + 2\mu$ for P waves

$M = \mu$ for S waves

λ, μ are the complex Lamé parameters.

The above definition for Q will be used for calculating
reflection and transmission coefficients for anelastic media.

In summary, the common measures of attenuation are
defined and related to one another as follows:

$$\frac{1}{Q} = \frac{\Delta E}{2\pi E} = \frac{\Delta A}{\pi A} = \frac{\delta}{\pi} = \frac{2\alpha c}{\omega} = \frac{Im[M]}{Re[M]}.$$
(1.17)

1.3 Experimental measurements of attenuation

The measurement of attenuation for earth materials
is well covered in the geophysical literature. The values
of Q can be determined in the laboratory, in the field or
by analyzing earthquake and normal mode data. In this section
a brief review of the experimental measurements of attenuation
will be made considering only laboratory data and field

experiments. Attenuation measurements from earthquake
records and normal mode data will not be discussed although
the literature is quite extensive in this area. Particular
attention will be given to the frequency dependence of Q
and the linearity of the absorption coefficient in terms of
frequency. Before going into the main discussion one has to
realize that the accurate measurement of attenuation is a
difficult task with experimental and interpretational prob-
lems. The choice of a particular technique is based largely
on the frequency range of interest, the actual values of
attenuation, and the physical conditions under which the
sample will be studied. The methods generally used for
measuring attenuation in the laboratory can be classified
into the following categories (Zener, 1948; Kolsky, 1953;
Schreiber et al. 1973):

1. Free vibration: In this technique a rod of rock
is suspended vertically so that a mass with a large moment
of inertia can be attached to its lower end. If the mass is
given a kick the system vibrates freely. The rate of decay
of the amplitude of these free oscillations is attributable
to energy loss in the rock. Define the logarithm decrement
as

$$\delta = \frac{\ln(A_1/A_2)}{(t_1-t_2)f}$$ (1.18)

where A_1 and A_2 are the amplitudes at times t_1 and t_2 and f
is the natural free-vibration frequency of the system, the

value of Q is calculated using $1/Q = \delta/\pi$.

2. <u>Forced vibration</u>: The method has been mentioned already where Q may be found from the width of the resonance curve. Equation (1.15) is used in the calculation of Q.

3. <u>Wave propagation method</u>: The transmission of a pulse through the rock and its detection is the basis of this technique. The method assumes an exponential decay of amplitude of the seismic pulse with distance or time and that one can correct for losses due to spreading, reflections, diffractions, etc.

4. <u>Observation of stress-strain curves</u>: For cyclical-ly stressed materials the energy loss per cycle, ΔE, is the area of the mechanical hysteresis loop, in which the phase of the strain lags behind that of the stress. Thus, Q can be calculated using equation (1.1).

The use of stress-strain curves will provide informa-tion at frequencies below 1 Hz, while resonance vibrations are used to measure the attenuation in the range of 100 Hz to 100 kHz. Wave-propagation experiments are commonly restricted to the ultrasonic range of 100 kHz or higher. Let us now discuss some key papers dealing with laboratory measurements of attenuation.

Birch and Bancroft (1938) measured the Q of a core of Quincy granite using the resonance technique. They concluded that Q of Quincy granite was approximately indepen-dent of frequency in the range of 140 to 1600 Hz.

Born (1941) used the same technique to measure the

logarithmic decrement of several rock cores taken from wells. He found that the logarithmic decrement for the dry rock samples was independent of frequency. His studies and measurements with water saturated samples showed that the total decrement was the sum of two terms, the first term was frequency independent and the second one which was proportional to frequency.

Bruckshaw and Mananta (1954) measured the quality factor Q on six different rock cores (granite, dolerite, diorite, sandstone, shelly limestone and oolitic limestone) in the frequency range 40 to 120 Hz. They concluded that Q was practically independent of frequency for these six rocks.

Peselnick and Zietz (1959) used a pulse-echo technique to measure the absorption coefficient in three different limestone samples. Using a piezoelectric crystal attached to one end of the specimen a short pulse of compressional or shear waves is generated. The first arrivals and multiply reflected signals are detected at the other end of the specimen by a second crystal. These arrivals are displayed on an oscilloscope and the decay in amplitude is measured, thus the absorption coefficient can be calculated. They found that the absorption coefficient was proportional to the frequency in the range of 3 Hz to 10 MHz for compressional and shear waves. The absorption coefficient calculated this way includes the effects of apparent losses due to geometrical spreading and the reflections and transmissions at the possible specimen boundaries. However, they found that these

losses were negligible in respect to the absorption.

Wylie et al (1962) studied the absorption of seismic waves in fluid saturated porous rocks. They proposed that the logarithmic decrement was the sum of two terms. The first term was practically independent of frequency while the second term was frequency dependent. They studied the absorption in terms of fluid saturation and they did not give any evidence showing the frequency dependence of the total logarithmic decrement.

Knopoff (1964) summarized the laboratory measurements of Q in metals, non-metals and rocks. In his article with the shortest title in the geophysical literature, "Q", Knopoff indicates that for small strains the absorption coefficient is a linear function of frequency and hence Q is constant.

Bradley and Fort (1966), Atwell and Ramana (1966) reviewed the literature and they concluded that Q is independent of frequency over a range of about 10^6 Hz. They tabulated laboratory and field measurements and measurements from earthquake records. Atwell and Ramana applied a least-squares analysis and concluded that the absorption coefficient was a linear function of frequency in the range 10^{-3} Hz to 100 MHz.

Toksoz et al (1979) studied the attenuation of seismic waves in dry and saturated rocks. Their laboratory measurements were made at ultrasonic frequencies (0.1 to 1.0 MHz) and they showed that attenuation coefficients increase

linearly with frequency (constant Q) for both P and S waves. in both dry and fluid saturated rocks. They found that the attenuation in water saturated rocks is greater than in dry rocks, while the attenuation in frozen rocks is very much lower than in saturated rocks. They also studied the effect of pressure on the attenuation of seismic waves and they concluded that attenuation decreases (Q increases) with increasing pressure for both P and S waves in all cases of saturation. The rate of increase of Q is high at low pressures and levels off at higher pressures.

Therefore, in looking at the laboratory data which has just been discussed, we find that for dry rocks and metals the absorption coefficient depends on the first power of frequency and thus Q is frequency independent. Laboratory measurements with fluid saturated rocks do not lead to the same conclusion. In liquids Q^{-1} is proportional to frequency (Pinkerton, 1947) so that in some highly porous and permeable rocks the total Q^{-1} may contain a frequency dependent component (Born, 1941; Wylie et al, 1962). There is also evidence that Q^{-1} is independent of frequency for saturated rocks as pointed out by McLeroy and DeLoach (1967) and Toksoz et al (1979). Most authors suggest some form of frequency dependence for Q for fluid saturated rocks. This form ranges from Q^{-1} varying directly as frequency to Q^{-1} varying inversely as the square root of frequency. It is evident that the rock texture, porosity, pressure, temperature and type of saturated fluid play an important role in the

relationship between attenuation and frequency for fluid
saturated rocks.

Let us now discuss briefly the field experiments
(in situ) for measuring Q. If the objective is to under-
stand the attenuation of seismic waves in the earth, then
the importance of measuring Q in situ is apparent. The most
common method of measuring the attenuation in situ is using
data from vertical seismic profiles (VSP). Seismic pulses
generated by a surface seismic source are recorded by a
single downhole seismometer positioned at various depths in
a well. The lateral separation between the source and the
well is generally small compared to the seismometer depth.
The spectral ratio method is then applied and Q estimates
are obtained. The spectral ratio method involves a Fourier
analysis of the data from which we can compute the value of
Q and the phase velocity. To explain the method consider
a pulse which has travelled a distance r_1 from the source
and another pulse which travelled a distance r_2 from the
source. Then, we get:

$$F_2(\omega) = F_1(\omega) e^{ik(r_2 - r_1)} \qquad (1.19)$$

where $F_1(\omega)$, $F_2(\omega)$ are the complex spectra of the two pulses
and k is the wavenumber. Make the wavenumber complex

$$k = \frac{\omega}{c(\omega)} + i\alpha \qquad (1.20)$$

where $c(\omega)$ is the phase velocity and α is the absorption coefficient. Substitute in (1.19) and take the ln of both sides we obtain

$$\ln\left[\frac{A_2(\omega)}{A_1(\omega)}\right] = -\alpha(r_2-r_1) \qquad (1.21)$$

and

$$c(\omega) = -\frac{\omega(r_2-r_1)}{\phi_2(\omega)-\phi_1(\omega)} \qquad (1.22)$$

where A_1, A_2 are the amplitude spectra and ϕ_1, ϕ_2 are the phase spectra of the two pulses. Equations (1.21) and (1.22) define the spectral ratio method. Equation (1.21) indicates that a plot of the natural logarithm of the ratio of the amplitude spectra against frequency can be used to determine the nature of the frequency dependence of the absorption coefficient. Equation (1.22) defines the dispersion curve, i.e. the phase velocity as a function of frequency.

The first such experiments were carried out in the Pierre Shale area near Limon, Colorado. This particular location was chosen because it provided a thick section (approximately 1000 m) of uniform shale very close to the earth's surface.

Ricker (1953) performed a series of field experiments in the Pierre Shale area in order to test the validity of his wavelet theory. According to Ricker a modified wave equation which includes a term with a first derivative with

respect to time, is used to explain the seismic phenomena. Ricker's model leads to an absorption coefficient which varies as the square of the frequency and it predicts that the wavelet breadth will increase as the square root of the travel time. He presented graphs which show the validity of his theory. However, in the discussion of his paper many authors pointed out serious problems in the comparison of observed and theoretical wavelets.

McDonald et al (1958) made attenuation measurements in the Pierre Shale area, in the same area where Ricker did his work. Shots at depths of 76.2 to 91.4 m were fired into five geophones at depths from 107 to 229 m. They used velocity log data to apply corrections for geometric spreading and they measured the absorption by Fourier analysis of the corrected waveforms. They concluded that for vertically travelling P waves the absorption coefficient was a linear function of frequency in the range of 100 to 600 Hz. They obtained similar results for horizontally travelling S waves. They also studied the decay of wavelet amplitude with travel time and they found that the wavelet broadening with travel time was less than Ricker had measured.

Wuenschel (1965) studied body wave attenuation and dispersion. The experimental data used in his study was the pulse-propagation experiment done by Mobil in the Pierre Shale (McDonald et al, 1958) and a model seismic analog of the Mobil experiment using ultrasonic pulses in a plexiglass sheet. He showed that the dispersion phenomenon was present

along with the observed absorption and he concluded that the field experiment conducted by McDonald et al (1958) in the Pierre Shale confirms Futterman's theory (1962). Futterman's theory provides the attenuation model used in this thesis, and a more detailed discussion will be found in the next sections of this chapter.

Cole (1965) studied reflections from the Newfoundland abyssal plane and the Gulf of Alaska. He approximated the reflection process by a three-layer fluid model, with attenuation in the second and third layers. He then calculated theoretical reflection coefficients considering the sediment attenuation as proportional to the one-half, first and second powers of the frequency for comparison with measured coefficients. For the frequency range 100-1000 Hz he found that the first power frequency attenuation law in the sediment is consistent with the observed dependence of the ocean-bottom reflectivity.

Tullos and Reid (1969) measured the attenuation of seismic energy in the sediments in the Gulf of Mexico. They used blasting caps as sources and geophones cemented to the earth at various depths in a borehole as receivers. They applied corrections to the data due to geometrical spreading and they removed the effects of constructive and destructive interference due to reflections by averaging the spectra of many traces over a small interval in depth. The ratio of spectra at different depths was then calculated and from this spectral ratio they determined the nature of the

frequency dependence of the absorption. They found that the absorption coefficient is a linear function of frequency in the range from 50 to 400 Hz.

Hamilton (1972) studied the compressional velocity and absorption in the sea floor off San Diego in the frequency range 3.5 KHz to 100 KHz. He concluded that attenuation is approximately dependent on the first power of frequency and that velocity dispersion is almost absent in water saturated sediments. He also indicated that intergrain friction appears to be, by far, the dominant cause of wave energy damping in marine sediments.

Ganley and Kanasewich (1980) measured the absorption and dispersion from seismic check-shot data using the spectral ratio method. The data was taken from a sedimentary basin in the Beaufort Sea. They showed that frequency dependent losses due to reflections and transmissions play an important role and they applied corrections due to these losses using synthetic seismograms. Their analysis showed that the value of Q is almost frequency independent and that the dispersion measured in the data is consistent with Futterman's model. Measured Q values were 43±2 for a depth interval from 549 to 1193m and 67±6 for a depth interval from 945 to 1311m.

Hauge (1981) used data from vertical seismic profiles to measure attenuation via the spectral ratio method. The data were taken from five detailed velocity surveys, one was carried out in West Texas and the other four in the Gulf

Coast area. Actual measured values of attenuation varied

by a factor of 10, ranging from less than 0.1 to 0.9 dB per

wavelength, depending on the lithology. He found that porous

sands have much larger attenuation than neighbouring shales.

Studying the shape of the seismic pulse, he concluded that

attenuation changes the pulse shape noticeably, which is

another indication that dispersion is an essential consequence

of absorption.

Spencer et al (1982) studied the basic problems

encountered in extracting estimates of seismic attenuation

from data recorded on vertical seismic profiles. They paid

particular attention to interference effects, spatial

resolution and frequency dependence of attenuation. They

found that for small receiver separations, the attenuation

computed from the spectral ratio method is much more strongly

influenced by the local stratigraphy in the immediate vicinity

of the seismometer than by the attenuation in the depth

interval between seismometers. They also showed that the

spatial resolution is strongly influenced by the local

stratigraphy and in most cases attenuation estimates would not

be possible to identify lithologies or conditions which are

the source of anomalous dissipation. Plotting the amplitude

ratios against frequency, they found that the graph exhibits

a linear trend which is in good agreement with previous

experimental results.

Summarizing the field measurements of attenuation it

is evident that the absorption coefficient is a linear function

of frequency and hence Q is constant. This statement is
true for frequencies in the range of 10 to 500 Hz and for
in situ rocks. Vertical seismic profiles (VSP) provide the
most successful method of obtaining in situ attenuation
estimates.

1.4 Attenuation mechanisms

In order to evaluate and interpret laboratory and
field measurements of attenuation, possible attenuation
mechanisms involved are needed. Numerous mechanisms have
been proposed and each may be considered to have a greater
degree of importance to the overall attenuation under
certain physical conditions. In this section a brief review
of possible attenuation mechanisms will be made, considering
only these mechanisms responsible for seismic attenuation
in upper crustal rocks. Studying attenuation mechanisms one
has to keep in mind that each mechanism depends on rock type,
saturation state, pressure, frequency range, amplitude of
the acoustic wave and other various rock properties.

Walsh (1966) proposed that the main source of attenu-
ation in dry rocks is based on the frictional dissipation as
crack surfaces in contact slide relative to one another
during passage of a seismic wave. He considered that all
other sources of attenuation are lumped together in the
intrinsic attenuation, which might include losses due to
thermoelastic effects, viscosity, etc. In his analysis,
Walsh formulated the problem by approximating the cracks as

ellipsoids and then he calculated Q values for P and S waves. The resulting expressions are rather complicated, nevertheless, the Q values obtained are frequency independent. Johnston et al (1979) utilized Walsh's formulation to model pressure dependence for the attenuation of ultrasonic waves. They showed that increasing pressure decreases the number of cracks contributing to attenuation by friction, thus the attenuation is decreased. Other authors (Mavko, 1979; Winkler et al, 1979) proposed that friction is not a dominant mechanism particularly at low strain amplitudes and low frequencies. However, under certain laboratory conditions, namely high amplitude ultrasonic experiments, it may be dominant.

Savage (1966) applied Zener's theory of thermoelastic attenuation to explain the attenuation of elastic waves in solids. He showed that thermoelastic losses are associated with long flat cavities which can represent cracks in the medium. This model predicts a decrease in attenuation with increasing pressure and an increase in Q for low frequencies. Recently, Armstrong (1980) has proposed another thermoelastic model for which attenuation is essentially frequency independent.

In a series of papers, Biot (1956, 1962) developed a mathematical theory for the dynamic response of a linear porous solid containing compressible fluid. According to Biot's theory attenuation is a result of the motion of the pore fluid relative to the rock frame and it depends on bulk

rock properties. This type of mechanism is generally concluded to produce negligible attenuation at low frequencies in consolidated rocks (White, 1965). However, it may be important at ultrasonic frequencies (Johnston et al, 1979) or in permeable, unconsolidated sediments at intermediate frequencies.

Biot-type mechanisms consider only bulk fluid flow in porous rock and they ignore inter- and intra-crack flow (local flow), both of which may dissipate seismic energy. Intercrack fluid flow, sometimes known as "squirt" flow, was first proposed as an attenuation mechanism by Mavko and Nur (1975).

Another type of mechanism is a stress induced diffusion model based on the thermally activated motions of atoms or defects on the lattice of a crystal under the influence of external stresses (Tittmann et al, 1980). This type of mechanism is similar to that due to viscous grain boundary damping, where there is a relaxation of stress at grain boundaries. Both mechanisms are relaxation mechanisms and they are generally described by

$$\frac{1}{Q} = D \frac{\omega t'}{1 + \omega^2 t'^2}$$
(1.23)

where D is the ratio of the greatest non-elastic stress to the elastic strain, t' is a relaxation time which varies with temperature T according to an equation of the form

$$t' = t°e^{-\frac{G}{kT}}$$
(1.24)

where G is an activation energy and k is Boltzman's constant.

Summarizing the attenuation mechanisms it seems that the most important absorption mechanism for sedimentary rocks at seismic frequencies would be sliding at cracks or grain boundaries. This mechanism implies a phase angle between stress and strain which leads to a hysteresis loop. Relaxation mechanisms such as grain boundary damping, thermal currents or stress induced diffusion play a secondary role in the attenuation of seismic waves. Finally, the presence of a fluid is a third possible source of absorption. Biot-type mechanisms and "squirt" flow can be considered as the most dominant mechanism in porous rocks.

1.5 Attenuation models

The necessity for incorporating the effect of atten-uation on wave propagation in realistic media is obvious to every geophysicist. Several models and mathematical theories have been developed which take into account the effects of anelasticity. In this section some key papers dealing with attenuation models will be discussed.

The simplest model which is the basis for further generalization is based upon linear elasticity and Stokes' viscosity. A material of this kind is called viscoelastic. Ricker (1953) in his classical paper tried to model the absorption by adding a single term to wave equation following

the work of Stokes (1845). He concluded that the absorption

coefficient varies as the square of the frequency and thus

Q is frequency dependent. It is now clear that Ricker's

model is not adequate to describe the anelasticity in earth

materials since the frequency dependence of Q contradicts

practically all experimental observations.

Kolsky (1956) studied the propagation of short

mechanical pulses along rods of three polymers, polythene,

polysterene and polymethylmethacrylate. He first calculated

theoretical curves showing the phase velocity and attenua-

tion for three models, the Maxwell model, the Voigt model

and the standard linear solid. The Maxwell model consists

of a perfectly elastic spring in series with a dashpot which

has Newtonian viscosity, in the Voigt model the spring is

joined across the dashpot and the standard linear solid is

represented by a second spring in series with a Voigt model.

He concluded that the standard linear solid model gives

better approximation to the behaviour of a real visco-

elastic solid but still can only be fitted over a limited

frequency range.

Futterman (1962) showed that dispersion is a necessary

consequence of the medium absorption and is determined

unambiguously by it. He assumed that the absorption

coefficient, $\alpha(\omega)$, is strictly linear in the frequency, over

the range of measurement and that the principle of super-

position is valid. Consider a one-dimensional plane wave

in the frequency domain as follows:

$$u(x,\omega) = u(o,\omega)e^{iKx} \qquad (1.25)$$

where K, the propagation constant, can be expressed in terms of the phase coefficient $k(\omega)$ and the absorption coefficient $\alpha(\omega)$ as follows:

$$K(\omega) = k(\omega) + i\alpha(\omega). \qquad (1.26)$$

Thus,

$$u(x,\omega) = u(o,\omega)e^{-\alpha(\omega)x}\, e^{ik(\omega)x} \qquad (1.27)$$

or

$$u(x,\omega) = u(o,\omega)e^{-\alpha(\omega)x}\, e^{i\frac{\omega}{c(\omega)}x} \qquad (1.28)$$

where $c = c(\omega)$ is the phase velocity.
Therefore, using the assumption of linear superposition the wave at (x,t) is

$$u(x,t) = \frac{1}{2\pi} \int_{-\infty}^{+\infty} u(o,\omega)e^{-\alpha(\omega)x}\, e^{i[\frac{\omega}{c(\omega)}x-\omega t]}\, d\omega. \qquad (1.29)$$

Equation (1.29) shows that if the absorption coefficient and phase velocity are known as functions of frequency then the effects of absorption and dispersion can be easily introduced in the frequency domain.

Futterman assumed a low cut-off frequency ω_o, characteristic of the material, below which no dispersion exists, and he expressed the complex wave number $K(\omega)$ in

terms of the index of refraction n defined as

$$n(\omega) = \frac{K(\omega)}{K_o(\omega)} = Re[n(\omega)] + iIm[n(\omega)] \qquad (1.30)$$

where $K_o(\omega)$ defines the nondispersive behaviour of K at the same frequency. He then used the principle of causality to derive relations of the Kramer-Krönig type relating the dispersive part of the index of refraction of the medium to the absorptive part by means of an integral over the entire frequency range. These K-K relations are a consequence of the principle of causality and follow without recourse to a specific wave equation. He considered three different forms of absorption which satisfy the assumption of linearity with respect to frequency. In this thesis the (A3) Futterman's absorption form is considered, namely:

$$Im[n(x)] = \frac{1}{2Q_o} (1-e^{-x}) \qquad (1.31)$$

where Q_o is the dimensionless factor of attenuation at ω_o and $x = \frac{\omega}{\omega_o}$. Then, for $Q >> 2\pi$ the phase velocity is given by

$$c(x) = c_o (1 - \frac{1}{\pi Q_o} \ln\gamma x)^{-1} \qquad (1.32)$$

and

$$Q(x) = Q_o (1 - \frac{1}{\pi Q_o} \ln\gamma x) \qquad (1.33)$$

where c_o is the phase velocity at ω_o

and $\ell n\gamma = 0.5772157...$ is the Euler's constant.

Equations (1.31), (1.32) and (1.33) describe the attenuation model used in this thesis. The low cutoff frequency ω_o does not correspond to any specific physical mechanism and it can be chosen sufficiently low. The values of Q, as obtained by equation (1.33), show that Q is practically constant and frequency independent. Futterman's model is in excellent agreement with experimental data (Wuenschel, 1965) and it has a major advantage in that we need not appeal to the physical details that are characteristic of a particular theory. They are bypassed to yield the dispersion directly from the absorption coefficient, in this case taken from experiment.

Lomnitz (1957) tried to explain the relationship between transient creep and interval friction in solid materials. He used Boltzmann's superposition principle to relate stress and strain as follows:

$$e(t) = \frac{1}{m}\left[p(t) + \int_{-\infty}^{t} p(t)\dot{f}(t-\tau)d\tau \right] \qquad (1.34)$$

where p(t) is the stress, e(t) is the strain, m is an elastic constant and f(t) is the creep function. The stress is related to strain as follows:

$$p(t) = m\left[e(t) + \int_{-\infty}^{t} e(t)\dot{y}(t-\tau)d\tau \right] \qquad (1.35)$$

where $y(t)$ is the relaxation function. Equations (1.34), (1.35) are convolution integrals, thus by Fourier transform we obtain

$$E(\omega) = \frac{P(\omega)}{m}(1+F(\omega)) \qquad (1.36)$$

$$P(\omega) = mE(\omega)(1+Y(\omega)). \qquad (1.37)$$

Lomnitz assumed a complex elastic modulus M to relate stress and strain as follows:

$$P(\omega) = ME(\omega) \qquad (1.38)$$

the quality factor Q is defined such that

$$M = m\left(1+i\frac{1}{Q}\right) \qquad (1.39)$$

He then showed that a creep function of the form

$$f(t) = \frac{q\omega_H}{1+\omega_H t} \qquad (t>0) \qquad (1.40)$$

could be used to derive the following expression for Q assuming that $Q \gg 1$ and $\frac{\omega}{\omega_H} \ll 1$

$$\frac{1}{Q} = \frac{q\pi}{2[1-q\ln(\gamma\frac{\omega}{\omega_H})]} \qquad (1.41)$$

where q is a constant and ω_H is a high frequency cutoff.

Equation (1.41) is very similar to the frequency dependence of Q given by Futterman in equation (1.33). Indeed, the two theories by Futterman and Lomnitz do not differ significantly (Savage and O'Neill, 1975). Futterman assumes a complex propagation constant while Lomnitz considers a complex elastic modulus. Neither theory provides any information about the physical mechanisms of absorption.

Carpenter (1966) calculated the impulse response of a system satisfying the constant Q hypothesis. He compared the models of Kolsky and Futterman and he concluded that they are very similar. He also concluded that in many cases it is more convenient to work in the frequency domain rather than in the time domain.

Azimi et al (1968) considered a model for which the absorption coefficient $\alpha(\omega)$ is of the form

$$\alpha(\omega) = \frac{\alpha_o \omega}{1+\alpha_1 \omega}, \qquad \begin{array}{l} \alpha_o (m^{-1} sec) \\ \\ \alpha_1 (sec) \end{array} \qquad (1.42)$$

in which α_o, α_1 are constants. This model has a linear dependence on frequency for $\alpha_1 \omega << 1$. They used Kramers-Krönig relations to derive the following expression for the phase velocity

$$\frac{1}{c(\omega)} = \frac{1}{c_\infty} + \frac{2\alpha_o}{\pi} \ln\left(\frac{1}{\alpha_1 \omega}\right) \qquad (1.43)$$

where c_∞ is the phase velocity as the frequency becomes infinite.

Strick (1967, 1970) used the following relation for the absorption coefficient:

$$\alpha(\omega) = b\omega^s \qquad\qquad (1.44)$$

where b is a constant and $0 < s < 1$. He then derived a dispersion relation for the above model and he noticed reasonable agreement with experimental data. He also developed an asymptotic expansion for the time domain shape of a travelling wave at large distances. He used a solid of $Q = 50$ and he compared his results with Futterman's theory. He found that the shapes of the pulses are similar but the time is very different. The difference in times is due to various approximations that Strick made, thus his theory is valid only for frequencies much greater than the low frequency cutoff.

Kjartansson (1979) presented a linear model for attenuation with Q exactly independent of frequency. According to his model the wave propagation is completely specified by two parameters, e.g. Q and c_o, a phase velocity at an arbitrary reference frequency ω_o. He started using Boltzmann's superposition principle with the following creep function

$$f(t) = \frac{1}{M_o \Gamma(1+2\gamma)} \left(\frac{t}{t_o}\right)^{2\gamma} \qquad t > 0$$

$$f(t) = 0 \qquad\qquad\qquad t < 0 \qquad (1.45)$$

where Γ is a function with a value close to unity, t_o is an arbitrary reference time and M_o is a constant. The value of γ is constant and is related to Q as follows

$$\gamma = \frac{1}{\pi} \tan^{-1}\left(\frac{1}{Q}\right) \approx \frac{1}{\pi Q}. \qquad (1.46)$$

He then derived a simple exact expression for the phase velocity as a function of frequency:

$$c(\omega) = c_o \left(\frac{\omega}{\omega_o}\right)^{\gamma}. \qquad (1.47)$$

Kjartansson's model is causal since both the creep and relaxation functions vanish for negative time, no strain can precede applied stress, nor can any stress precede applied strain.

Finally, the standard linear solid model will be examined. This model is well described by Zener (1948). The stress-strain relation is of the following form

$$p + e_p \dot{p} = m(e + p_e \dot{e}) \qquad (1.48)$$

where e_p is the relaxation time for stress corresponding to

a step change in strain, p_e is the relaxation time of

strain under an applied step in stress and m is a constant.

The Q is obtained as a function of ω and the relaxation

times

$$\frac{1}{Q} = \frac{\omega(p_e - e_p)}{1 + \omega^2 p_e e_p} . \tag{1.49}$$

The above equation shows that Q^{-1} is not constant but it

behaves as a resonance curve as a function of ω. The

attenuation, Q^{-1}, is concentrated near the frequency

$(p_e e_p)^{-\frac{1}{2}}$, with Q^{-1} behaving like ω for frequencies below

this central peak and like ω^{-1} for frequencies above it.

The corresponding expression for the phase velocity shows

a monotonical increase with frequency.

In order to reproduce the effectively constant Q^{-1}

values observed at seismic frequencies, Liu et al (1976)

assumed that attenuation is due to a superposition of

different relaxation phenomena, each of which corresponds

to a relaxation peak and is represented by the stress-

strain relation of equation (1.48). Thus, by superposition

of twelve relaxation peaks of this type they obtained a

model with constant Q^{-1} over the range 0.0001 to 10 Hz.

They also showed that the dispersion relation for such a

model is very similar to that arising from Futterman's

theory.

CHAPTER 2

2.1 Introduction

Generalized ray theory was introduced by Van der Pol and Bremmer (1937) in a classical paper on electromagnetic radiation from a point source. The integral terms in the infinite expansion were described clearly as unique reflected or multiply reflected rays from the boundaries in the layered medium. Beginning with Cagniard (1939) and Pekeris (1940) various forms of this technique have been applied to the study of elastic wave propagation. A definitive exposition was given by Pekeris et al (1965) for the case of a solid layer over a half space. They describe the elastic wave solution as a double power series over indices μ and ν ($\mu, \nu = 0, \ldots, \infty$) in which each term in the expansion represents a ray that has been reflected μ times as a compressional (P) wave and ν times as a shear (S) wave. The term "generalized reflection and transmission coeffi- cients" was introduced by Spencer (1960) and "generalized rays" by Cisternas et al (1973).

In this thesis we follow the development of generalized ray theory for the case of a point stress pulse in an elastic layer over a half space. Exact synthetic seismo- grams are obtained by computer modelling for a number of cases of interest in exploration and earthquake geophysics. These include the weathered layer problem where recordings close to the source may be difficult to interpret since they are not analogous to intuitive experience obtained from far-

field observations or plane wave modelling. Another case examines the simple model of a "crustal" layer over a "mantle" half space for a horizontal point force. Finally in the fourth chapter we examine the region where head waves separate from the reflected arrivals in a typical sedimentary section consisting of a low velocity layer over a thick high velocity one.

Consider the propagation of waves from a buried stress discontinuity to a surface receiver in a solid elastic layer over a half-space. The exact analytic solution in the Laplace transform domain has the following form:

$$\bar{u}_i(p,r) = \frac{\bar{F}_1(p)}{4\pi\mu_1} \sum_{\mu=0,}^{M} \sum_{\nu=0}^{\infty} \bar{G}_{\mu\nu}(p,r,i,j) \quad i,j=1,2,3 \qquad (2.1)$$

The transformed displacements ($\bar{u}_1 = \bar{q}$; $\bar{u}_2 = \bar{V}$; $\bar{u}_3 = \bar{w}$) are in cylindrical coordinates (r,ϕ,z) in which circular symmetry is assumed about the z axis and the source is placed at a depth d below the origin. The source function $\bar{F}$ will be a stress pulse of type j with a triangular shaped time dependence when viewed in the far-field. The algorithms will be computed for a horizontally polarized torque (j=1); a vertically (j=2) and a horizontally (j=3) concentrated force. The Laplace transform variable is p($=i\omega$) where ω is the angular frequency. M equals infinity unless compressional waves are absent in which case it is zero. The shear modulii, shear and compressional velocities in the layer and half space are $\mu_1,\mu_2, \beta_1,\beta_2, \alpha_1$ and α_2. The response of

each generalized ray is given by $\bar{G}$, an integral involving integers μ and ν, where μ is the number of times the energy is reflected as a P wave and ν the number of times as an S wave. The response of each generalized ray has the following form:

$$\bar{G}_{\mu\nu} = \int_0^\infty \frac{px^2}{\beta_1} \left[J_{n(j)} \left(\frac{prx}{\beta_1} \right) \left(R_i^P E_{ij} + R_i^S F_{ij} \right) + J'_{n(j)} \left(\frac{prx}{\beta_1} \right) \left(r_i^P e_{ij} + r_i^S f_{ij} \right) \right] dx$$

(2.2)

where x is a scaled integration variable $\left(= \frac{\beta_1 \xi}{p} \right)$ in which ξ is a spatial wave number measured in the direction of wave propagation. J_n is the Bessel function of order n=0 or 1 and J'_n is its derivative. R_i^P and r_i^P are generalized reflection coefficients for the ith displacement for the totality of rays starting as P and arriving at the receiver after being reflected μ times as P and ν times as S waves. Functions R_i^S and r_i^S play a similar role for rays starting as S. As will be illustrated, each μ, ν pair represents several distinct ray paths and the generalized reflection coefficients are the sum of all their reflection coefficients. E, e, F and f are spatial coefficients which determine the phase delay and amplitude change. They are products of rational functions of x and exponential terms involving velocities and ratio of depth of source to thickness. The explicit relations or their references for the three types of sources are as follows:

$$j = 1; \text{SH Torque} \quad i = 2; \quad n(1) = 1$$

$$F_1 = 8\pi\mu_1 f(t)H(t) \tag{2.3}$$

where $f(t)$ is the shape of the source in time, a quadrature pulse being used, and $H(t)$ is the Heaviside function.

$$E_{21} = e_{21} = f_{21} = 0 \tag{2.4}$$

$$F_{21} = \frac{\delta_{\mu\nu}}{\sqrt{1+x^2}} e^{-(\nu+\frac{1}{2})\left[Hp\sqrt{x^2+1}/\beta_1 \right.} \tag{2.5}$$

$$R_2^S = R^{I[(\nu+1)/2]} \tag{2.6}$$

where $\delta_{\mu\nu}$ is the Kronecker delta, I is the integer part and R is the Laplace transformed representation of the generalized reflection coefficient for SH waves as given by Pekeris et al (1963).

$$j = 2; \quad \text{Vertical Force}$$

$$i = 1 \text{ and } 3; \quad n(2) = 0; \quad F_2 = Z_o f(t)H(t) \tag{2.7}$$

where Z_o is the excess normal load.

$$E_{12} = F_{12} = e_{32} = f_{32} = 0 \tag{2.8}$$

$$e_{12} = \frac{e^{-AMH-B\nu H}}{p} \; ; \qquad f_{12} = \frac{e^{-A\mu H-BNH}}{p}$$

$$\text{(2.9)}$$

$$E_{32} = \frac{\sqrt{x^2+\varepsilon_1^2}}{xp} \, e^{-AMH-B\nu H} \; ; \qquad F_{32} = \frac{x}{p\sqrt{x^2+\eta_1^2}} \, e^{-AMH-BNH}$$

The operational forms of the reflection coefficient are given by Abramovici (1970); Abramovici and Gal-Ezer (1978) as R_1 and R_2 for R_3^P and R_3^S and S_1 and S_2 for r_1^P and r_1^S. The other constants are

$$\varepsilon_1 = \beta_1/\alpha_1; \quad \eta_1 = \beta_1/\beta_2; \quad A = \frac{p}{\beta_1}\sqrt{x^2+\varepsilon_1^2}; \quad B = \frac{p}{\beta_1}\sqrt{x^2+1} \quad \text{(2.10)}$$

$$N = \begin{cases} \nu+1-d/H \\ \nu+d/H \end{cases} ; \quad M = \begin{cases} \mu+1-d/H & ; \quad F \quad \text{even} \\ \mu+d/H & ; \quad F \quad \text{odd} \end{cases} \quad \text{(2.11)}$$

where F is the Family ray number ($=\mu+\nu+1$), H is the layer thickness and d is the depth of the source.

$$j = 3; \quad \text{Horizontal Force}$$

$$i = 1,2,3; \quad n(3) = 1; \quad F_3 = \underline{Y}f(t)H(t) \quad \text{(2.12)}$$

where $\underline{Y} = Y_x\underline{i} + Y_y\underline{j}$ is the strength of the source in the horizontal plane ($Y_x = Y_y = 1$); $\underline{i},\underline{j}$ are unit vectors.

$$E_{13} = e_{23} = e_{33} = f_{33} = 0 \tag{2.13}$$

$$F_{13} = \frac{2\delta_{\mu\nu} i\beta_1}{r p^3 x^2} \frac{e^{-BNH}}{\sqrt{x^2+\eta_1^2}} \quad ; \quad e_{13} = \frac{jx}{p^2} e^{-AMH-B\nu H} \tag{2.14}$$

$$f_{13} = \frac{-j\sqrt{x^2+\eta_1^2}}{xp^2} e^{-A_1\mu H - BNH} \quad ; \quad E_{23} = \frac{i\beta_1}{p^3 r} \frac{e^{-AMH-B\nu H}}{\sqrt{x^2+\epsilon_1^2}} \tag{2.15}$$

$$F_{23} = \frac{i\beta_1 \sqrt{x^2+\eta_1^2}}{p^3 x^2} e^{-A\mu H - BNH} ; \quad f_{23} = \frac{-i2\delta_{\mu\nu} e^{-BNH}}{x\sqrt{x^2+\eta_1^2}} \tag{2.16}$$

$$E_{33} = \frac{j}{p^2} e^{-AMH-B\nu H}; \quad F_{33} = \frac{-j\sqrt{x^2+\epsilon_1^2}\sqrt{x^2+\eta_1^2}}{p^2 x^2} e^{-A\mu H - BNH} \tag{2.17}$$

where the reflection coefficients are

$$r_2^S = R_1^S = R^{I[(\nu+1)/2]}; \quad R_2^P = r_1^P = S_3 \tag{2.18}$$

$$R_2^S = r_1^S = S_4; \quad R_3^P = R_3; \quad R_3^S = R_4 \tag{2.19}$$

where R_3, R_4, S_3 and S_4 are derived in the Appendix A.

The displacements in the time domain are obtained by an inverse Laplace transform following the methods of Cagniard (1939), Pekeris (1940), and de Hoop (1960). The details of the transformation follow the method of Longman (1961) as generalized by Abramovici (1978).

The complete mathematical solution for the case of a horizontal stress discontinuity is given in the Appendix A.

2.2   The Weathered Layer Model

The seismic weathered layer or zone is a surficial deposit that has a profound influence on all studies of the elastic propagation of waves. The properties of the weathered layer are:

(a)   a low compressional wave velocity (300 to 2000 m/s) and an anomalously low shear velocity (100 to 1000 m/s);

(b)   high energy absorption or low Q (5-100);

(c)   a heterogeneous composition with the thickness varying from 3 to 100 meters. However the lateral variation usually has a long wave length except at geologically significant interfaces;

(d)   a large change in acoustic impedance across the inter-face separating the weathered layer from underlying consolidated medium.

The properties arise because the rocks near the surface are relatively unconsolidated, mechanically and chemically altered and highly aerated. In some areas the base of the weathered layer is related to the average level of the water table but even in areas where the water table is at the surface there is a well defined seismic weathered layer presumably caused by repeated hydration-dehydration, precipitation of salts, fracturing and decomposition of minerals.

The effect of the weathered layer on a surface record-ing or on seismic waves impinging on it from greater depths is out of all proportion to its relative thickness or

transit time through it. The weathered layer produces anomalous scattering of energy, magnification of amplitudes, and large energy dissipation, particularly in the desired high frequency part of the spectrum. It acts as a wave guide which converts a large amount of the energy into surface waves and generally introduces undesirable reverberation patterns into the seismograms.

An accurate determination of the weathered layer is of value in making static corrections for reflection seismic studies and it has potential in the derivation of deconvolution operators. The subject is of interest by itself in the study of the water table, buried channel deposits and the exploration of coal and other surficial deposits which may be subject to strip mining. Because of the heterogeneous nature of the weathered layer its properties may only be determined by seismic studies employing short source to receiver distances. Elastic wave recordings in the near and intermediate distance range are difficult to interpret because seismologists have been trained in and use far-field models for most of their studies. In general, more care must be taken in the type of instrumentation used for near surface studies because of the difficulties in identifying several kinds of phases. We shall see that three component recordings are essential since the radial direction often contains the strongest compressional or P wave arrivals. In fact, P velocity arrivals may be found on synthetic seismograms in the transverse direction in the near field.

As a guide to the study of seismic recordings for the structure of shallow layers, a series of exact synthetic seismograms have been computed using generalized ray theory. The model to be used is idealized in that it consists of a source within or on an elastic layer over a half-space. The incorporation of attenuation will be considered in the next chapter.   Good approximations to a low velocity layer over a half-space are found quite frequently in sedimentary basins. More complex layered structure could be modelled but usually with objectionable approximations in the algorithm or with prohibitively expensive computer operations. Before attempting these more elaborate models the considerable complexity in the results from these simpler examples should be explored.

In the following synthetic seismograms the complete solution is given up to a selected time after the first arrival. An important advantage of the generalized ray method is that one may examine individual generalized rays or groups of them. This allows one to determine if the numerical integration procedures are stable and accurate for each generalized ray. It is also possible to determine whether a significant peak is due to a single ray or, as often happens, because of a cluster of arrivals.

Figure 1 gives the model for the weathered layer and also the shape of the source pulse in the far field. The triangular width of the pulse is 0.0021 s and it is placed

Figure 1. Model of a layer over a half space with the

source at a shallow depth. The model simulates

wave propagation in a weathered layer. The

source is a stress impulse with a triangular

shape in time.

SOURCE

MODEL

$\alpha_1 = 1000 m/s$ $\rho_1 = 2.09 g/cc$

$\beta_1 = 577 m/s$

$\alpha_2 = 2000 m/s$ $\rho_2 = 2.29 g/cc$

$\beta_2 = 1160 m/s$

2δ

t

$0m$

5

20

x

z
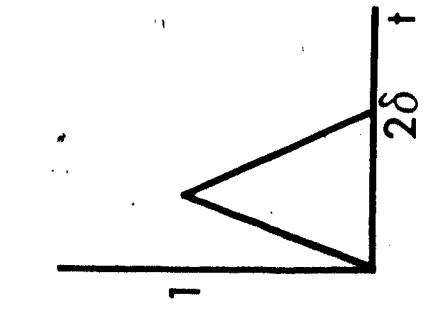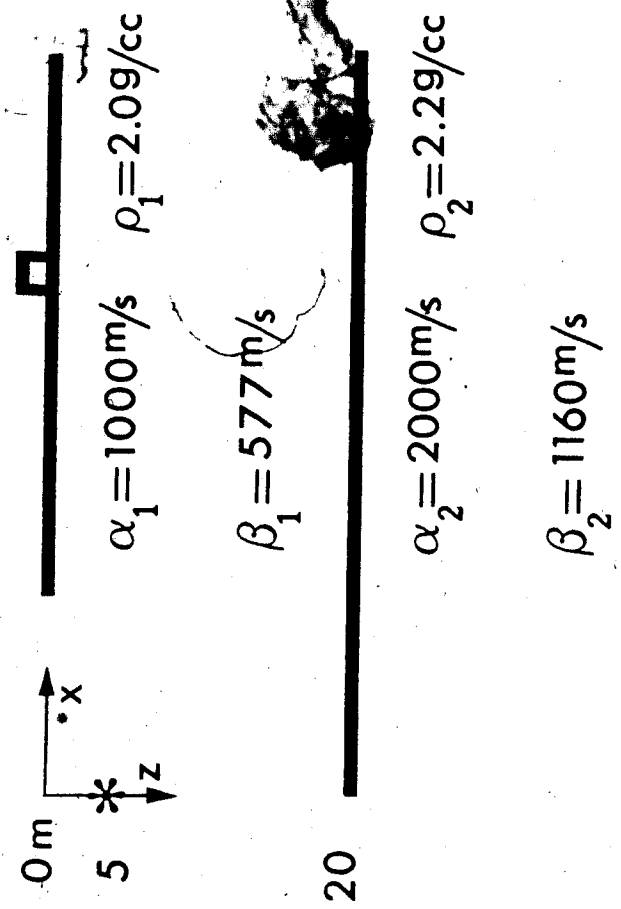
Figure 2.   Synthetic seismograms for a horizontally
            polarized torque as the source in the model of
            figure 1.   The surface transverse displacement
            is shown in a three dimensional plot using an
            algorithm called ASPEX.   The figure viewed for
            an azimuth of 340°, an altitude of 18° from the
            horizontal at the center of the graph to the
            observer and a distance of 25m from the graph
            to the observer.
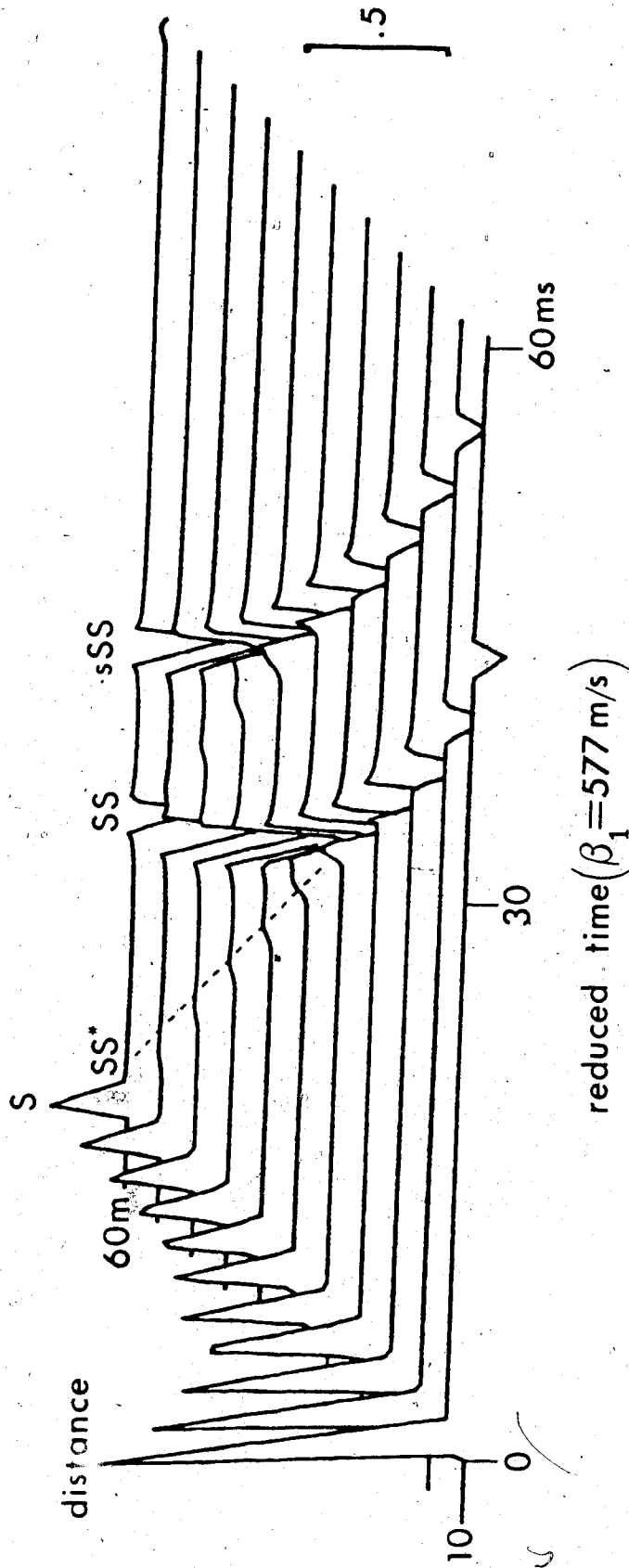
SH-TORQUE

either at 5 m or at the surface. The first seismograms (Fig. 2) are of the transverse component at distances of 10 to 60 m for a torque with the axis in the vertical direction. For an experimentalist an SH torque is not a very interesting model since it is difficult or impossible to produce in the field. For the theoretician and programmer it is the first step in producing a well tested algorithm since only horizontally polarized waves are produced. The results are of some interest, since apart from velocity scaling, an explosive source in a liquid medium produces a similar seismogram on a pressure transducer. Note the well developed head wave (labelled SS*= $S_1 S_2 S_1$) separating from the first reflected wave (SS).

The next source is of far greater interest to the experimentalist, being a concentrated vertical force produced by a jump in normal stress at a particular depth on the z axis. A vertical force is used instead of a buried compressional pulse since a hammer impact, a vibratory device or a cylindrically shaped tube of explosive chemical in a lightly tamped borehole produces a dominantly vertical force. The difference in the displacement components for a surface source and one at a depth of 5 m is shown in figure 3. The displacement for the surface source is similar to the classical Lamb (1904) solution up to the time of the reflected (PP) ray. Dramatic changes occur when the source is buried. The amplitude of the Rayleigh wave is over one magnitude greater for a surface

Figure 3. Synthetic seismograms for a surface and a

buried (5m) source for a point vertical force.

The model parameters are given in figure 1.

The decay of the surface head wave sP* is shown

to the right of the seismograms.
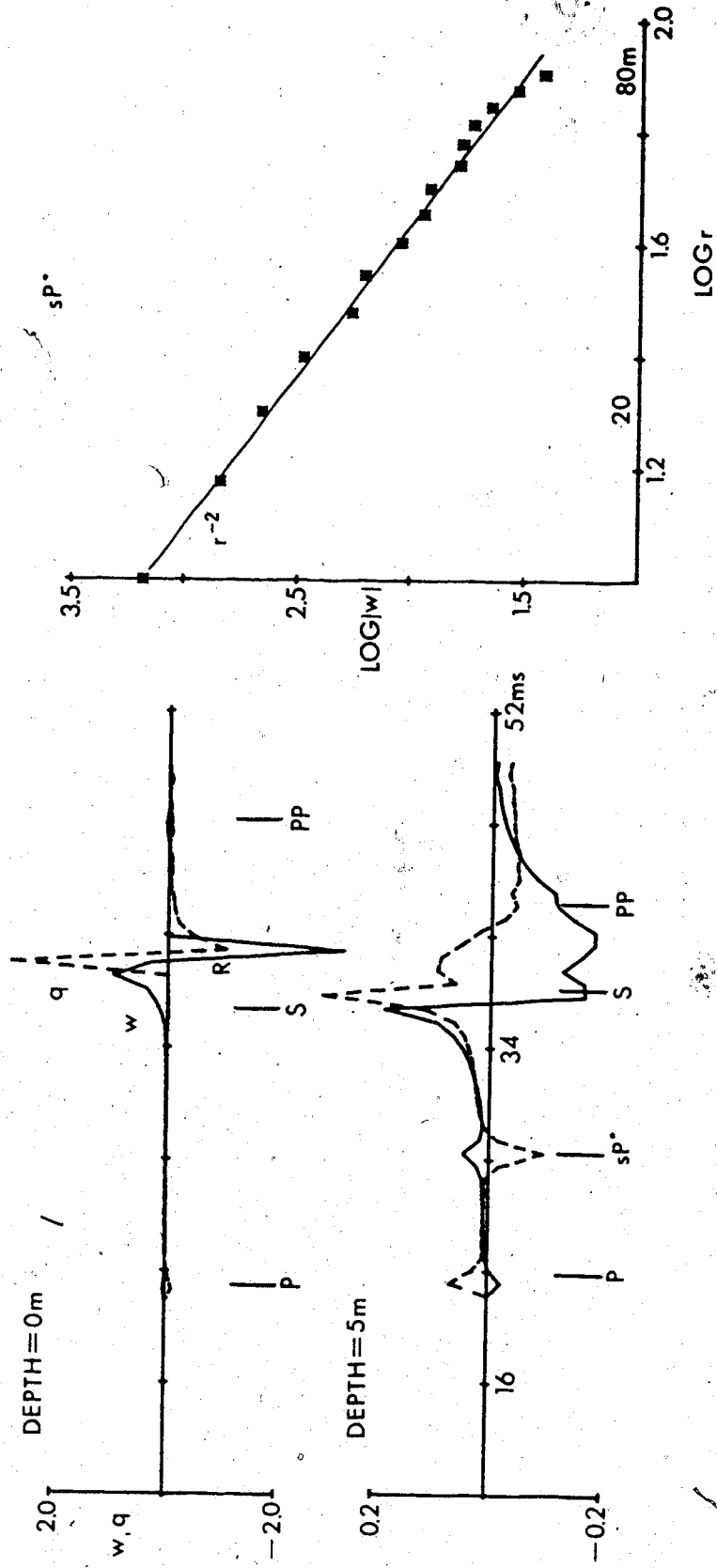
impulse.

More importantly, there is a new diffracted pulse labelled sP* which travels to the surface as an S wave and along the surface as a P wave. This "surface head wave" was predicted theoretically by Petrashin (1959) who called it a shear head wave. Numerical seismograms for this phase which they called a diffracted $\bar{S}*$ were first shown by Abramovici and Gal-Ezer (1978). The particle motion is linear and 180° out of phase with the direct P or S waves. The surface head wave does not occur if the source is purely compressional since no S waves are generated. From theoretical considerations the surface head wave should decay as $r^{-3/2}$ close to critical distance and as r^{-2} at distances where the path in the lower interface is large. This is confirmed by the modelling studies (Figure 3).

For the buried source the emergent Rayleigh wave clearly precedes and overlaps the direct shear wave. This behaviour can be interpreted physically as due to the arrival of the direct spherical P wave front at the surface near the source and generating a displacement which forms the early part of the Rayleigh wave. The interference pattern formed by the strong direct shear wave and the Rayleigh waves will certainly create difficulties in interpreting field recordings if only a single component is available. The interpretation of the displacement of generalized rays is facilitated if they are grouped into families defined by a parameter F

Figure 4. Classification of 30 physical rays into

generalized rays, having a unique value of μ

and ν into the first three families. The

partial seismograms, using the vertical

component at a distance of 40m and a vertical

force buried at 5m, are used to illustrate each

family of rays.
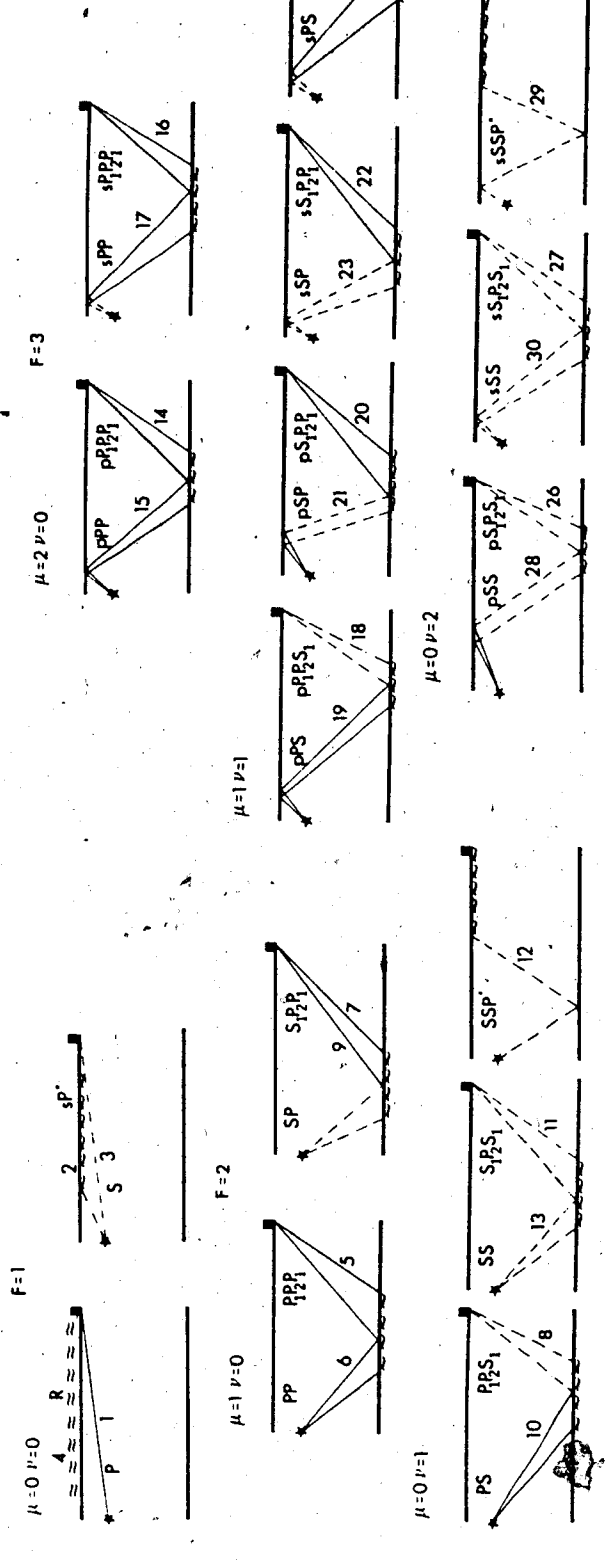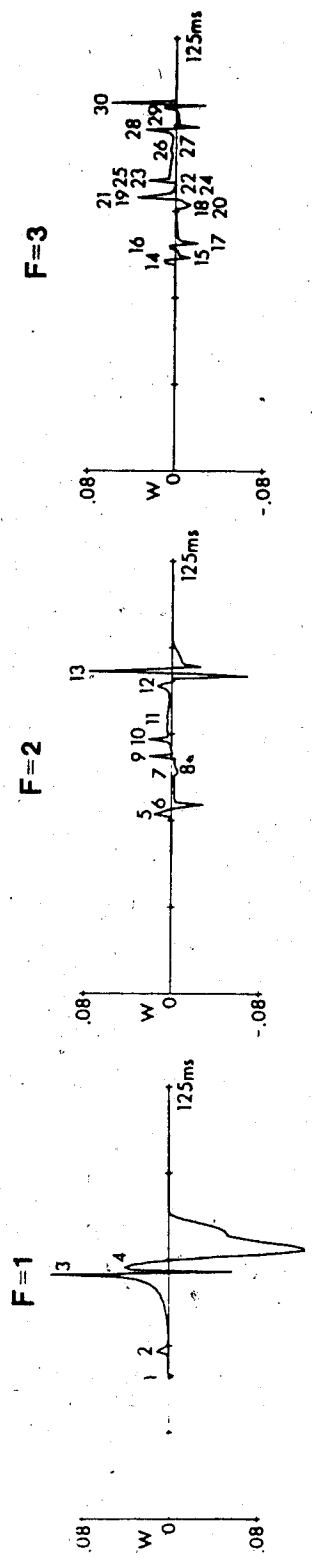
$$F = \mu + \nu + 1 \qquad F = 1,2... \qquad (2.20)$$
$$\mu,\nu = 0,1,2...$$

F is equal to the number of encounters that the curve makes with all available interfaces. In figure 4 all the rays in the first 3 families are illustrated together with their displacement for a buried source and a surface receiver at a distance of twice the layer thickness (40 m). The complete seismogram is the sum of all the families of rays up to any particular time. This may be viewed in figure 5 which shows the suite of seismograms from 10 to 60 m. As will be shown in the next section of the chapter, each individual generalized ray has its component impulsive ray arrivals superimposed upon an "exponentially" growing tail which is not evident on the complete seismogram. The tail in each generalized ray may be thought of as due to Rayleigh waves generated as the spherical P and S wave fronts interact with the surface. When all the generalized rays within each family are combined the tails cancel completely after the arrival of the last ray. A relict of the tails is physically observable by the non-zero offset of the displacement between individual rays. The partial seismograms in figure 4 reproduce faithfully the ground displacement including the non-zero plateaus between the impulsive arrivals.

Note that the odd numbered families originate as up-going waves at the source and even numbered familites initiate as downgoing waves. The amplitude of phases in family 3 are

Figure 5. Synthetic seismograms for a point vertical
source buried at 5m for the model shown in
figure 1. The three dimensional plot has the
same parameters as figure 2 except that the
reduction velocity is 1000 m/s.

VERTICAL

60m P sP⋅ PP SP S R SS

distance

50

40

30

20

10

PS⋅

PPS sSP⋅

sSS

.5

RADIAL

60m P sP⋅ PP SP S R SS

distance

40

10

0

PS⋅

40

60

PPS sSP⋅80ms

sSS

reduced time $\left(\alpha_1 = 1.0 \text{Km/s}\right)$
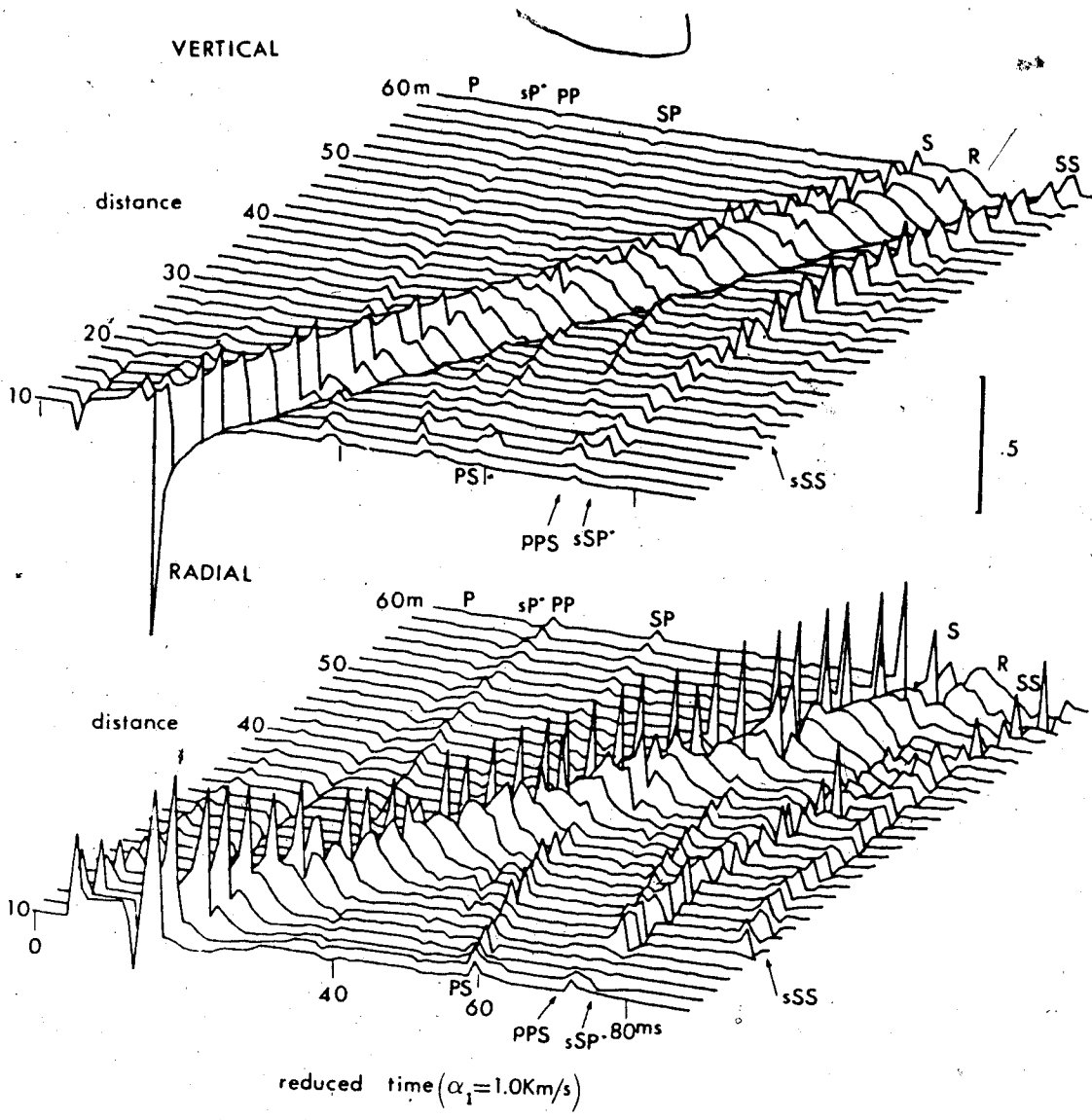
only slightly less than those of family 2. This is to be
expected since the extra encounter is as a perfect reflection
at the surface. In field recordings this will seldom occur
and the rays from family 3 would diminish by an amount
determined by the roughness of the surface and dominant
wavelength of wave and surface irregularities. Rays from
higher order families have amplitudes much diminished. This
is evident in figure 5 which also includes rays from families
4 and 5. These arrivals are the ones not labelled with a
code.

In the synthetic for a buried vertical force (figure 5)
one should note the prominence of the first two compressional
waves on the radical component. These are the direct P and
the surface head wave, sP*. At intermediate distances, 10
to 40 m from the source, the shear (S) arrival is more
prominent on the vertical receiver. There are a great
multiplicity of reflected and related head waves in the
seismograms. These exact seismograms include 20 pairs of
generalized waves originating as P or S waves from the source.
The total computation time for all figure 5 seismograms on
an Amdahl 470 V/6 was 25 minutes at a nominal cost of $500.
Unfortunately the integration noise increases greatly and
the CPU time mounts rapidly if longer seismogram intervals,
after the first arrivals, are required.

When the buried source is a force in an arbitrary
horizontal direction all three components of motion are

Figure 6. Synthetic seismograms for a point horizontal
source buried at 5m for the model shown in
figure 1. The ray paths for a few principal
rays are shown on the right.

VERTICAL

30m P

S SP PS SS

distance

20

10 PP

RADIAL

30m P sP' S SP PS sSP' SS

distance

20

10 PP

.2

TRANSVERSE

30m S SS

distance

20

10

0 (P) 40 60ms

reduced time($\alpha_1 = 1.0$Km/s)

KEY TO PHASES

P

sP'
S

PP

PS

SP

SS
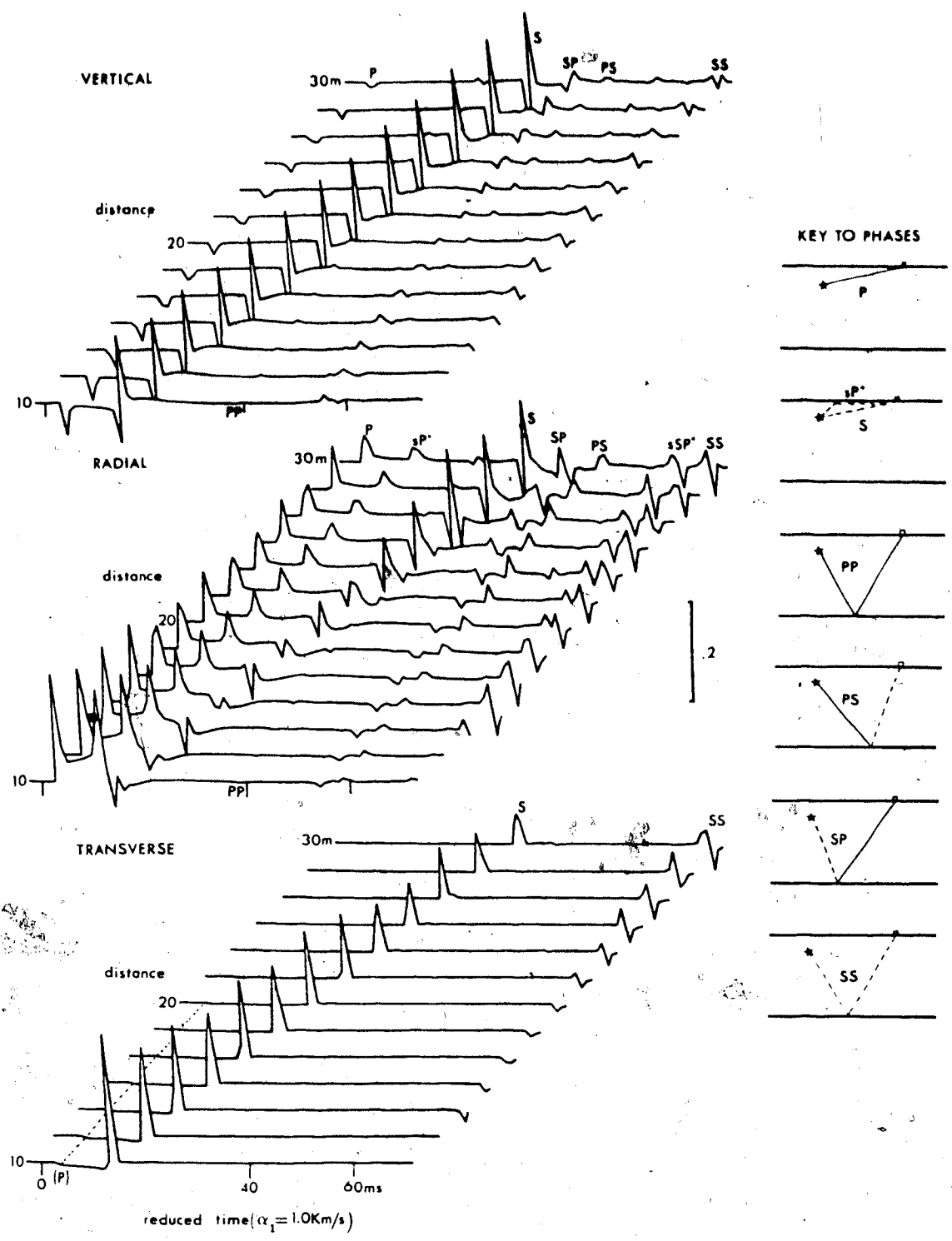
excited. In the examples shown in figure 6 a unit impulse
of equal strength in the x (=x_1) and y (=x_2) direction was
used. The source acts like a shear dislocation with a stress
discontinuity along an open surface. Although the system of
equations is expanded conveniently into an SH set with
transverse motion and a P-SV set with radial and vertical
motion, both sets have arrivals with P and S wave velocities.
Thus the transverse (SH) component shows an initial wave
arriving with a P wave velocity at near and intermediate
distances (10-20 m). We have observed this with hammer
seismograph sources in field experiments during studies of
the weathered layer and the theoretical confirmation is
gratifying.

The direct P wave is the strongest arrival on the
radial component while the shear (S) arrival is the strongest
on the vertical component. Excitation of this type of
source is particularly desirable since the Rayleigh waves
are minor and the seismogram is dominated by a clear set of
reflected impulses. A comparison of figure 5 with a verti-
cal force and figure 6 with a horizontal force makes the
point clearly. The surface head wave, sP*, is the only head
wave with a well defined signature and it appears strongly
on the radial component only.

2.3 The crustal layer model

Synthetic seismograms are computed for a horizontal point force in the x_1-x_2 plane for the model ~~~~~~ in Fig. 7. The model velocities and densities are ~~~~~ for a 40 km thick crustal layer over a mantle half-space. Synthetics are computed for two different depths (figures 8 and 9) and for distances of 20 to 60 km. In all cases the receivers were placed on the surface on the x_1-axis. The x_1-component of the force gives rise to radial, q, and vertical, w, components of motion. The components of the force along the x_2-axis gives only an angular displacement called the transverse component, V. As in refraction seismology the seismograms are plotted against reduced time $(t-r/\alpha_1)$ where t is the actual time in seconds, r is the distance from the source to receiver along the x_1-axis α_1 is the velocity of compressional waves in the layer.

Some of the rays are marked by the convention employed in earthquake seismology. An initial wave propagating toward the surface has the ray segment designated by a lower case letter (p or s). A star is used as a superscript to indicate a head wave of that type. The solution is complete and includes all the generalized rays arriving within 23 seconds after the first compressional wave front. At most distances this included about 15 generalized rays starting at a compressional wave velocity and 12 starting at a shear wave velocity. The integer μ is again a generalized

Figure 7.   The crustal model of an elastic layer over a
            half space. The source is at a depth of either
            1/2 (figure 8) or 1/5 (figure 9) of the layer
            thickness. Velocities (α and β) are in km/s
            while density (ρ) is in gm/mℓ.

Receivers

X_1

x Source (figure 9)

X_3

■ Source (figure 8)

X_2

0

40 Km

$\alpha = 8.15$
$\beta = 3.55$
$\rho = 2.74$

$\alpha = 8.14$
$\beta = 4.70$
$\rho = 3.30$
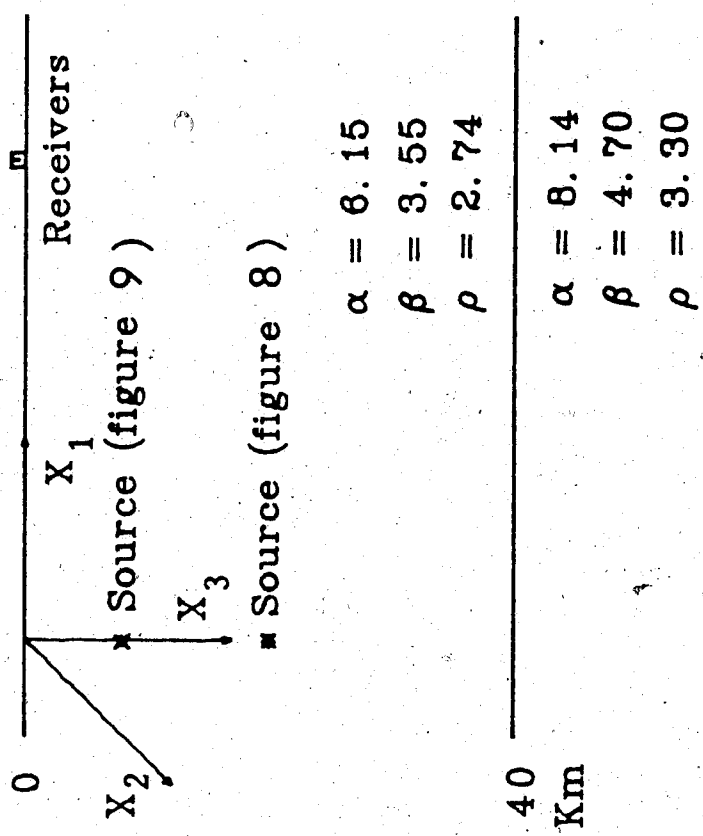
Figure 8. Synthetic seismograms for a source buried in
the middle of the layer of figure 7. The ray
paths for a few of the principal generalized
rays are shown on the right. The figure is a
three dimensional plot for an azimuth of 340°,
an altitude of 18° from the horizontal at the
center of the graph to the observer and a
distance of 25 km from the graph to the
observer.

VERTICAL 60Km — P s SS

40

20 PP SP PS PPS sSP

RADIAL 60Km P sP s SS

40

20 PP SP PS PPS sSP

.0005

TRANSVERSE 60Km s SS

40

20
0 10 20sec

REDUCED TIME = $\left(t - R/6.15\right)$

Source
1.0
2.5sec
DEPTH = 20Km
KEY TO PHASES

P

sP s

PP

PS

SP

SS

PPS
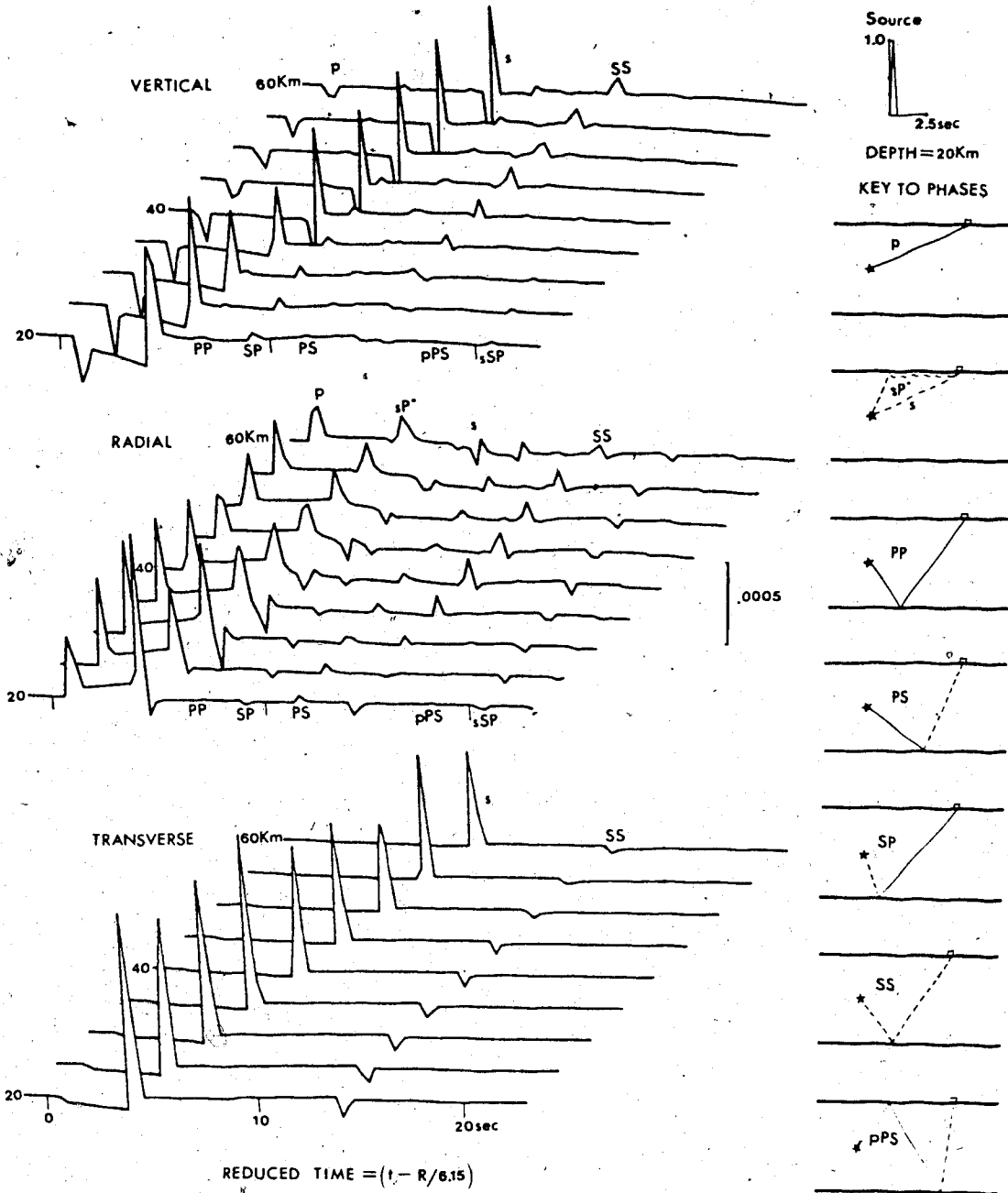
ray index which may be interpreted as one less than the
number of interactions with the available boundaries as an
indicent P wave. Similarly ν is a generalized ray index
which specifies the number of boundary interactions minus
one as an incident S wave. As in the previous section,
one can define the integer F

$$F = \mu + \nu + 1 \qquad F = 1,2,\ldots \quad (2.21)$$

$$\mu,\nu = 0,1,2,\ldots$$

In the illustrations for figures 8 and 9 the generalized
ray parameters which needed to be included for the desired
span of time were $\mu \leq 6$; $\nu \leq 2$, $F \leq 7$.

Although the source is due only to a horizontal force
there is a prominent p or compressional wave generated by
the first generalized ray ($\mu=0$, $\nu=0$, $F=1$) at close distances.
The vertical and transverse components become negligible
within a distance equal to the thickness of the first layer
but the radial component is substantial at all distances.
This result is of significance when interpreting seismograms
from horizontal sources in exploration seismology. The
direct s or shear wave shows some interesting variations
in amplitude on the radial component when the source is
shallow (figure 9). It is also possible to see the head
wave generated by shear waves incident on the boundaries,
sP*, on the radial component.

Figure 9. Synthetic seismograms similar to those shown in
figure 8 but with the horizontal point source
at a depth of 1/5 of the layer thickness. The
three dimensional plot uses the same parameters
as in figure 8.

VERTICAL   60Km   P   s   PS   pPS   SS   pSS

DEPTH = 8 Km

KEY TO PHASES

P

sP*

s

40

20

PP   SP   sSP

RADIAL   60Km   P   sP*   s   PS   pPS   SS   pSS

PP

.0008

PS

40

20

PP   SP   sSP   sSS

SP

TRANSVERSE   60Km   s   SS   sSS

sSS

40

SS

20

0   10   20sec
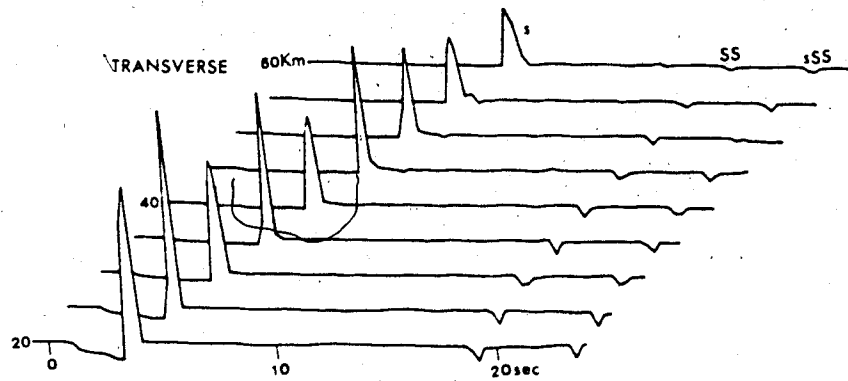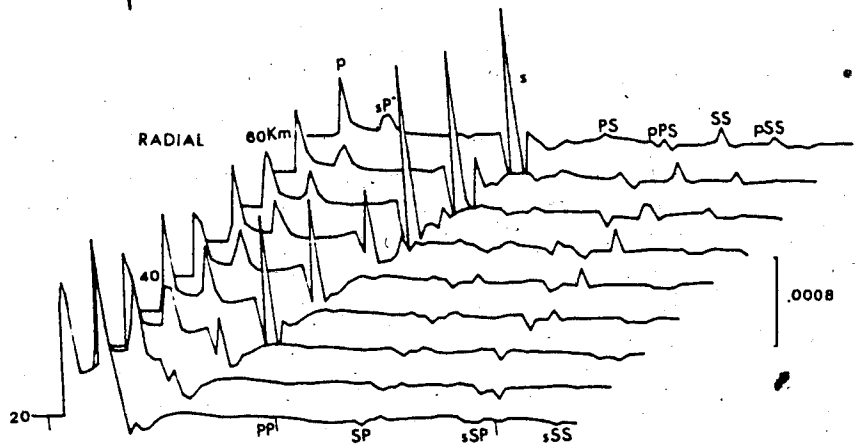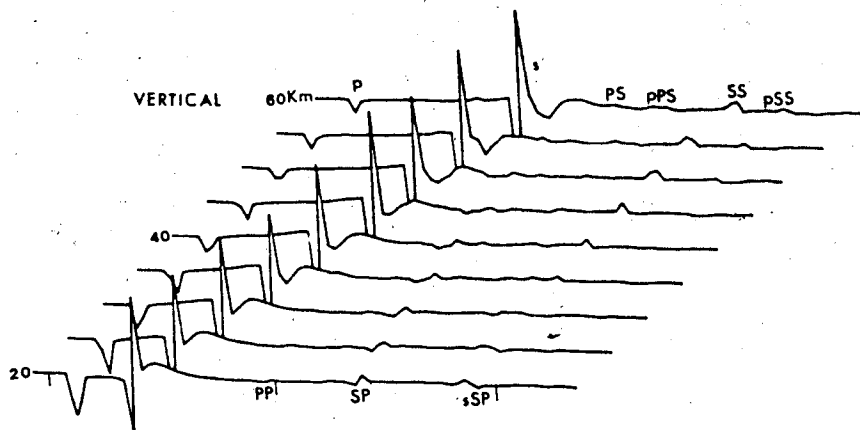
REDUCED TIME = (t − R/6.15)
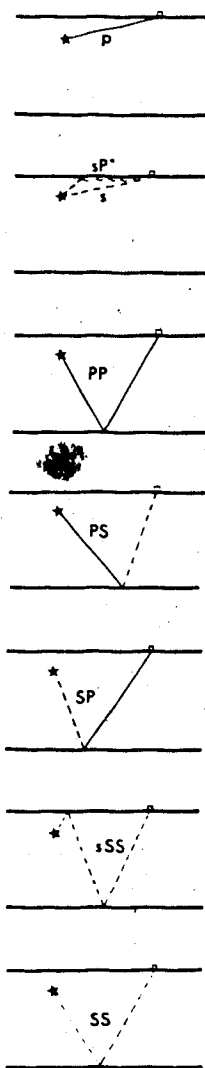
Figure 10. Phase relationship in the near field for a

buried horizontal source in a layer over a

half space. The transverse (V) radial (Q) and

vertical (W) component are shown for a receiver

at a distance of 20 km. The source is buried

at a depth of 8 km. The model is shown in

figure 7.
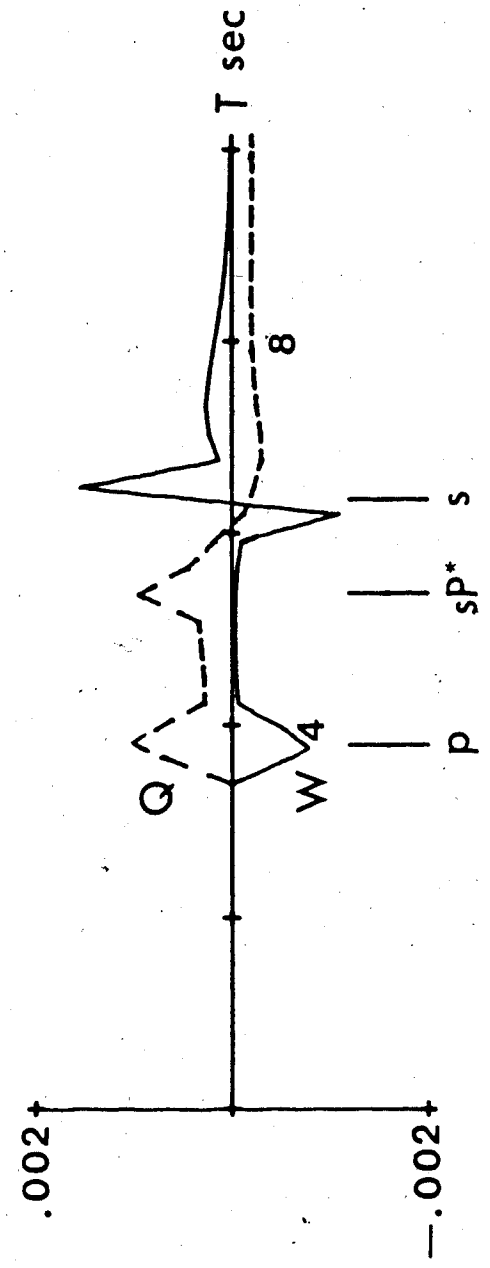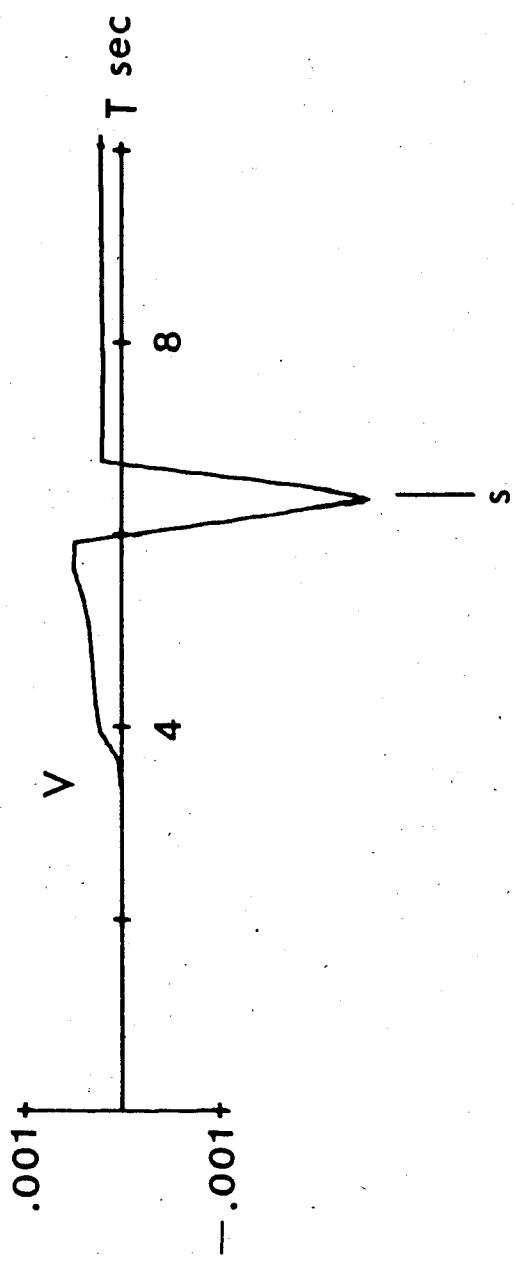
For horizontal force sources the vertical and radial components are close to 0° or 180° in phase for most generalized rays at medium recording distances. However surface recordings close to the source show large phase differences at times close to the direct s wave arrival. This is shown more clearly in figure 10 which is an enlargement of the seismogram at 20 km in figure 9. The radial and vertical components following the s phase show that a small "Rayleigh" wave has been generated from contributions of integrals with indices $\mu = 0$, $\nu = 0$ (F = 1).

Since the final seismograms were computed from a linear superposition of generalized rays, it is possible to disassemble the contributions. Examination of the individual generalized rays allows one to make a better physical interpretation and to check on the numerical stability when evaluating complex integrals on a digital computer. In addition it may be possible to compute an ad hoc synthetic seismogram including attenuation by treating each generalized ray individually and incorporating atten-uation in a process involving a discrete Fourier transform (chapter 3).

The generalized rays may be grouped using Eq. (2.21) according to families based on the value of F. Thus, F = 1 defines the first family which include the direct p and s arrivals and their associated Rayleigh wave due to the interaction with the free surface. Figure 11 shows the
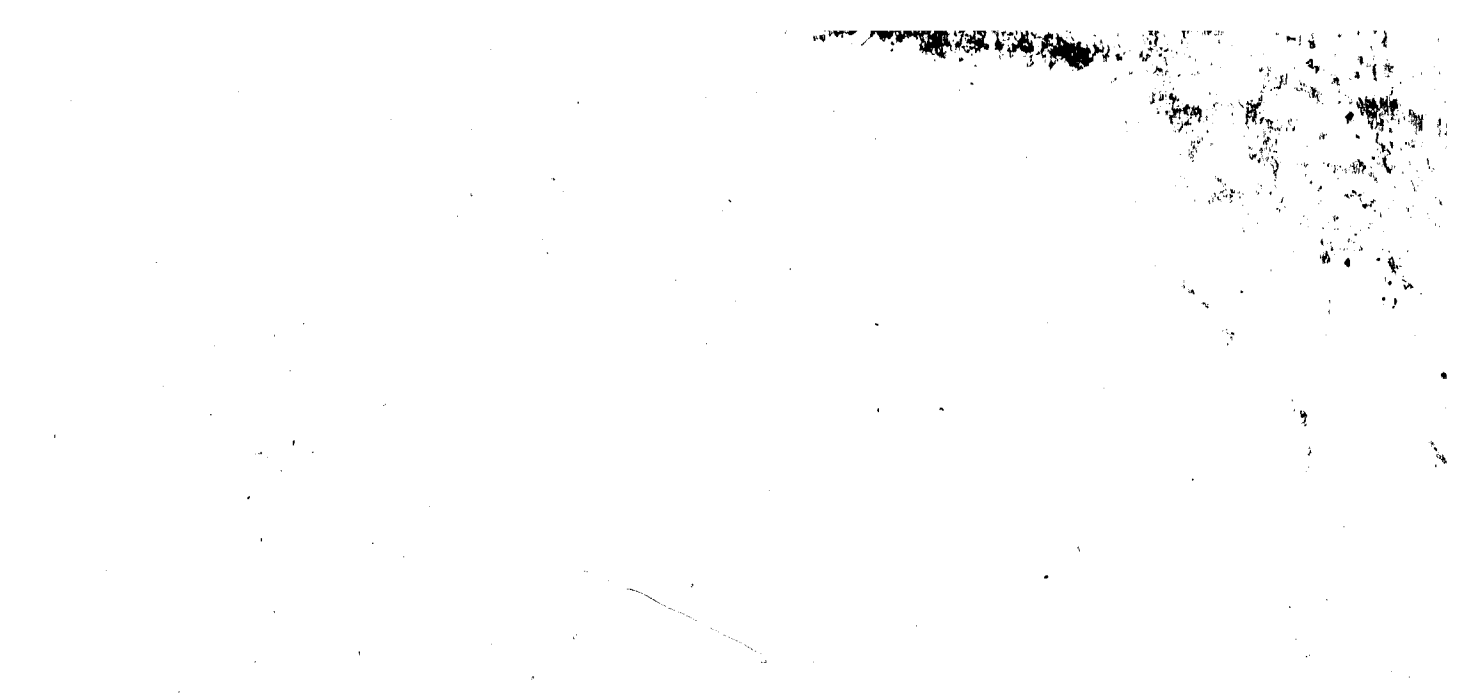
Figure 11. Synthetic seismograms decomposed into families
of generalized rays for a distance of 40 km
and a point horizontal force in the middle of
the crustal layer. P and S indicate that the
ray starts as a compressional or shear wave
from the source. All the partial seismograms
start at a real time of 6.8s. Note that when
all the generalized ray contributions in each
family are summed (Σ), the exponentially
growing tails cancel.

F = 1

F = 2

VERTICAL

(P) $\mu = 0$ $\nu = 0$

(S) $\mu = 0$ $\nu = 0$

Σ

P   s

RADIAL

(P) $\mu = 0$ $\nu = 0$

(S) $\mu = 0$ $\nu = 0$

Σ

p   sP*   s

TRANSVERSE

(P) $\mu = 0$ $\nu = 0$

(S) $\mu = 0$ $\nu = 0$

Σ

s

.004

VERTICAL

(P) $\mu = 1$ $\nu = 0$

(P) $\mu = 0$ $\nu = 1$

(S) $\mu = 1$ $\nu = 0$

(S) $\mu = 0$ $\nu = 1$

Σ

PP   SP   PS   SS

RADIAL

(P) $\mu = 1$ $\nu = 0$

(P) $\mu = 0$ $\nu = 1$

(S) $\mu = 1$ $\nu = 0$

(S) $\mu = 0$ $\nu = 1$

Σ

PP   SP   PS   SS

TRANSVERSE

(P) $\mu = 1$ $\nu = 0$

(P) $\mu = 0$ $\nu = 1$

(S) $\mu = 1$ $\nu = 0$

(S) $\mu = 0$ $\nu = 1$

Σ

SS

.0004

— 5 —
Sec

— 5 —
Sec
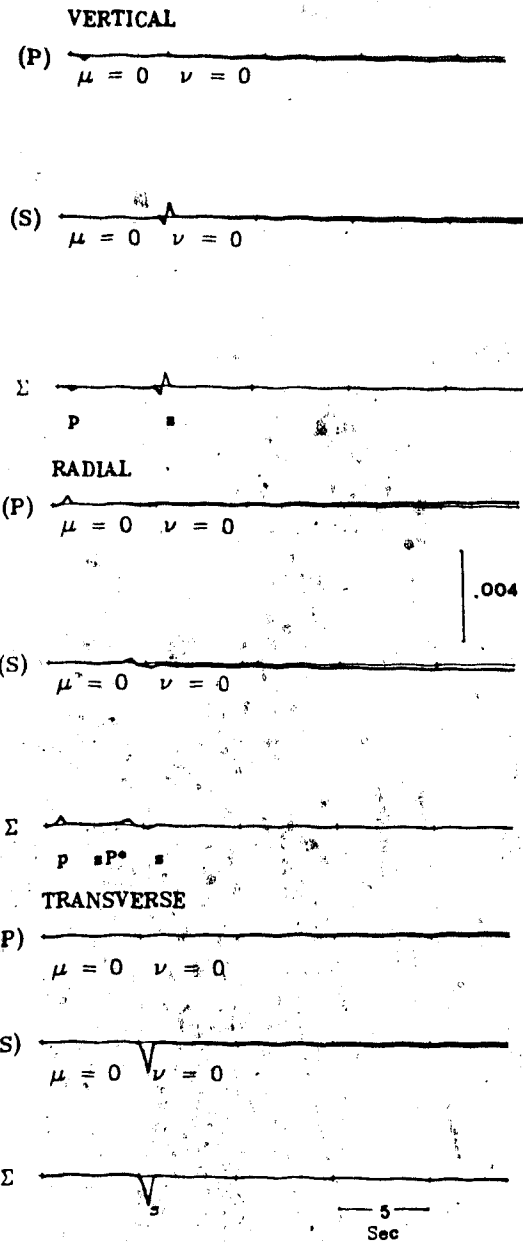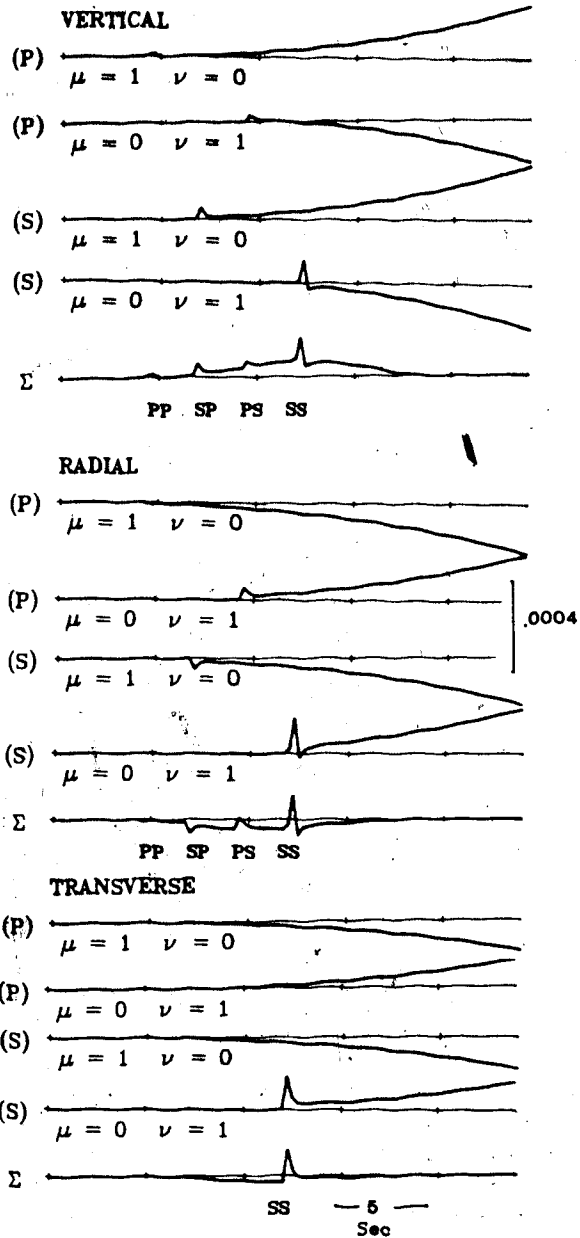
individual generalized rays for each component of motion and their summation into a family of rays. Each individual generalized ray shows the principal arrival as a P or an S wave but it also shows a tail which does not vanish with time. The tails are related to the generation of an interface (Rayleigh) wave as the curved wave front expands to cover a continuous range of ray parameters. As shown in figure 11 the tails disappear when all the generalized rays from each family ($F = \mu + \nu + 1 =$ constant) have arrived and are incorporated into the seismogram. It is seen that from a physical point of view F is a measure of the number of encounters each ray has had with the available boundaries. The classification of generalized rays into families appears to be useful and should allow one to form an alternate method of truncating a seismogram when it is too expensive to incorporate computationally all the rays to a particular time.

The synthetic seismograms should be of use in interpreting field results close to small earthquakes where the source can be modelled by a horizontal stress discontinuity at some depth within the crust. The importance of the direct compressional wave and many converted phases has been illustrated. The results should be of interest in exploration studies where a shear source is generated by a hammer mechanism or by a vibrator. Since the solution is analytic and the numerical results are complete up to any desired

time the results are useful in checking other methods

which may be adapted more easily to a complex elastic

layered medium.

CHAPTER 3

3.1 Introduction

It is becoming increasingly important to include the
effects of anelasticity in the computation of synthetic
seismograms and in other seismic modelling techniques. A
method of introducing the effects of attenuation and
dispersion into the synthetics will be shown. The general-
ized ray theory is used to calculate exact synthetic
seismograms for a layered homogeneous isotropic medium and
the effects of anelasticity such as attenuation and dispersion
of seismic waves are modelled using the linear theory of
viscoelasticity combined with Futterman's model (1962).

According to the generalized ray theory the response
of a layered medium to a disturbance is expressed as a
superposition of individual generalized rays. By decomposing
the seismogram into rays, one can study each ray individually
and the effects of absorption and dispersion can be incor-
porated in the frequency domain using Futterman's theory.
In addition, the effects of viscoelastic interfaces are
taken into account by calculating reflection coefficients
for anelastic media. Therefore, by summing all the rays a
synthetic seismogram which includes the effects of anelas-
ticity can be computed.

Futterman's theory provides an excellent model of
attenuation and dispersion that is in good agreement with
experimental data (Wuenschel, 1965). It is based on the

principle of superposition and on the linearity of
absorption coefficient as a function of frequency. Reflec-
tion and transmission coefficients for anelastic media are
calculated using the correspondence principle. Lockett
(1962) described the method for setting up the equations
which must be solved for the reflection and transmission
coefficients in the anelastic problem. The boundary
conditions are the same as for the elastic case and the
only change is that elastic modulus, phase velocity and
wave number are complex functions of frequency. Buchen
(1971) and Borcherdt (1973) set up the general theoretical
framework for plane waves in linear viscoelastic media by
considering inhomogeneous waves, where the direction of
propagation is different from the direction of attenuation.
Schoenberg (1971) solves the problem of a plane harmonic
wave impinging on a plane interface between an elastic and
a linearly viscoelastic medium. Borcherdt (1977) gives a
complete theoretical description of SH-waves in anelastic
media and derives reflection and transmission coefficients
for the SH-waves. Krebes and Hron (1980a,b), following
Borcherdt's formulation, calculate reflection and trans-
mission coefficients for the SH-anelastic case and compare
them with the coefficients for the perfectly elastic case.
They use these coefficients for computing synthetic seismo-
grams for SH-waves in a layered anelastic medium using the
asymptotic ray theory. In this chapter we consider
attenuation for both the SH and P-SV cases by a modification

of an exact and complete solution obtained from generalized ray theory.

3.2 Attenuation and dispersion along the path

A complete description of Futterman's model of attenuation was given in the first chapter. Equations (1.31), (1.32) and (1.33) describe the attenuation model used in this thesis. They provide the absorption coefficient, the phase velocity and the dimensionless factor Q as functions of frequency. Then, the effects of attenuation and dispersion along the ray path can be easily incorporated into the frequency domain by multiplying the amplitude spectrum of each ray by an exponential decay and by adding a phase shift in the phase spectrum. The ray is obtained in the time domain using an inverse Fourier transform (Eq. 1.29).

3.3 The effect of the viscoelastic interface

The stress-strain relation for a homogeneous isotropic linear viscoelastic medium is given by

$$\sigma_{ij} = \delta_{ij} \int_{-\infty}^{t} \lambda(t-\tau) \frac{de_{kk}(\tau)}{d\tau} d\tau + 2 \int_{-\infty}^{t} \mu(t-\tau) \frac{de_{ij}(\tau)}{d\tau} d\tau. \quad (3.1)$$

where σ_{ij} is the stress tensor, λ and μ are the complex Lamé parameters and e_{ij} is the stress tensor (Borcherdt, 1973, 1977). Substitution of (3.1) into the equation of motion gives

$$[\lambda(t)+\mu(t)]*d(\nabla(\nabla.\vec{u}) + \mu(t)*d(\nabla^2\vec{u}) = \rho\vec{u} \qquad (3.2)$$

after some calculation where the symbol * denotes the Stieltjes convolution. Taking the Fourier transform of (3.2) and writing the transform of the displacement vector in terms of the Helmholtz potentials, we obtain the well known Helmholtz equation

$$\nabla^2\vec{F} + K^2\vec{F} = 0$$

where K is now complex.

Equation (3.3) is similar in form to the corresponding equation of linear elasticity except that the Lamé constants are now complex. Therefore, any formal solution of Helmholtz equation in the theory of elasticity offers a corresponding solution for a linear viscoelastic body, if the elastic modulii that occur in the elastic solution are replaced by the corresponding complex modulii (Correspondence-Principle; Ben-Menahem, Singh, 1981). Thus, reflection/transmission/coefficients for a viscoelastic interface may be obtained from the analogue in the elastic case. In appendix B we show how complex modulii are calculated using the phase velocity and the attenuation factor as functions of frequency.

Figure 12 shows the amplitude and phase for the PP and PS reflection coefficients. The solid lines represent the elastic case while the dashed lines correspond to the

Figure 12.   The amplitude and phase for PP and PS plane

wave reflection coefficients are plotted against

the angle of incidence θ.   The solid lines

correspond to the elastic case while the

dashed lines correspond to the anelastic case

The velocities, densities and Q values are

shown in figure 15.
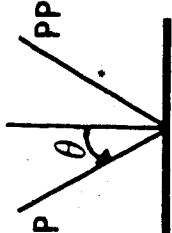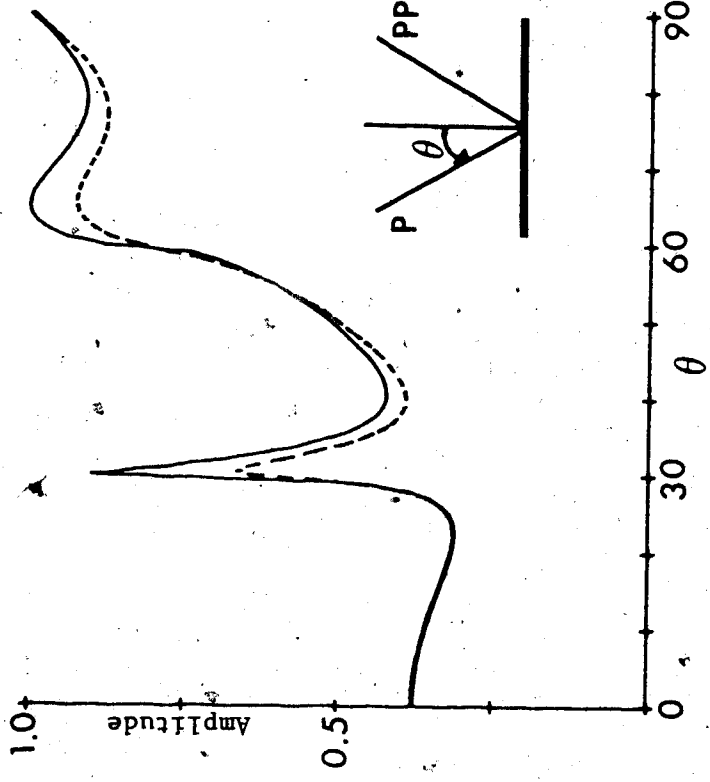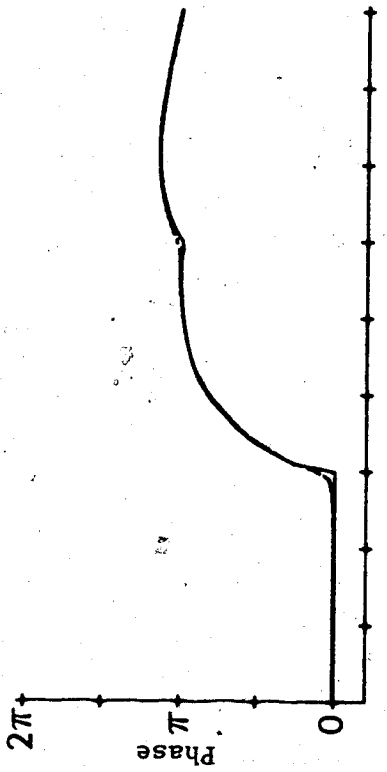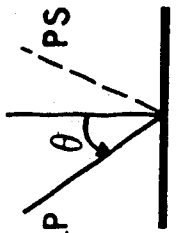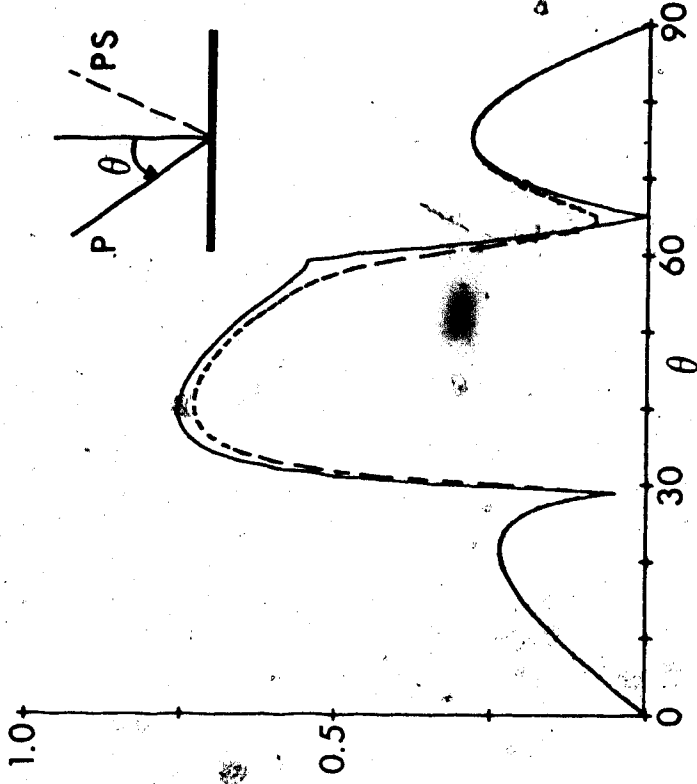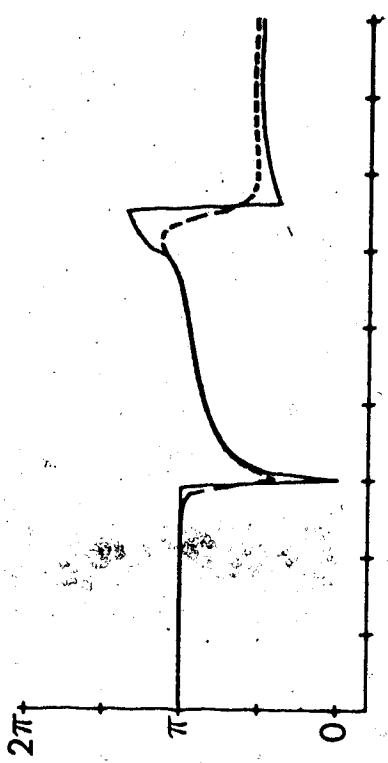
viscoelastic case. In order to examine the frequency
dependence of the reflection and transmission coefficients
for a viscoelastic interface, we have studied several simple
models. We found that these coefficients are not sensitive
functions of frequency unless the values of Q are very low.
Therefore, the effect of a viscoelastic interface can be
modelled by calculating frequency independent reflection
and transmission coefficients for anelastic media. As
Figure 12 indicates, in order to take into account a visco-
elastic interface, we have to apply a correction to the
amplitude spectrum of the pulse and to add another term in
the phase spectrum.

3.4 The attenuation algorithm

      Figure 13 is a flow chart which illustrates the
algorithm used in order to introduce the effects of atten-
uation and dispersion in the seismograms. The synthetic
is first decomposed into individual generalized rays, and
each ray is transformed into the frequency domain using a
fast Fourier transform (FFT). The absorption and disper-
sion along the ray path is then introduced using
Futterman's model. The effect of the viscoelastic interface
is also taken into account by calculating reflection
coefficients for anelastic media.

      The procedure for one generalized ray is illustrated
in Figure 14 for the case of a horizontally polarized head
wave and reflection near the critical distance. A Fourier

Figure 13. Flow chart showing the algorithm used in order
to introduce the effects of anelasticity into
each generalized ray.

ATTENUATION — DISPERSION

1. ALONG THE PATH
2. INTERFACE

1.

```
┌──────────────┐
│   GENER.     │
│   RAY        │
└──────────────┘
        │
        ▼
┌──────────────┐
│     FFT      │
└──────────────┘
```

2.

```
┌──────────────┐
│  REFLECTION  │
│    COEF.     │
└──────────────┘
        │
        ▼
┌──────────────┐
│   CO...      │
│   λ, ...     │
└──────────────┘
```
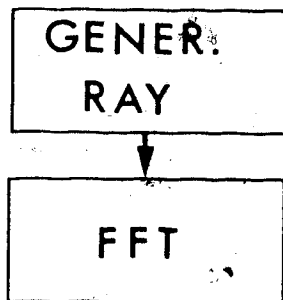
```
┌──────────────┐
│  FUTTERMAN   │
│    MODEL     │
└──────────────┘
        │
        ▼
┌──────────────┐
│   INVERSE    │
│    FFT       │
└──────────────┘
        │
        ▼
┌──────────────┐
│   ∑ RAY      │
└──────────────┘
        │
        ▼
┌──────────────┐
│   SEISMOG.   │
└──────────────┘
```
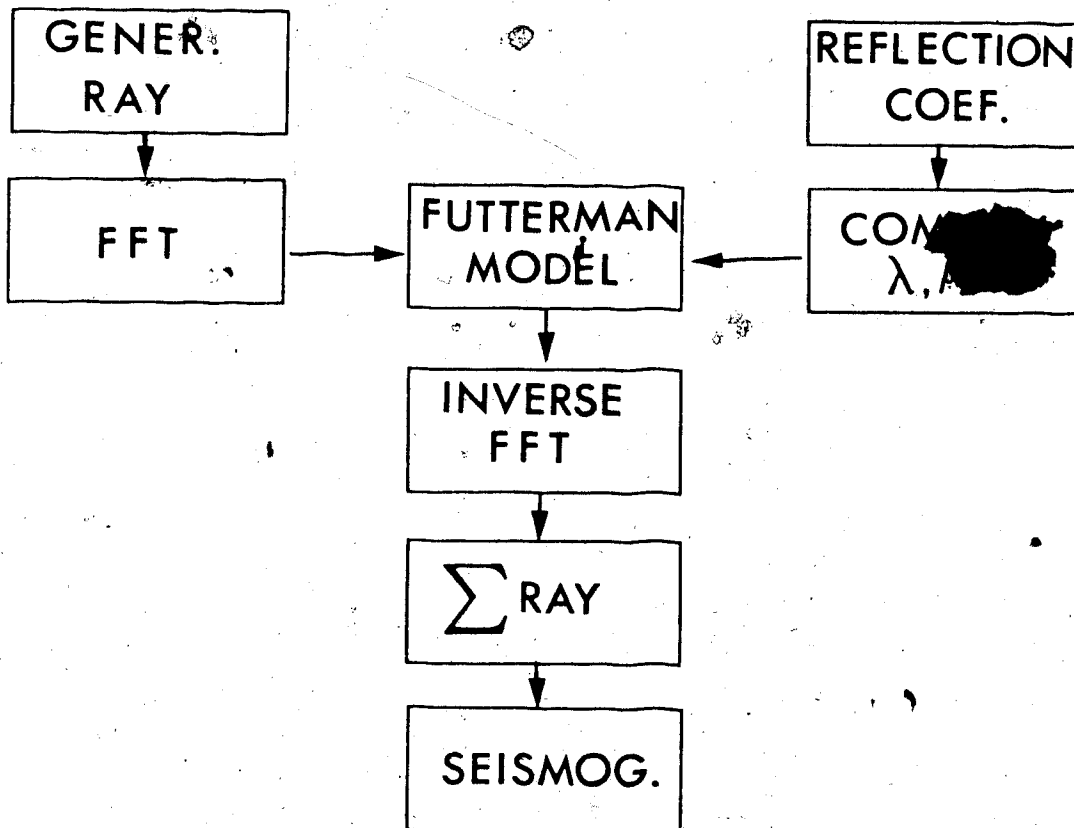
Figure 14.   Steps involved for the inclusion of attenuation

into one generalized ray.   The horizontal

distance between source and receiver is 30m.

The source is an SH-torque for the model of

figure 15.   (a) Partial seismogram for one

generalized ray ($\nu=1$) in the case of a layered

elastic medium.   (b) The amplitude spectrum for

(a) as obtained from a fast Fourier transform

algorithm.   (c) The phase spectrum for (a).

(d) The unwrapped hase for (c).   (e) Partial

seismogram with the effects of anelasticity.

(f) The amplitude spectrum for the attenuated

pulse.   (g) The velocity dispersion curve for

the first anelastic layer in figure 15.

(h) The unwrapped phase for the attenuated

pulse.

(a) (b) (c) (d) (e) (f) (g) (h)
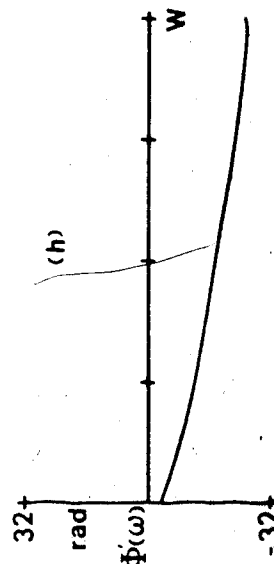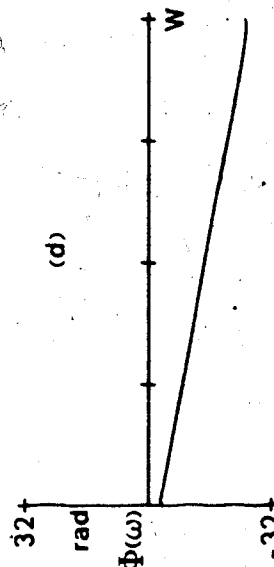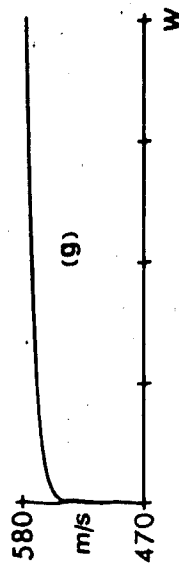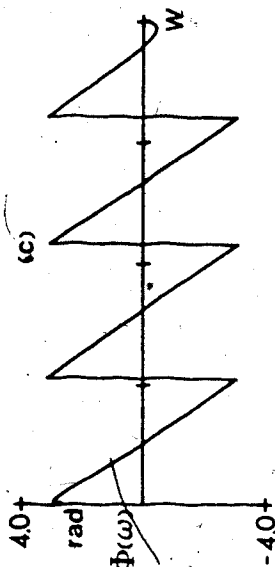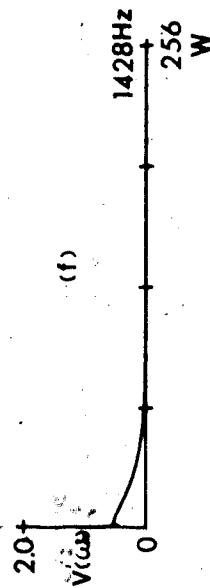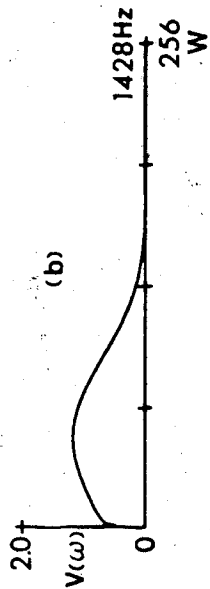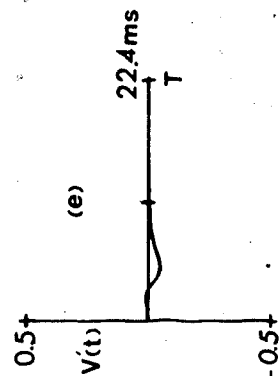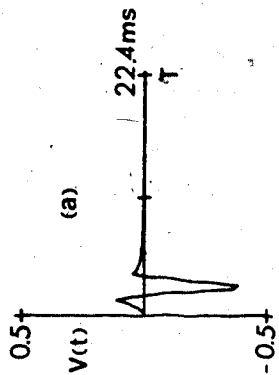
Figure 15. The anelastic weathered layer model. The

source is a stress impulse with a triangular

shape in time. The attenuation is indicated

by the quality factor Q.

SOURCE

2δ

MODEL

x

z,

0m

5

20
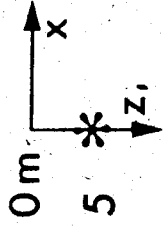
$\alpha_1 = 1000 \text{m/s}$ $\rho_1 = 2.09 \text{/cc}$

$\beta_1 = 577 \text{m/s}$ $Q_1 = 30$

$\alpha_2 = 2000 \text{m/s}$ $\rho_2 = 2.29 \text{/cc}$

$\beta_2 = 1160 \text{m/s}$ $Q_2 = 80$
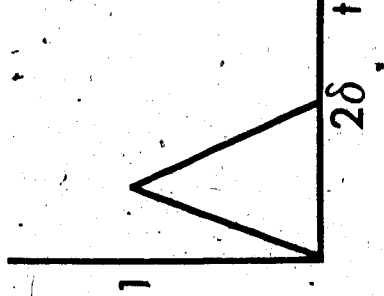
transform is taken of the original seismogram for one generalized ray. Its phase is unwrapped and then a phase term is added using the phase velocity $c(\omega)$ in equation (1.32). The modulus or amplitude function is multiplied by an exponential decay involving the absorption coefficient. The effective change due to the viscoelastic reflection coefficient is introduced similarly and the final pulse is obtained by an inverse fast Fourier transform.

3.5 The weathered layer model

A model which simulates the weathered layer is shown in Figure 15. It consists of a single homogeneous isotropic layer overlying a homogeneous isotropic half space. The compressional (α) and shear (β) velocities along with the densities (ρ) and the Q values are also indicated. Synthetic seismograms for the elastic and anelastic case are calculated for two different sources, an SH-torque and a vertical stress discontinuity.

Figure 16 shows the synthetic seismograms with and without anelasticity for the weathered layer model using a point SH torque as a source. The displacements are presented in a three-dimensional graph with one of the dimensions being reduced time. The seismograms are at intervals of 5m for a surface receiver at distances of 10 to 60 m. The direct wave S, the reflection SS with the corresponding head wave SS* ($=S_1S_2S_1$), and the multiple, sSS, are shown.

Figure 16. Synthetic seismograms for an SH-torque source

for the elastic and anelastic case for the

model of figure 15. The algorithm ASPEX is

used to produce a three dimensional plot for an

azimuth of 340°, an altitude of 18° from the

horizontal at the center of the graph to the

observer and a distance of 25m from the graph.

to the observer.

SH-TORQUE

ANELASTIC

S SS'   SS   sSS

60m

distance

10

ELASTIC

S SS'   SS   sSS

60m

distance

10

0

30   60ms

reduced time $(\beta_1 = 577\,m/s)$

.5
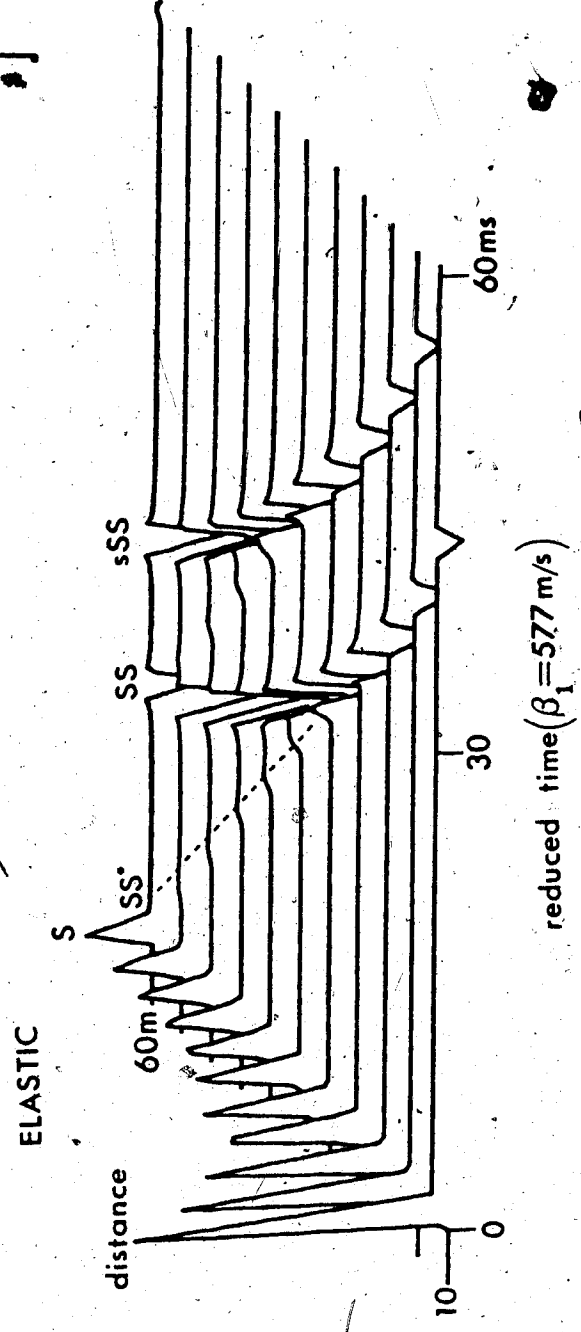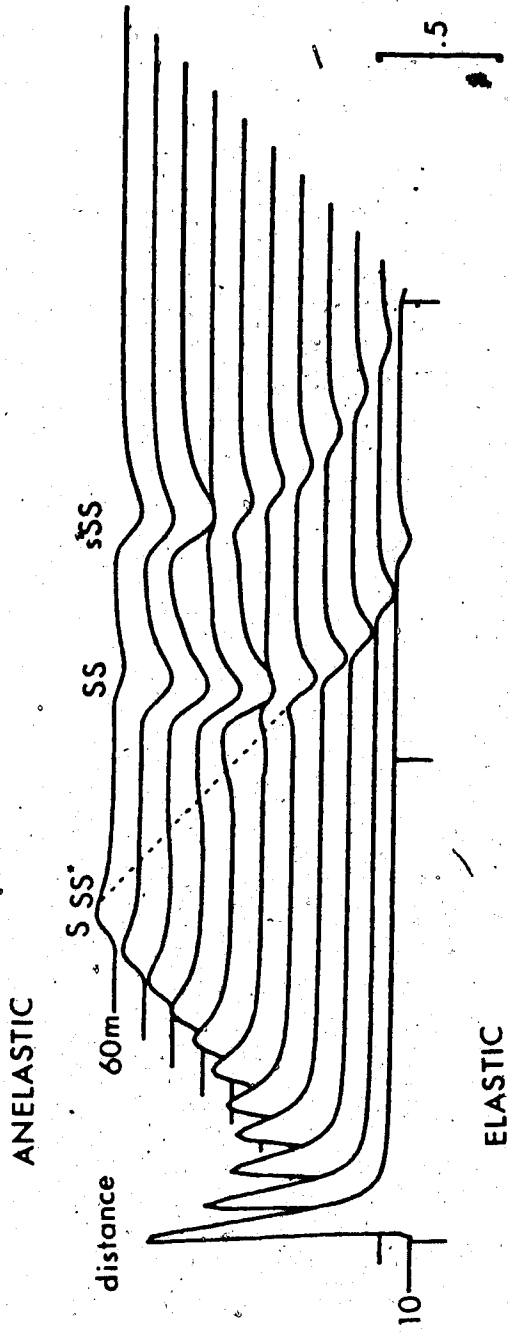
Notice the decrease in amplitude and the widening of the pulses in the anelastic version. The decrease in amplitude is due to the exponential decay while the increased pulse breadth is due to the loss of high frequencies and the effects of dispersion.

The P-SV case is illustrated in Figures 17, 18 and 19 in which a buried point vertical force is used as a source. Figure 17 shows the vertical and radial components of individual rays resulting from the decomposition of a seismogram from a vertical stress discontinuity. The horizontal distance between source and receiver is 20m. The rays of the first two families (F=1, F=2) are shown. Each family is completely defined by an integer F which indicates the number of interactions of the ray with the two boundaries. A Fourier transform of a tapered form of each generalized ray is obtained and the attenuated pulse is obtained following the procedures outlined in Figures 13 and 14. The complete synthetics for the vertical and radial component are shown in Figures 18 and 19 respectively. The seismograms for the elastic and anelastic cases are plotted from 10 to 30m at an interval of 4/3m. For short distances between the source and receiver the path of the head waves was taken to be the same as for the reflected waves. Similarly, the generalized ray which includes the direct wave and the Rayleigh wave was treated identically for the purpose of attenuation. Note the dominance of the

Figure 17. The vertical and radial components for the generalized rays making up the first two families (F=1, F=2). (P) and (S) indicate rays beginning from the source as compressional and shear waves respectively. The sums of the generalized rays making up each family are labelled by a Σ. Note the cancellation of the tails in the partial seismograms for each family.

F=1   F=2

VERTICAL

(P) $\mu = 0$ $\nu = 0$

(P) $\mu = 0$ $\nu = 1$

.4

.1

(S) $\mu = 0$ $\nu = 0$

(S) $\mu = 1$ $\nu = 0$

(S) $\mu = 0$ $\nu = 1$

Σ P sP· S

Σ PP SP SS· PS SS PS·

RADIAL

(P) $\mu = 1$ $\nu = 0$

(P) $\mu = 0$ $\nu = 0$

(P) $\mu = 0$ $\nu = 1$

(S) $\mu = 0$ $\nu = 0$

(S) $\mu = 1$ $\nu = 0$

(S) $\mu = 0$ $\nu = 1$

Σ P sP· S   ←20ms→

Σ PP SP SS· PS SS PS·
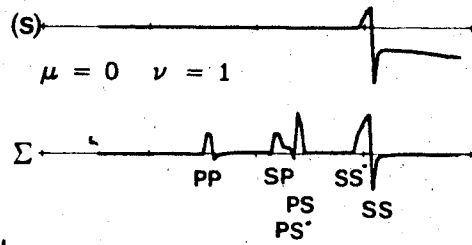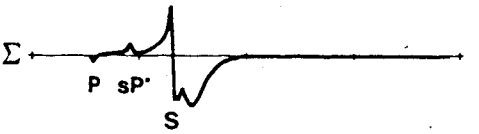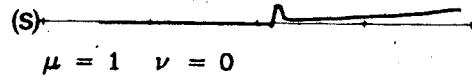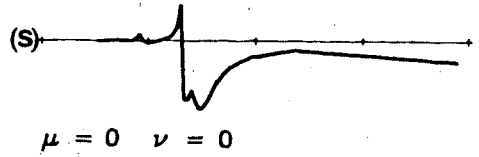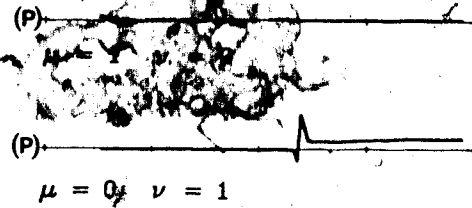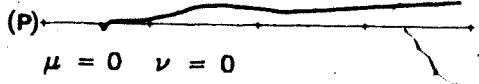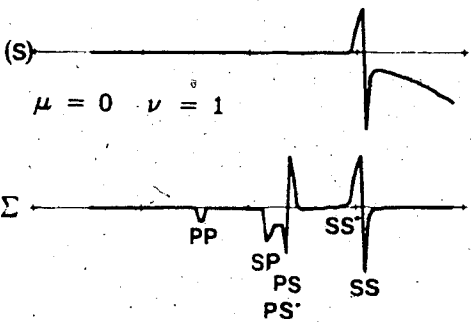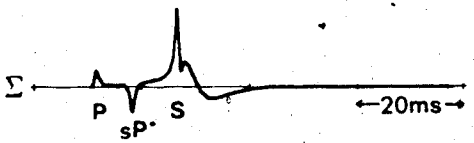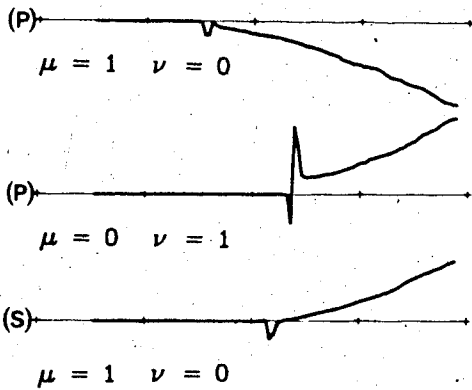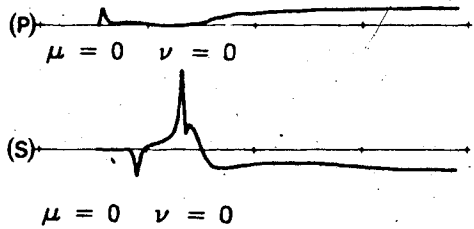
Figure 18. The vertical component for a vertical point

force for the elastic and anelastic case for

the weathered layer model of figure 15. ASPEX

uses the same parameters as figure 16.

VERTICAL   ANELASTIC

30m   P   sP·   S   R   PS

distance

20

10

.5

PP

ELASTIC

30m   P   sP·   S   R   PS   pPS   SS

distance

20

10
0

PP   40   60ms

reduced   time$(\alpha_1 = 1.0 Km/s)$
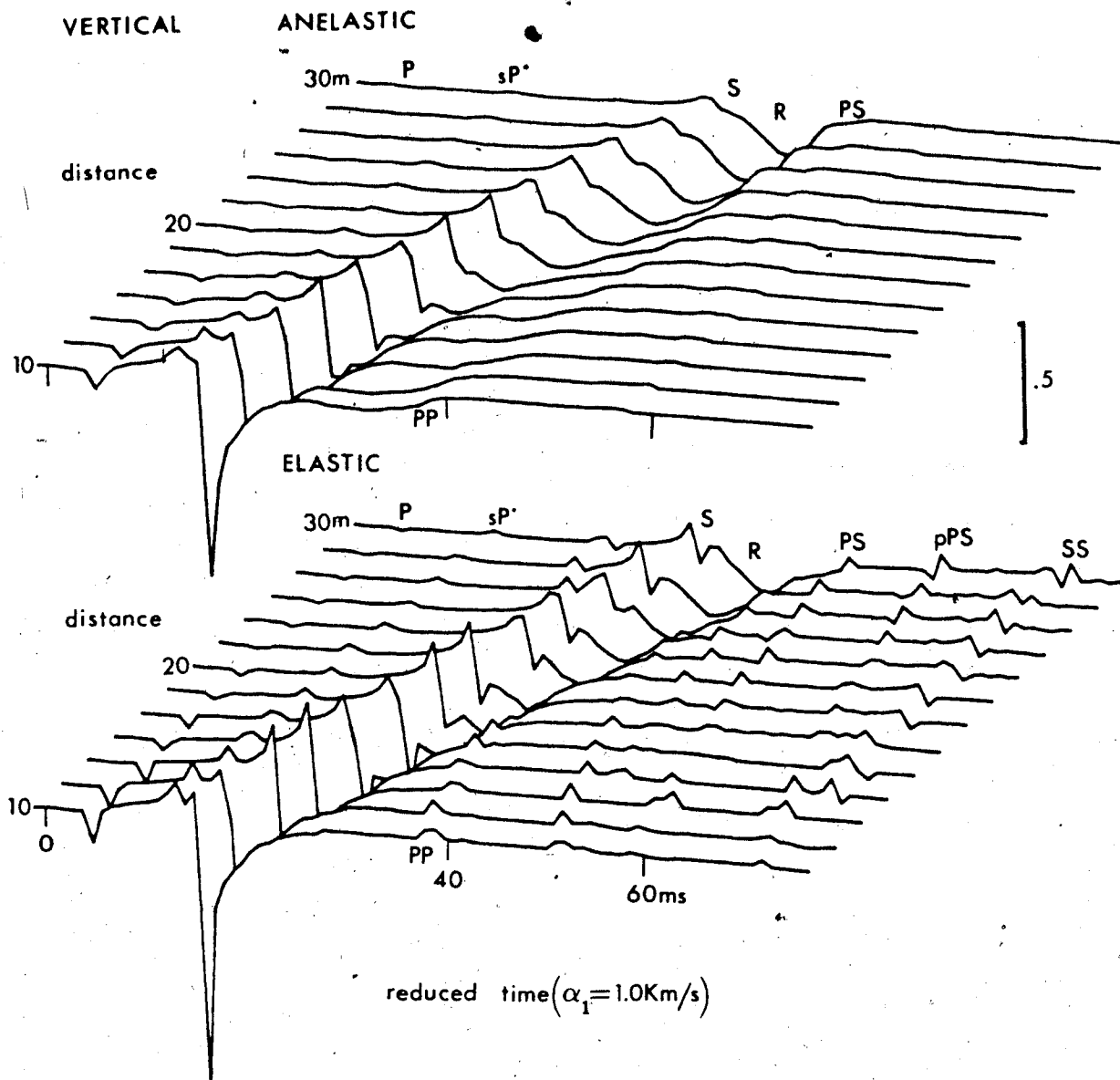
Figure 19. The radial component for a vertical point force

for the elastic and anelastic case for the

weathered layer model of figure 15. ASPEX uses

the same parameters as figure 16.

RADIAL   ANELASTIC
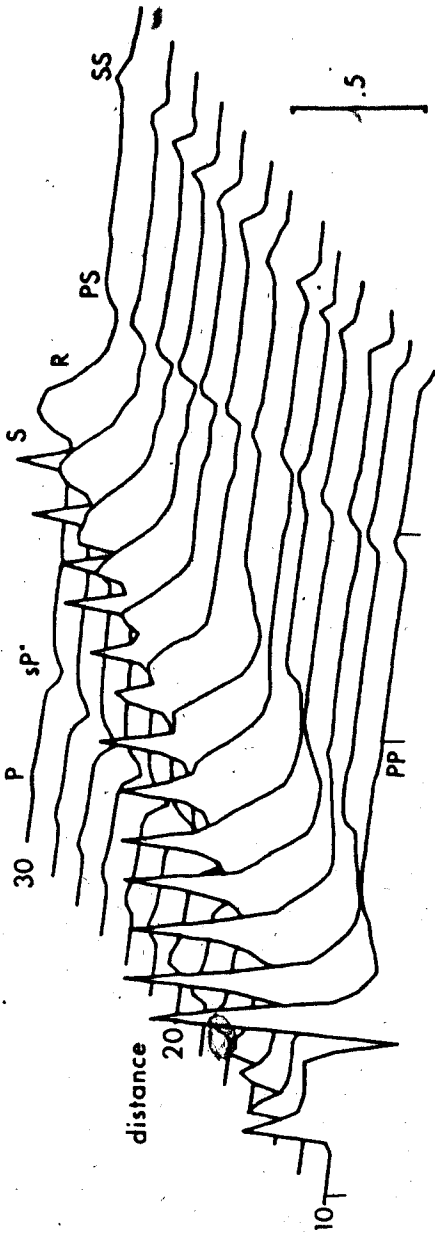
ELASTIC
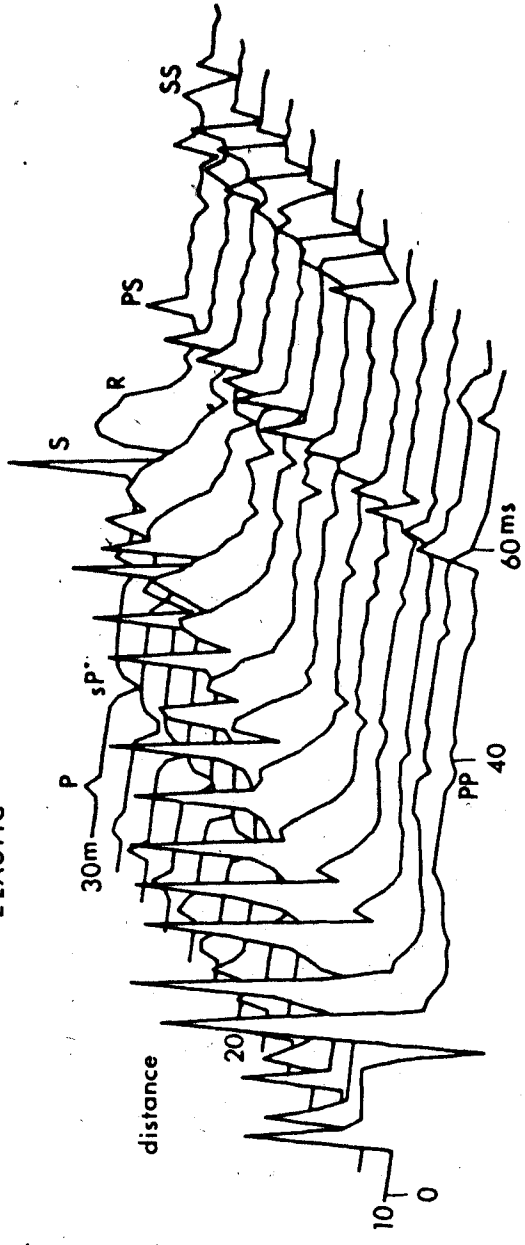
reduced time $(\alpha_1 = 1.0 \text{Km/s})$

Rayleigh wave as the high frequency components in the head
wave are strongly attenuated. The head waves and
reflections are strongly attenuated and show pulse widen-
ing due to the filtering of the high frequencies and the
effects of dispersion.

CHAPTER 4

4.1 The "Alberta" Model

Many sedimentary basins may be modelled, in a first approximation, as a thick, relatively uniform, low velocity layer overlying a thick high velocity section. A good example is the Alberta basin which extends into the Rocky Mountains on the west. In the foothills it consists of a 3 km section of alternating shales and sands of Mesozoic age with a mean velocity of 4200 m/s (13800 ft/s) overlying Paleozoic and Precambrian beds with a mean velocity of 6400 m/s (21000 ft/s). The high velocity in the Paleozoic rocks is due to a large proportion of limestone and dolomite while the Precambrian section, of similar velocity, consists of 2 billion year old gneisses, metasediments and igneous intrusives (Porter et al., 1982).

The mean velocity contrast between the two sections is so large that special techniques may be used in mapping the contrast as discussed by Blundun (1959) and Richards (1960). Nevertheless, the identification of the phases used in mapping has been difficult because of the interference of many types of wide angle reflections and head waves. The computation of exact synthetic seismograms is also very difficult and has only been accomplished recently with large digital computers. Our own approach to this problem involves generalized ray theory and a Cagniard-Pekeris inversion because the method yields the complete and exact

Figure 20. Model of a layer over a half space with a

vertical point force as source situated at a

depth of 100m. The model simulates an

"Alberta" sedimentary section. The source

function in time and the first part of the

travel time curve are shown on the right.

SOURCE

ALBERTA MODEL
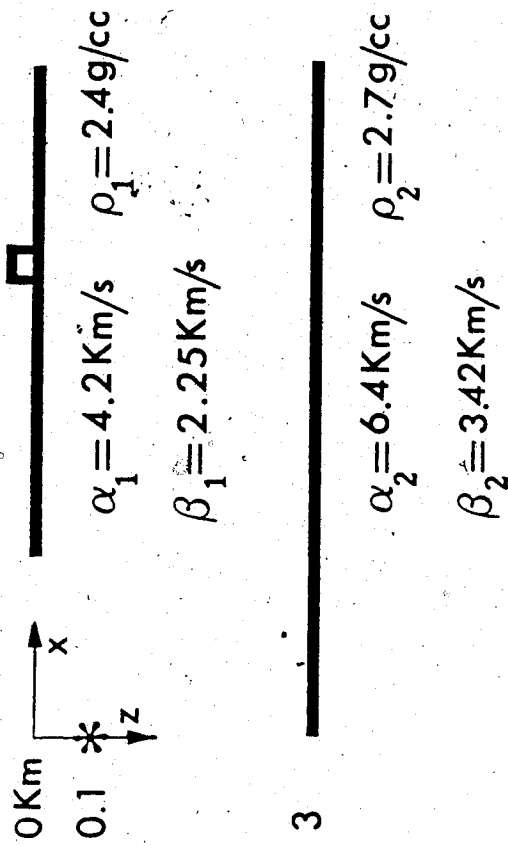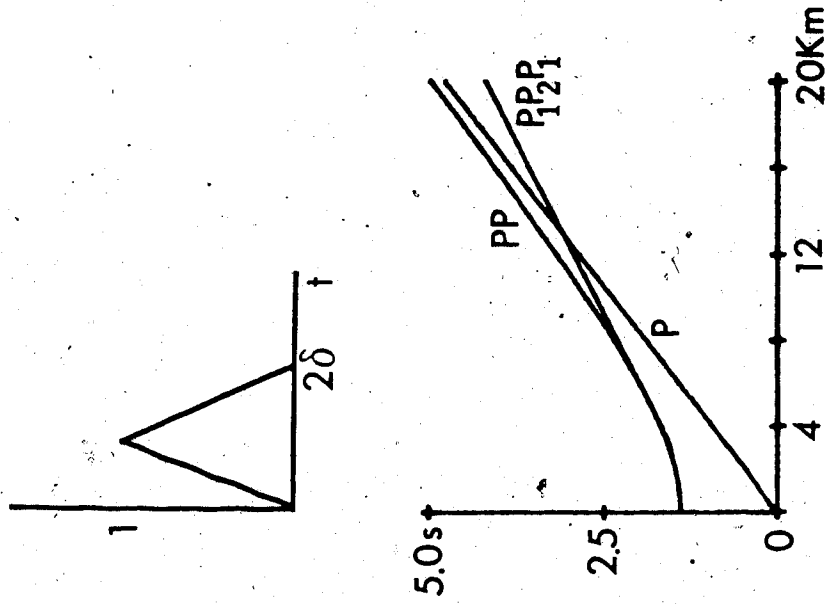
solution, and also allows one to decompose the results into
individual generalized rays for detailed analysis.

A concentrated vertical force at a particular depth
is used instead of a buried compressional pulse since a
vibratory device or a cylindrically shaped tube of explo-
sive chemical in a lightly tamped borehole produces a
dominantly vertical force. Mathematically it is simulated
by a jump in normal stress across a boundary at the source
level placed on the z axis. The model of a buried source
in a layer over a half space is a gross simplification of
the actual crustal section in the Alberta basin. A more
complex layered structure could be modelled but with
objectionable approximations in the algorithms or with
prohibitively expensive computer operation. Before
attempting these more elaborate models the complexity of
the results from these simpler examples will be explored.

4.2 Synthetic seismograms

The basic model used is given in Figure 20. Other
velocities will be illustrated after the results for this
case are shown. To obtain a perspective on the relative
amplitudes exact seismograms were computed for distances
of 4 to 8 km from the source (Figure 21). The Rayleigh
waves dominate the recording and the earlier portion of the
seismogram with the head and reflected waves is not seen
clearly. Since we are interested in this earlier section

Figure 21. Synthetic seismograms for the model shown in

figure 20. The vertical and radial components

are superimposed to show the phase relation for

distances of 4 to 8 km from the source.

reduced   time (α_1=4.2Km/s)
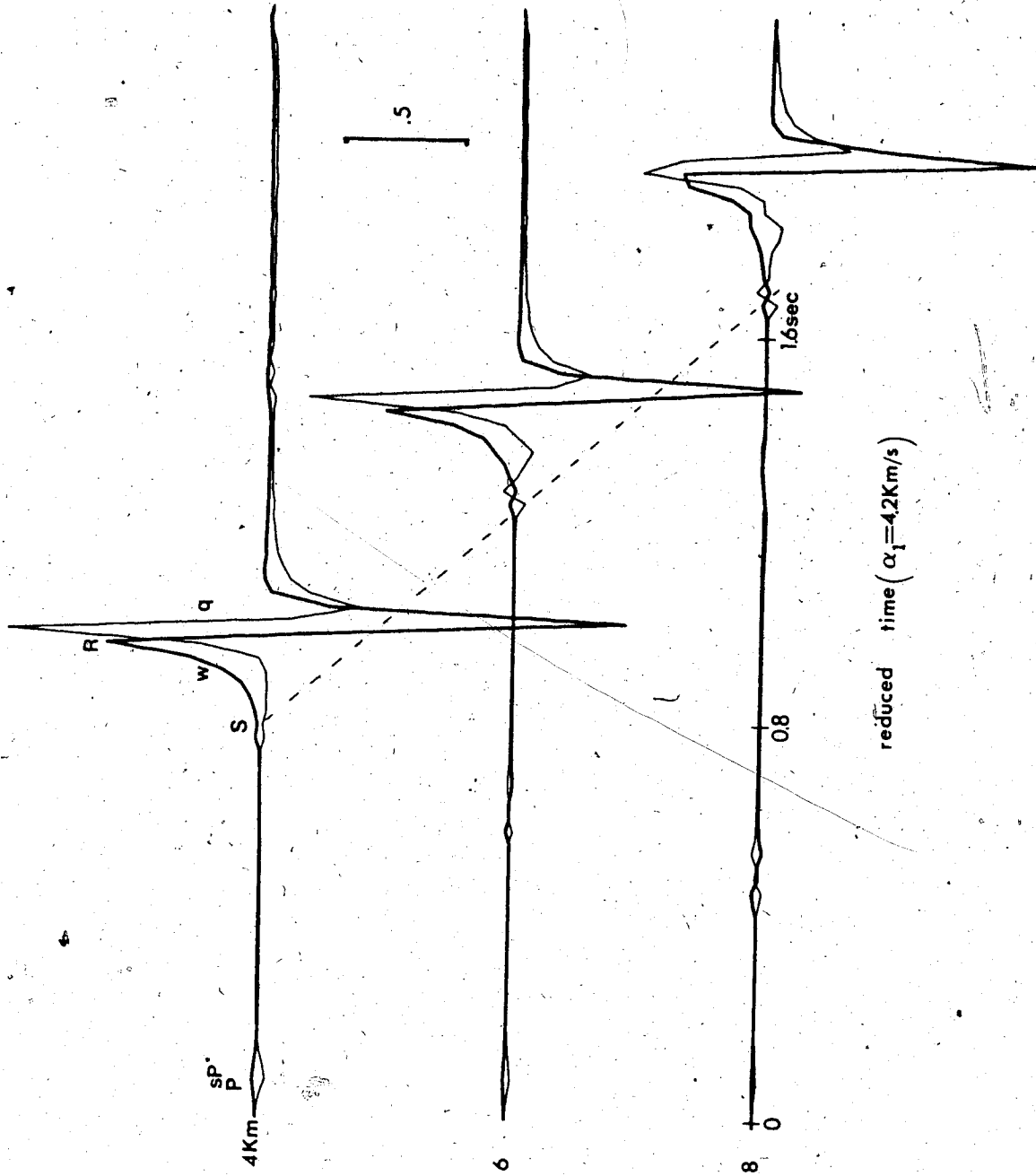
Figure 22. Synthetic seismograms for the model of figure

20. The head wave from the half space is a

first arrival beyond a distance of 13 km. The

algorithm ASPEX is used for the three dimen-

sional plot with an azimuth of 340°, an

altitude of 18° from the horizontal at the

center of the graph to the observer and a

distance of 25 km from the graph to the

observer.
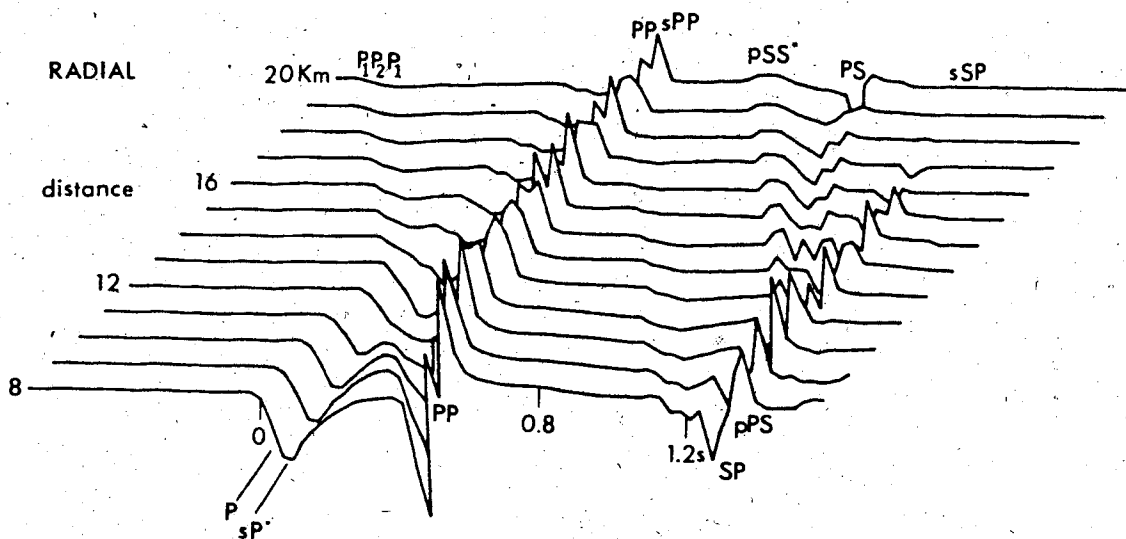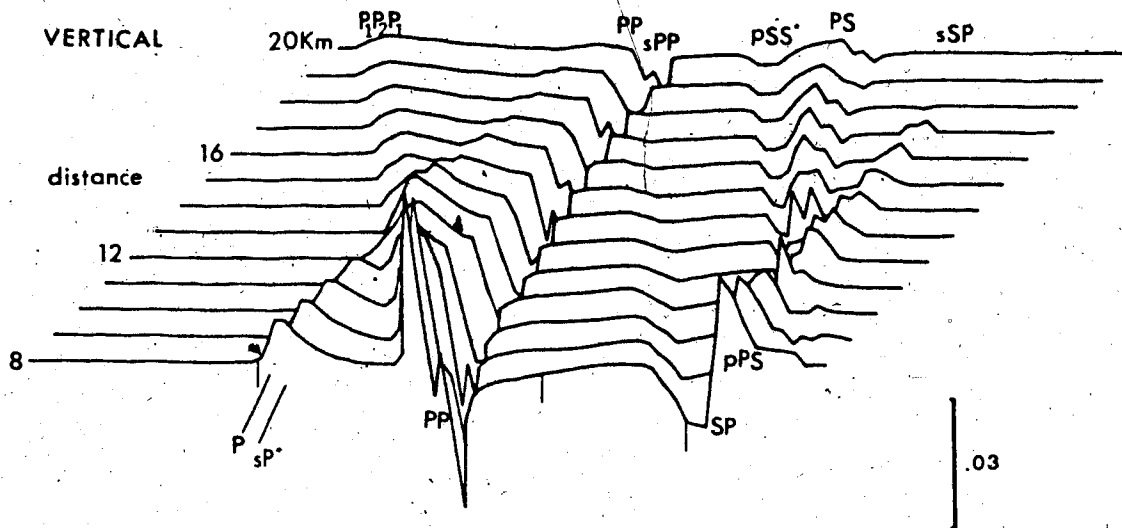
reduced   time$\left(\alpha_1 = 4.2\,Km/s\right)$

but at critical distances, we will restrict the display to the time before the surface waves arrive. Figure 22 shows the vertical and radial displacement for a vertical point force at distances of 8 to 20 km (5 to 12.4 miles). These may be compared to the field recordings of Richards (1960) in the foothills belt of Stolberg over a distance range of 5.3 to 18.8 km.

The major event on the seismograms in Figure 22 is the PP reflection from the half space. It is followed immediately by two generalized pPP and sPP, which also have strong amplitudes. These two rays reflect off the surface close to the source. Their ray paths may be seen in Figure 4 . Their visible effect depends upon the depth of the source and the roughness of the reflecting surface which could be modelled as a parameter. The theoretical relative strength of the interfering phases may be seen in Figure 23.

The synthetic seismograms in Figure 22 also show strong arrivals for the SP and PS phases (see the second family, $F=2$ in Figure 4). The SP ray occurs only at close distances because a critical angle is reached when the compressional wave is travelling horizontally. At distances of 18 km the PS reflected ray may be interpreted. Note that the pSS* head wave in Figure 22 may be well enough defined to be of value in structural modelling. These head waves belong to the second and third families with ray paths labelled $pS_1P_2S_1$ and $S_1P_2S_1$ in Figure 4.

Figure 23.   The main reflected, and head waves for the
             model in figure 20.   Three generalized rays
             are shown ($\mu=1$, $\nu=0$ (P): $\mu=2$, $\nu=0$ (P) : $\mu=2$,
             $\nu = 0$ (S)).

VERTICAL

$\mu=1\ \nu=0$

$\mu=2\ \nu=0$

$\mu=2\ \nu=0$

8Km

12

16

20

PPP
1 2 1

PP

pPPP
1 2 1

PPP

sPPP
1 2 1

sPP

RADIAL

].03

—0.5s—
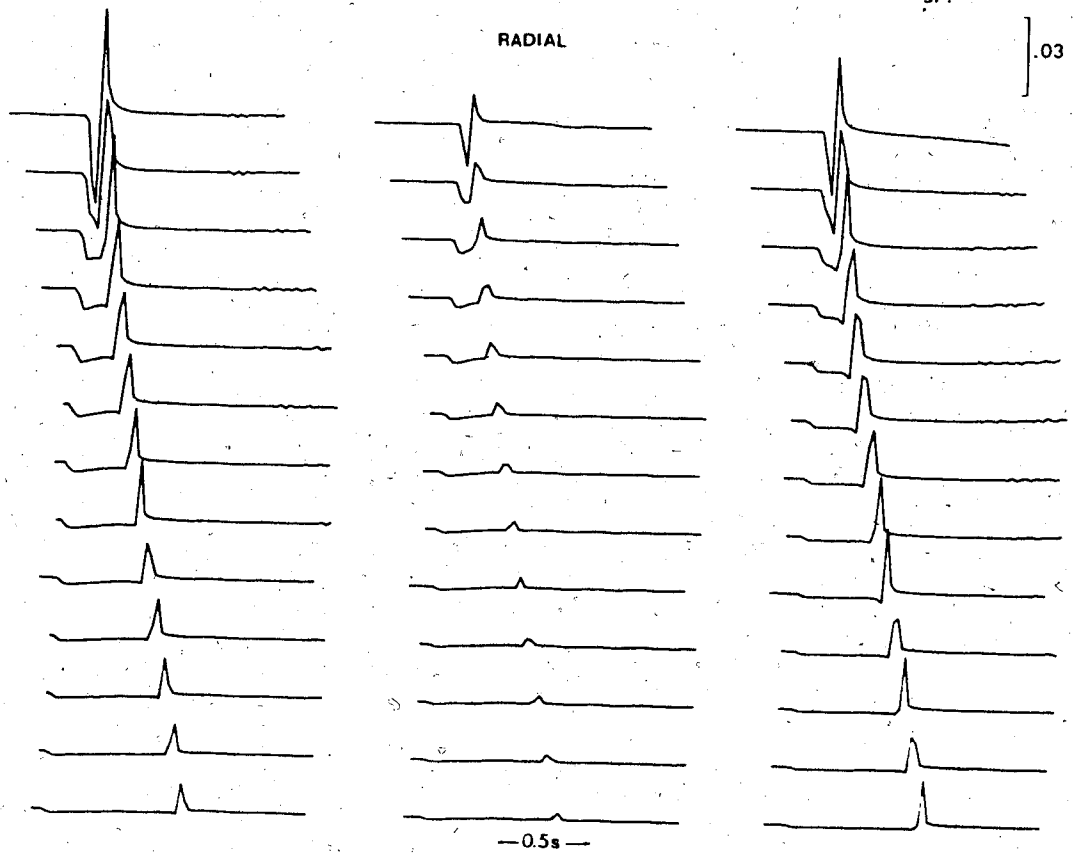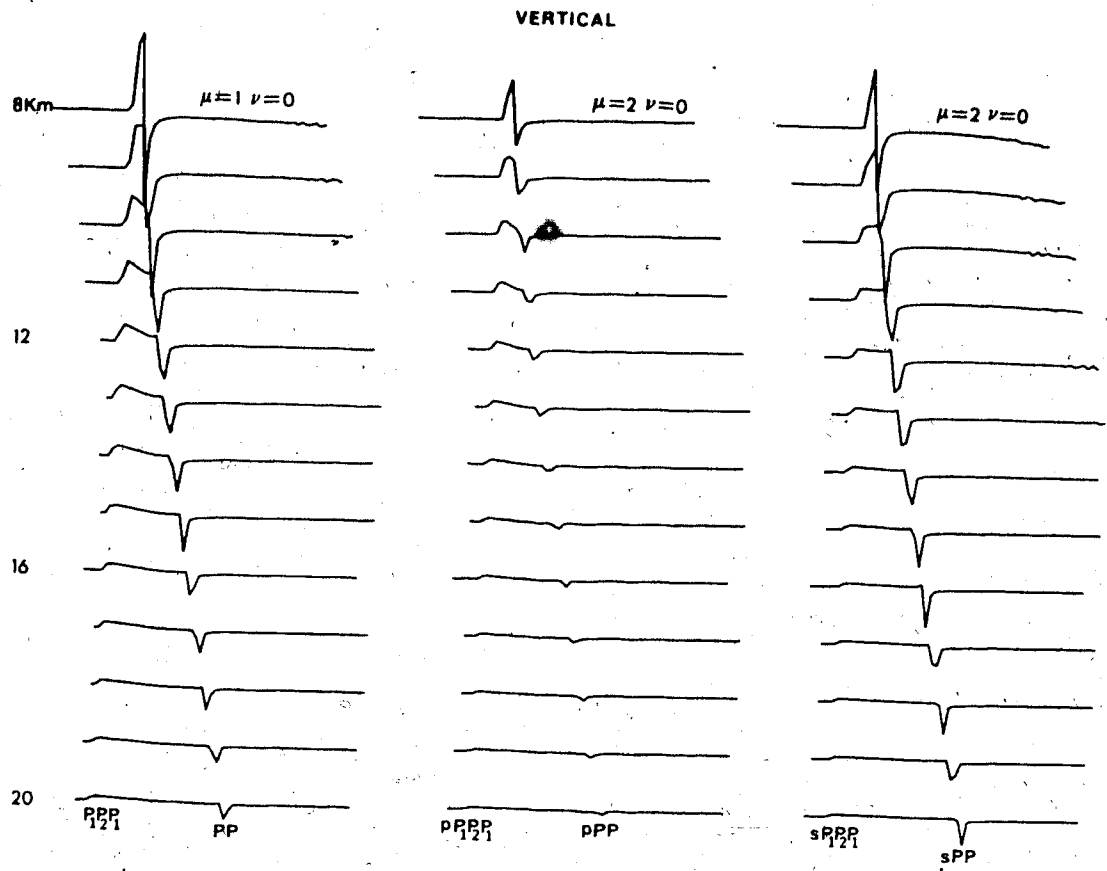
Figure 24. Synthetic seismograms for a vertical point force
and variations on the model shown in figure
20. The only parameters that are changed are
the P and S velocities in the half space. The
P velocities vary from 5600 to 6800 m/s and
the Poisson's ratio is 0.3.
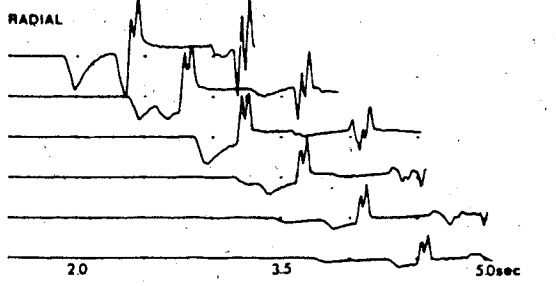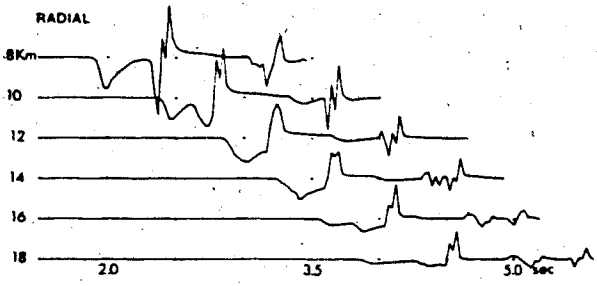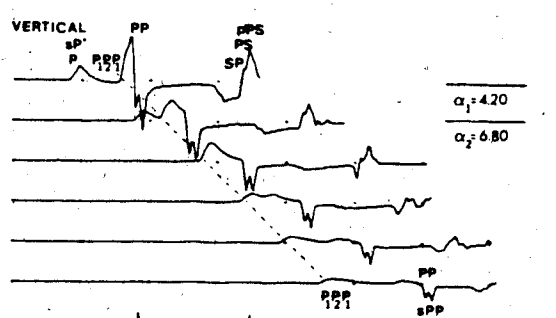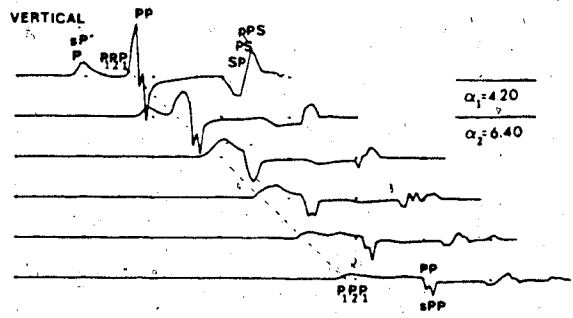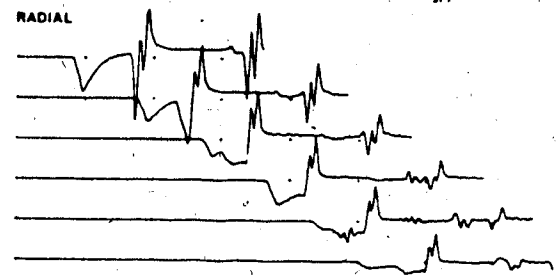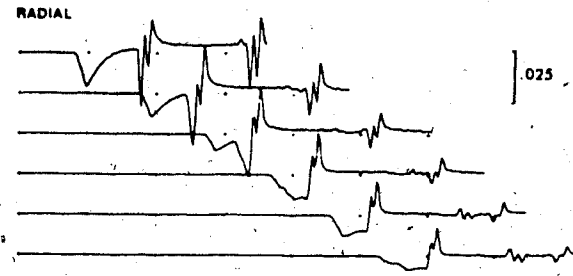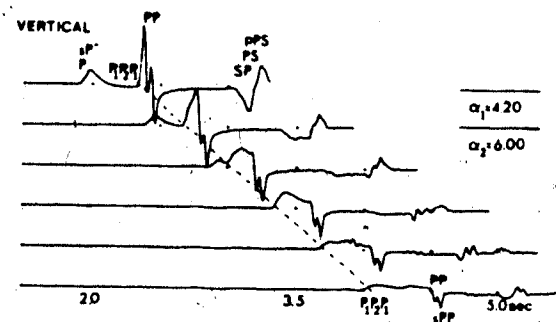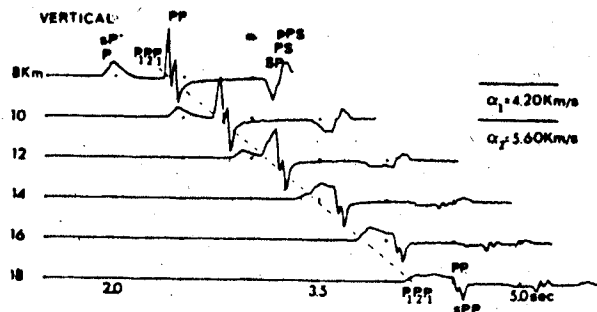
The effect of changes in the velocity of the Paleo-
zoic half space is shown in Figure 24. The interference
of the direct P wave, the $P_1P_2P_1$ head wave, and the PP
reflection makes it imperative that an exploration program
be carefully designed based on the thickness and velocities
encountered. Note that the radial component has well
defined impulsive phases and it would be advantageous to
record on horizontal motion seismometers when carrying out
seismic surveys for wide angle reflections. The results
from Figures 23 and 24 show that one should keep the source
at as uniform and shallow a depth as possible to avoid the
interference created by sPP and pPP rays with the primary
reflection, PP. A pattern of multiple sources would also
help in reducing the interference of converted and direct
shear waves.

CHAPTER 5

Conclusions

It is possible to obtain exact synthetic seismograms
for various kinds of impulsive forces using generalized
ray theory and an algorithm that performs an inverse
Laplace transform. Decomposition into generalized rays
allows one to analyse component phases and interpret the
results physically. In addition, the numerical stability
of the integration for each generalized ray may be monitored
independently. Synthesis of the generalized rays into
families is also of value in the study of groups of rays
and the influence of each additional interaction with an
interface.

The individual generalized rays are examined and
modified and the effects of attenuation and dispersion can
be incorporated in the frequency domain. Futterman's
theory is used to model the anelasticity along the ray path.
The effect of the viscoelastic interface is also taken into
account by calculating reflection coefficients for anelastic
media. Novel to this thesis is the incorporation of
attenuation along the path and at the viscoelastic interface
for the P-SV case. In addition, use of a Laplace transform
in the formulation of the problem insures that the final
synthetic seismograms have a causal source pulse.

In the near-field and at intermediate distances the
field seismograms may be difficult to interpret without the

use of model results. The weathered layer case is illus-

trated with a buried source in a layer over a half space.

A new surface head wave (sP*) which is not generated when

the source is compressive is a prominent second arrival,

particularly on the radial component. A wave travelling with

a compressional wave velocity is also visible on the trans-

verse (SH) component for an impulsive horizontal force in

an arbitrary direction. At near and intermediate distances

the direct compressional wave is much stronger on the radial

component while the direct shear wave is best seen on the

vertical seismometer.

The same algorithm may be used to study a thick

lower velocity layer over a high velocity section (Alberta

model), a solution seen in some sedimentary basins. The

complexity of head waves and reflected arrivals near the

critical distance makes it imperative that model studies

accompany the interpretation of data recorded at wide angles

of incidence.

Most of the synthetic seismograms are plotted in a

three-dimensional way using an algorithm called ASPEX.

Seismograms for different distances are plotted against

reduced time and the main arrivals can be easily identified.

We found that this particular presentation of seismic data

is very helpful and it may be of use in seismic studies.

We also found that the algorithm ASPEX gives a better

graphical representation than the well known algorithm

SURFACE II.

The models that we have studied are rather simple, in that they consist of a single layer over a half space. The obtained exact seismograms show the complexity of the results. More complex layered structures could be modelled but usually with objectionable approximations in the algorithm or with prohibitively expensive computer operations. Before attempting these more elaborate models this thesis examined and studied in detail the considerable complexity in the results from simple models.

REFERENCES

Abramovici, F. (1964). Propagation of a seismic pulse in
    a layered solid. Ph.D. thesis. Hebrew University,
    Israel.

Abramovici, F. (1970). Numerical seismograms for a layered
    elastic solid. Bull. Seism. Soc. Am., 60, 1861-1876.

Abramovici, F. (1978). A generalization of the Cagniard
    method. Journal of Comp. Phys., 29, 328-343.

Abramovici, F. and J. Gal-Ezer (1978). Numerical seismo-
    grams for a vertical point force in a single layer
    over a half space. Bull. Seism. Soc. Am., 68, 81-101.

Abramovici, F., E.R. Kanasewich and P.G. Kelamis (1982).
    Seismic waves from a horizontal stress discontinuity
    in a layered solid. Bull. Seism. Soc. Am., 72, 1483-1498.

Aki, K. and P.G. Richards (1980). Quantitative Seismology -
    Theory and Methods. Vols. 1 and 2. W.H. Freeman Co.,
    San Francisco.

Armstrong, B.H. (1980). Frequency independent background
    internal friction in heterogeneous solids.
    Geophysics, 45, 1042-1054.

Atwell, P.B. and Y.V. Ramana (1966). Wave attenuation and
    internal friction of frequency in rocks. Geophysics,
    31, 1049-1056.

Azimi, S.A., A.V. Kalinin, V.V. Kalinin, and B.L. Pivovarov.
    (1968). Impulse and transient characteristics of
    media with linear and quadratic absorption laws.
    Izvestia (Earth Physics), 42-54. (Translation pages 88-93).

Ben-Menahem, A. and S.J. Singh (1968). Multipolar elastic
    fields in a layered half-space. Bull. Seism. Soc.
    Am., 58, 1519-1572.

Ben-Menahem, A. and S.J. Singh (1981). Seismic waves and
    sources. Springer-Verlag Inc., New York.

Biot, M.A. (1956). Theory of propagation of elastic waves
    in a fluid saturated porous solid (parts 1 and 2).
    Jour. Acoust. Soc. Am., 28, 168-191.

Biot, M.A. (1962a). Mechanics of deformation and acoustic
    propagation in porous media. Jour. Appl. Phys. 33,
    1482-1498.

Biot, M.A. (1962b). Generalized theory of acoustic propagation in porous dissipative media. Jour. Acoust. Soc. Am. 34, 1254-1264.

Birch, F. and D. Bancroft. (1938). Elasticity and internal friction in a long column of granite. Bull. Seism. Soc. Am., 28, 243-254.

Blundun, G.J. (1959). The Mississippian in the Alberta plains and the reflection seismograph. Geophysics 24, 426-442.

Borcherdt, R.D. (1973). Energy and plane waves in linear viscoelastic media. Jour. of Geophys. Res., 78, 2442-2453.

Borcherdt, R.D. (1977). Reflection and transmission of type II S waves in elastic and anelastic media. Bull. Seism. Soc. Am., 67, 43-67.

Born, W.T. (1941). The attenuation constant of Earth materials. Geophysics 6, 132-148.

Bradley, J.J. and A. Fort. (1966). Internal friction in rocks. Section 8 in Handbook of Physical Constants edited by Syndey P. Clark Jr., Mem. 97 of Geol. Soc. Am.

Bruckshaw, J. and P.C. Mananta. (1954). The variation of the elastic constants of rocks with frequency. Petroleum, 17, 14-18.

Buchen, P.W. (1971). Plane waves in linear viscoelastic media. Geophys. Jour., 23, 531-542.

Cagniard, L. (1939). Reflexion et Refraction des Ondes Seismiques Progressives. Gauthier-Villars, Paris, France.

Carpenter, E.W. (1966). Absorption of elastic waves - An operator for a constant Q mechanism. UK Atom. Energy Auth. AWRE. 43, 66.

Cisternas, A., O. Betancourt and A. Leiva (1973). Body waves in a "real earth". Part I. Bull. Seism. Soc. Am., 63, 145-156.

Cole, B.F. (1965). Marine sediment attenuation and ocean bottom reflected sound. Jour. Acoust. Soc. Am., 37, 291-297.

De Hoop, A.T. (1960). A modification of Cagniard's method for solving seismic pulse problems. Appl. Sci. Res., 8, 349-356.

Futterman, W.I. (1962). Dispersive body waves. Jour. of Geophys. Res., 67, 5279-5291.

Ganley, D.C. (1980). The seismic measurement of absorption and dispersion. Ph.D. thesis. The University of Alberta, Edmonton, Alberta.

Ganley, D.C. and E.R. Kanasewich (1980). Measurements of absorption and dispersion from check shot surveys. Jour. of Geophys. Res., 85, 5219-5226.

Hamilton, E.L. (1972). Compressional wave attenuation in marine sediments. Geophysics 37, 620-646.

Hauge, P.S. (1981). Measurements of attenuation from vertical seismic profiles. Geophysics, 46, 1548-1558.

Johnston, D.H., N.M. Toksoz, and A. Timur. (1979). Attenuation of seismic waves in dry and saturated rocks: Part II, Mechanisms. Geophysics, 44, 691-711.

Kanasewich, E.R. (1981). Time sequence analysis in Geophysics (3rd Edition). The University of Alberta Press. Edmonton, Alberta.

Kanasewich, E.R., P.G. Kelamis and F. Abramovici. (1982). Exact seismograms for a point force using generalized ray theory. Geophysics (submitted).

Kjartansson, E. (1979). Constant Q-wave propagation and attenuation. Jour. of Geophys. Res., 84, 4737-4748.

Knopoff, L. (1964). Q. Rev. of Geophysics, 2, 625-660.

Kolsky, H. (1953). Stress waves in solids. Oxford, Clarendon Press.

Kolsky, H. (1956). The propagation of stress pulses in viscoelastic solids. Philosophical Magazine, 1, 693-710.

Krebes, E.S. (1980). Seismic body waves in anelastic media. Ph.D. thesis. The University of Alberta, Edmonton, Alberta.

Krebes, E.S. and F. Hron. (1980a). Ray-synthetic seismograms for SH-waves in anelastic media. Bull. Seism. Soc. Am., 70, 29-46.

Krebes, E.S. and F. Hron. (1980b). Synthetic seismograms

for SH-waves in a layered anelastic medium by asymptotic ray theory. Bull. Seism. Soc. Am., 70, 2005-2020.

Lamb, H. (1904). On the propagation of tremors over the surface of an elastic solid. Philosophical Transactions, Roy. Soc. (London) A, 203, 1-42.

Liu, H.P., D.L. Anderson, and H. Kanamori. (1976). Velocity dispersion due to anelasticity; implications for seismology and mantle composition. Geophys. Jour. 47, 41-58.

Lockett, F.J. (1962). The reflection and refraction of waves at an interface between viscoelastic materials. Jour. Mech. Phys. Solids, 10, 53-64.

Lomnitz, C. (1957). Linear dissipation in solids. Jour. of Appl. Phys., 28, 201-205.

Longman, I.M. (1961). Solution of an integral equation occurring in the study of certain wave-propagation problems in layered media. Jour. Acoust. Soc. Am., 33, 954-958.

Maruyama, T. (1963). On the force equivalents of dynamic elastic dislocations with reference to the earthquake mechanism. Bull. Earthquake Res. Inst. Tokyo Univ., 41, 467-486.

Mavko, G.M. (1979). Frictional attenuation: An inherent amplitude dependence. Jour. of Geophys. Res., 84, 4769-4776.

Mavko, G.M. and A. Nur. (1975). Melt squirt in the aesthenosphere. Jour. of Geophys. Res., 80, 1444-1448.

McDonald, F.J., F.A. Angona, R.L. Mills, R.L. Sengbush, R.A. van Nostrand, and J.E. White. (1958). Attenuation of shear and compressional waves in Pierre shale. Geophysics, 23, 421-439.

McLeroy, E.G. and A. DeLoach. (1967). Sound speed and attenuation from 15 to 1500 KHz measured in natural sea-floor sediments. Jour. Acoust. Soc. Am., 44, 1148-1150.

O'Connell, R.J. and B. Budiansky. (1978). Measures of dissipation in viscoelastic media. Geophys. Res. Lett., 5, 5-8.

Pekeris, C.L. (1940). A pathological case in the numerical solution of integral equations. Proc. Nat. Acad. Sci. U.S.A., 26, 433-437.

Pekeris, C.L. (1948). Theory of propagation of explosive sound in shallow water. Geol. Soc. Am. Mem., 27.

Pekeris, C.L., Z. Alterman, and F. Abramovici. (1963). Propagation of an SH-torque pulse in a layered solid. Bull. Seism. Soc. Am., 53, 39-59.

Pekeris, C.L., F. Abramovici, and H. Jarosch. (1965). Propagation of a compressional pulse in a layered solid. Rev. of Geophysics 3, 25-47.

Petrashin, G.E. (1959). Elements of the dynamic theory of the propagation of seismic waves: Part 1 in Collection III, edited by G. Petrashin, Leningrad University, 11-106.

Peselnick, L. and I. Zietz. (1959). Internal friction of fine-grained limestones at ultrasonic frequencies. Geophysics, 24, 285-296.

Pinkerton, J.M.M. (1947). A pulse method for the measurement of ultrasonic absorption in liquids, results for water. Nature, 160, 128-129.

Porter, J.W., R.A. Price and R.G. McCrossan (1982). The Western Canada Sedimentary Basin. Phil. Trans. Roy. Soc. London A 305, 169-192.

Richards, T.C. (1960). Wide angle reflections and their applications to finding limestone structure in the foothills of Western Canada. Geophysics, 25, 385-407.

Richards, T.C. (1961). Motion of the ground on arrival of reflected longitudinal and transverse waves at wide-angle reflection distances. Geophysics, 26, 277-297.

Ricker, N. (1953). The form and laws of propagation of seismic wavelets. Geophysics, 18, 10-40.

Savage, J.C. (1966). Thermoelastic attenuation of elastic waves by cracks. Jour. of Geophys. Res., 71, 3929-3938.

Savage, J.C. and M.E. O'Neill. (1975). The relation between the Lomnitz and Futterman theories of internal friction. Jour. of Geophys., 80, 249-251.

Schreiber, E., O.L. Anderson, and N. Soga. (1973). Elastic constants and their measurements. New York, McGraw-Hill Book Co., Inc.

Schoenberg, M. (1971). Transmission,reflection of plane waves at an elastic-viscoelastic interface. Geophys. Jour. 25, 35-47.

Singh, S.J., A. Ben-Menahem and M. Vered (1973). A unified approach to the representation of seismic sources. Proc. Roy. Soc. London A. 331, 525-551.

Spencer, T.W. (1960). The method of generalized reflection and transmission coefficients. Geophysics, 25, 625-641.

Spencer, T.W., J.R. Sonnad and T.M. Butler (1982). Seismic Q-Stratigraphy or dissipation. Geophysics, 47. 16-24.

Stokes, G.G. (1845). Trans. Cambridge Phil. Soc., 8, 287-319 (Part III).

Stratton, J.A. (1941). Electromagnetic Theory. McGraw-Hill, New York.

Strick, E. (1967). The determination of Q, dynamic viscosity, and transient creep curves from wave propagation measurements. Geophys. Jour., 13, 197-218.

Strick, E. (1970). A predicted pedestal effect for pulse propagation in constant-Q solids. Geophysics, 35, 387-403.

Tittmann, B.R., V.A. Clark, J. Richardson, and T.W. Spencer. (1980). Possible mechanism for seismic attenuation in rocks containing small amounts of volatiles. Jour. of Geophys. Res., 85, 5199-5208.

Toksoz, M.N., D.H. Johnston, and A. Timur. (1979). Attenuation of seismic waves in dry and saturated rocks: Part I. Laboratory measurements. Geophysics, 44, 681-690.

Tullos, F.N. and A.C. Reid. (1969). Seismic attenuation of gulf-coast sediments. Geophysics, 34, 516-528.

Van der Pol, B. and H. Bremmer. (1937). The diffraction of electromagnetic waves from an electrical point source round a finitely conducting sphere, with

applications to radio telegraphy and the theory of the rainbow. Part II. Philosophical Magazine, S. 7, 24, Suppl. 825-864.

Walsh, J.B. (1966). Seismic wave attenuation in rocks due to friction. Jour. of Geophys. Res. 71, 2591-2599.

White, J.E. (1965). Seismic waves. New York McGraw-Hill Book Co. Inc.

Winkler, K., A. Nur and M. Glandwin. (1979). Friction and seismic attenuation in rocks. Nature, 277, 528-531.

Wuenschel, P.C. (1965). Dispersive body waves – An experimental study. Geophysics, 30, 539-551.

Wylie, M.F.J., G.H.F. Gardner, and A.R. Gregory (1962). Studies of elastic wave attenuation in porous media. Geophysics, 27, 569-589.

Zener, C.M. (1948). Elasticity and Anelasticity of Metals. The University of Chicago Press.

APPENDIX A

A1. Introduction

The displacement components for a concentrated horizontal force in an elastic homogeneous layer on top of an elastic half space are given analytically in terms of generalized rays. Before going into the mathematical details let us give an overall picture of how the solution is obtained by reviewing briefly the various stages involved.

The starting point is the representation of the solution for a stress discontinuity along a given finite surface Σ in a homogenous elastic solid in a convenient way. The solution in the frequency domain was given by Maruyama (1963) for a discontinuity in both stress and displacement, in terms of solutions of the wave equation that are spherically symmetric with respect to points on Σ. Thus, the displacement components are written as finite combinations of integrals of such functions over Σ. When the medium has horizontal boundaries, the spherical symmetry is replaced by cylindrical symmetry with respect to the vertical through points of Σ and the boundary conditions are satisfied accordingly after rewriting the solution. This task was accomplished by Ben-Menahem and Singh (1968) and Singh, Ben-Menahem and Vered (1973) using the so-called Hansen solution (Stratton, 1941). We followed closely the treatment used by Ben-Menahem and Singh in their 1969 paper and

122

split the corresponding non-homogeneous system of equations of motion into one involving P-SV waves and another one representing SH-waves only. These solutions were expanded in series of generalized rays, each ray being inverted in the time domain by a generalization of the Cagniard-Pekeris method (Abramovici, 1978).

A2. The formal solution

Consider an elastic solid consisting of a homogeneous layer of depth H over a homogeneous half-space (Fig. 1) and assume that inside the layer there is a time-dependent stress discontinuity of components

$$\Delta \tau_{\kappa \ell} = f_{\kappa \ell}(t) \qquad \qquad \text{(A.1)}$$

along a finite open surface Σ.

Our problem is to find the displacement vector $\underset{\sim}{u} = \underset{\sim}{u}(t)$, i.e. the solution of the momentum equations

$$\mu \nabla^2 \underset{\sim}{u} + (\lambda+\mu) \underset{\sim}{\nabla} (\underset{\sim}{\nabla} \cdot \underset{\sim}{u}) = \rho \frac{\partial^2 \underset{\sim}{u}}{\partial t^2} \qquad \qquad \text{(A.2)}$$

where λ, μ are the Lamé parameters and ρ is the density satisfying

1. zero initial conditions,

$$\underset{\sim}{u} = 0 \text{ and } \frac{\partial \underset{\sim}{u}}{\partial t} = 0 \text{ for } t = 0 \qquad \qquad \text{(A.3)}$$

2. vanishing of stress on the upper surface,

$$\underset{\approx}{T} = 0 \text{ for } z = 0 \tag{A.4}$$

3. continuity of displacement and stress at interface, of layers 1 and 2

$$\underset{\sim}{u}_1 = \underset{\sim}{u}_2 \text{ and } \underset{\approx}{T}_1 = \underset{\approx}{T}_2 \text{ for } z = H \tag{A.5}$$

4. the radiation condition

$$\underset{\sim}{u} \to 0 \text{ for } z \to \infty \tag{A.6}$$

5. the source condition: when approaching Σ the displacement $\underset{\sim}{u}$ tends to $\underset{\sim}{s}$, the displacement corresponding to the given stress discontinuity in a homogeneous medium with the same density and Lamé parameters as the layer.

The Laplace transform of the displacement

$$\underset{\sim}{\bar{u}} = \underset{\sim}{\bar{u}}(p) = \int_0^\infty \underset{\sim}{u}(t) e^{-pt} dt \tag{A.7}$$

is found as a superposition between the transform of the solution corresponding to the source $\underset{\sim}{\bar{s}}(p)$ and the transform $\underset{\sim}{\bar{U}}(p)$ of the solution of (A.2) chosen so that

$$\bar{\underset{\sim}{u}} = \bar{\underset{\sim}{U}} + \bar{\underset{\sim}{s}} \qquad (A.8)$$

satisfies the transform of conditions (A.4)-(A.6). The initial conditions are taken care of when finding $\bar{\underset{\sim}{U}}$ as a solution of

$$(\mu\nabla^2 - \rho p^2)\bar{\underset{\sim}{U}} + (\lambda+\mu)\underset{\sim}{\nabla}(\underset{\sim}{\nabla}\cdot\bar{\underset{\sim}{U}}) = \underset{\sim}{0} \qquad (A.9)$$

and the source condition is met due to the superposition (A.8).

A2a. The source solution in cartesian coordinates

According to Maruyama (1963), the transform of the displacement components for a stress discontinuity along Σ in a homogeneous medium are

$$\bar{s}_j = - \iint\limits_{\Sigma} \frac{\bar{f}_{k\ell}}{4\pi} \bar{s}_{jk} \, \nu_\ell \qquad (A.10)$$

where $\bar{f}_{k\ell}$ are the transforms of the jumps in the stress components, ν_ℓ are the components of the unit normal to Σ at the running point (ξ_1, ξ_2, ξ_3) and the definition of $\bar{s}_{jk}$ is

$$\bar{s}_{jk} = h/(\lambda+2\mu)\left[\frac{-\delta_{jk}}{3} h_0^{(2)}(-ihR) + \left(\frac{-\delta_{jk}}{3} + \frac{R_j R_k}{R^2}\right)h_2^{(2)}(-ihR)\right]$$

$$+ (k/\mu)\left[-\frac{2}{3}\delta_{jk}h_0^{(2)}(-ikR) + \left(\frac{\delta_{jk}}{3} - \frac{R_j R_k}{R^2}\right)h_2^{(2)}(-ikR)\right]$$

$$(A.11)$$

Here $h_0^{(2)}$, $h_2^{(2)}$ are spherical Hankel functions of the second kind, δ_{mk} is the Kronecker symbol, and

$$k = p/\beta, \quad h = p/\alpha; \quad R_j = \zeta_j - x_j, \quad R = (R_j R_j)^{\frac{1}{2}} \qquad (A.12)$$

α, β being the P and S velocities respectively, x_j being the coordinates of the receiver and the summation being used whenever two indices in the same term coincide. Maruyama gave the Fourier transform of the displacement components so that in order to obtain the Laplace transform we change $i\omega$ into p.

A2b. Free solutions of the momentum equations.

In order to be able to satisfy the boundary conditions, one must look for vector solutions of (A.9) that are separated in cylindrical coordinates. Guided by Hansen's solutions for the Maxwell equations (Stratton 1941), Ben Menahem and Singh (1968) considered the following independent solution of (A.9):

$$L_m^\pm = (1/h) \; \mathrm{grad}\phi_m^\pm$$

$$M_m^\pm = (1/\zeta) \; \mathrm{curl}(\psi_m^\pm e_z) \qquad (A.13)$$

$$N_m^\pm = (1/\zeta k) \; \mathrm{curl}(\mathrm{curl}(\psi_m^\pm e_z))$$

where

$$\phi_m^\pm = J_m(\zeta r)e^{im\phi \pm \Gamma z}, \quad \psi_m^\pm = J_m(\zeta r)e^{im\phi \pm \Delta z}$$

$$(A.14)$$

$$\Gamma = (\zeta^2 + h^2)^{\frac{1}{2}}, \quad \Delta = (\zeta^2 + k^2)^{\frac{1}{2}}$$

$\underset{\sim}{e}_r$, $\underset{\sim}{e}_\phi$, $\underset{\sim}{e}_z$ being unit vectors, ζ - a separation constant and J_m the Bessel function of order m.

These vector solutions represent upgoing and downgoing cylindrical waves, $\underset{\sim}{L}_m^\pm$ corresponding to P-waves $\underset{\sim}{M}_m^\pm$ to SH-waves and $\underset{\sim}{N}_m^\pm$ to SV-waves. The general solution of (A.9) in terms of such waves is therefore

$$\underset{\sim}{\bar{U}} = \sum_m \int_0^\infty \underset{\sim}{\bar{u}}_m(\zeta)\zeta d\zeta \qquad (A.15)$$

where

$$\underset{\sim}{\bar{u}}_m(\zeta) = h(a_m^+ \underset{\sim}{L}_m^+ + a_m^- \underset{\sim}{L}_m^-) + k(b_m^+ \underset{\sim}{N}_m^+ + b_m^- \underset{\sim}{N}_m^-) + k(c_m^+ \underset{\sim}{M}_m^+ + c_m^- \underset{\sim}{M}_m^-). \quad (A.16)$$

The factors h,k and ζ were introduced here for convenience, a_m^+, etc. being arbitrary functions of ζ.

It seems that all we have to do now is to write the source term in the same form, to add it to $\underset{\sim}{\bar{U}}$ and impose the boundary conditions. It may be, however, not so convenient to proceed in this manner, even if the source term will turn out to contain only a few upgoing and downgoing waves and therefore only a finite number of terms will appear in the sum (A.15). The boundary conditions will result in

vector relations between $L_m^{\pm}$, etc. at $z = 0$ and $z = H$ involving six coefficients in the layer and three in the half-space. These coefficients depend only upon ζ and it may not be so easy to eliminate r and ϕ, the source of the trouble seemingly being the fact that although $L_m^{\pm}$, etc. are independent solutions of (A.9), at each point they are not linearly independent, their number being more than three.

Ben-Menahem and Singh showed an elegant way out by expressing the solution in terms of the following system of independent vectors:

$$P_m = e^{im\phi} J_m(\zeta r) e_z$$

$$B_m = e^{im\phi} \left\{ \frac{1}{\zeta} \frac{\partial J_m(\zeta r)}{\partial r} e_r + im \frac{J_m(\zeta r)}{\zeta r} e_\phi \right\} \qquad \text{(A.17)}$$

$$C_m = e^{im\phi} \left\{ im \frac{\partial J_m(\zeta r)}{\zeta r} e_r - \frac{1}{\zeta} \frac{\partial J_m(\zeta r)}{\partial r} e_\phi \right\}.$$

The upgoing and downgoing waves are expressed in terms of this system as follows:

$$L_m^{\pm} = \frac{1}{h} e^{\pm \Gamma z} (\pm \Gamma P_m + \zeta B_m)$$

$$\qquad \text{(A.18)}$$

$$M_m^{\pm} = e^{\pm \Delta z} C_m$$

$$N_m^{\pm} = \frac{1}{k} e^{\pm \Delta z} (\pm \Delta B_m + \zeta P_m).$$

Using (A.18), Ben-Menahem and Singh (1969) write $\bar{u}_m(\zeta)$ in the form

$$\bar{u}_m(\zeta) = (\zeta f_{m_1} + f'_{m_2}) B_m + (f'_{m_1} + \zeta f_{m_2}) P_m + k f_{m_3} C_m \quad (A.19)$$

where

$$f_{m_1} = a_m^+ e^{\Gamma z} + a_m^- e^{-\Gamma z}$$

$$f_{m_2} = b_m^+ e^{\Delta z} + b_m^- e^{-\Delta z} \quad (A.20)$$

$$f_{m_3} = c_m^+ e^{\Delta z} + c_m^- e^{-\Delta z}$$

f'_{m_j} being the derivative of f_{m_j} with respect to z. The stress on a horizontal plane is expressed in a similar manner as a sum over m with:

$$\tau_m = 2\mu(\zeta f'_{m_1} + \Omega f_{m_2}) B_m + \mu k f'_{m_3} C_m + 2\mu(\Omega f_{m_1} + \zeta f'_{m_2}) P_m \quad (A.21)$$

where

$$\Omega = \zeta^2 + k^2/2. \quad (A.22)$$

A2c. The source term in cylindrical coordinates.

Following closely Ben-Menahem and Singh, the

components $\bar{s}_{mk}$ given by (A.11) are first expressed in terms of the spherical wave functions

$$\psi_{j,n}^{e,c} = h_n^{(2)} \ (-ipr/c) \ P_n^j(\cos\theta) \ \cos j\phi \qquad (A.23)$$

$$\psi_{j,n}^{\theta,c} = h_n^{(2)} \ (-ipr/c) \ p_n^j(\cos\theta) \ \sin j\phi$$

where ϕ,θ are spherical coordinates centered at the running point (ξ_1,ξ_2,ξ_3) on Σ and P_n^{ℓ} are the associated Legendre functions. Using the Erdely identity expressing the product $h_n P_n^{\ell}$ as an integral of scalar cylindrical wave functions, the components $\bar{s}_{jk}$ are obtained as follows:

$$\bar{s}_{11} = \int_0^{\infty} a(\zeta)J_0(\zeta r)d\zeta + \cos 2\phi \int_0^{\infty} b(\zeta)J_2(\zeta r)d\zeta$$

$$\bar{s}_{12} = \sin 2\phi \int_0^{\infty} b(\zeta)J_2(\zeta r)d\zeta$$

$$\bar{s}_{13} = \epsilon \ \cos\phi \int_0^{\infty} c(\zeta)J_1(\zeta r)d\zeta$$

$$\bar{s}_{22} = \int_0^{\infty} a(\zeta)J_0(\zeta r)d\zeta - \cos 2\phi \int_0^{\infty} b(\zeta)J_2(\zeta r)d\zeta \qquad (A.24)$$

$$\bar{s}_{23} = \epsilon \ \sin\phi \int_0^{\infty} c_1(\zeta)J_1(\zeta r)d\zeta$$

$$\bar{s}_{33} = \int_0^{\infty} c_2(\zeta)J_0(\zeta r)d\zeta$$

where

$$a(\zeta) = -(X\zeta^2/2\Gamma) + (k^2+\zeta^2/2)Y/\Delta$$

$$b(\zeta) = (X/\Gamma-Y/\Delta)\zeta^2/2$$

$$c_1(\zeta) = (X-Y)\zeta \; ; \quad c_2(\zeta) = \Gamma X-\zeta^2 Y/\Delta \qquad (A.25)$$

$$X = \frac{\zeta}{(\lambda+2\mu)h^2} e^{-\Gamma|z-d|}, \quad y = \frac{\zeta}{\mu k^2} e^{-\Delta|z-d|}$$

$$\varepsilon = \begin{cases} 1 & \text{for } z > d \\ -1 & \text{for } z < d \end{cases}$$

d being the depth of the source.

The expression for the displacement vector corresponding to the source in terms of the harmonic vectors $\underset{\sim}{B}_m$, $\underset{\sim}{C}_m$, $\underset{\sim}{P}_m$ is obtained using also the relations giving the connection between cartesian and cylindrical coordinates as well as some relations between Bessel functions. The result is

$$\bar{\underset{\sim}{s}} = \iint_{\Sigma} \int_0^{\infty} \text{Re}[\bar{\underset{\sim}{s}}(\zeta)]\zeta d\zeta d\sigma \qquad (A.26)$$

$$\bar{\underset{\sim}{s}}(\zeta) = \frac{\bar{F}_1}{4\pi}\left\{ -\frac{k^2}{\Delta} iY\underset{\sim}{C}_1 - (\frac{\zeta^2 X}{\Gamma^2}-\Delta Y)\ \underset{\sim}{B}_1 + \varepsilon\zeta(X-Y)\underset{\sim}{P}_1 \right\}$$

$$+ \frac{\bar{F}_2}{4\pi}\left\{ -\frac{k^2}{\Delta^2} Y\underset{\sim}{C}_1 + (\frac{\zeta^2 X}{\Gamma} - \Delta Y)\ i\underset{\sim}{B}_1 - \varepsilon\zeta(X-Y)i\underset{\sim}{P}_1 \right. \qquad (A.27)$$

$$+ \frac{\bar{F}_3}{4\pi}\left\{ -\varepsilon\zeta(X-Y)\underset{\sim}{B}_0 + (\Gamma X - \frac{\zeta^2 Y}{\Delta})\ \underset{\sim}{P}_0 \right\}$$

with

$$\bar{F}_j = \bar{f}_{j\ell}\nu_\ell . \qquad (A.28)$$

Thus, the displacement due to the source is expressed as an integral over Σ of a sum of the form (A.15) including only two terms: $m = 0$ and $m = 1$. If the surface Σ is reduced to a point, i.e. the source is a space concentrated force, the integration with respect to Σ will result in $\bar{F}_1, \bar{F}_2, \bar{F}_3$ representing the strength of such a concentrated force in the directions of the coordinate axes and the surface integral in (A.26) will disappear.

The expression of $\bar{s}(\zeta)$ in terms of $\underset{\sim}{L}_m^{\pm}$, etc. was given by Singh, Ben-Menachem and Vered (1973).

In order to add the source solution (A.26) to the free solution represented by (A.19) it is convenient to write (A.27) in the same form:

$$\bar{s}(\zeta) = (\zeta Z_{m_1} + Z'_{m_2})\underset{\sim}{B}_m + (Z'_{m_1} + \zeta Z_{m_2})\underset{\sim}{P}_m + kZ_{m_3}\underset{\sim}{C}_m \qquad (A.29)$$

where

$$Z_{m_1} = i_m e^{-\varepsilon\Gamma(z-d)}\varepsilon^{m+1}$$

$$Z_{m_2} = j_m e^{-\varepsilon\Delta(z-d)}\varepsilon^m \qquad (A.30)$$

$$Z_{m_3} = \kappa_m e^{-\varepsilon\Delta(z-d)}\varepsilon^{m+1} .$$

For a horizontal force in x_2-direction with m taking the values 0 and 1 we obtain

$$i_0 = j_0 = \kappa_0 = 0$$

$$i_1 = -\frac{\zeta \bar{F}_1}{4\pi\Gamma\mu k^2}, \quad j_1 = \frac{\bar{F}_1}{4\pi\mu k^2}, \quad \kappa_1 = \frac{i\bar{F}_1}{4\pi\Delta\mu k}. \qquad (A.31)$$

For a horizontal force in the x_1-direction

$$i_0 = j_0 = \kappa_0 = 0$$

$$(A.32)$$

$$i_1 = \frac{\zeta i\bar{F}_2}{4\pi\Gamma\mu k^2}, \quad j_1 = \frac{i\bar{F}_2}{4\pi\mu k^2}, \quad \kappa_1 = -\frac{\bar{F}_2}{4\pi\Delta\mu k}.$$

For a vertical force

$$i_0 = -\frac{\bar{F}_3}{4\pi\mu k^2}, \quad j_0 = -\frac{\zeta\bar{F}_3}{4\pi\mu k^2\Delta}, \quad \kappa_0 = 0$$

$$(A.33)$$

$$i_1 = j_1 = \kappa_1 = 0.$$

The total displacement for a point force, obtained superposing the source and the free solution is therefore of the following form (Ben-Menahem and Singh, 1968):

in the layer:
$$\bar{u}_1(p) = \mathrm{Re} \int_0^\infty \bar{u}_1(\zeta)\zeta d\zeta$$

$$\bar{u}_1(\zeta) = [\zeta(f_{m_1}+z_{m_1})+(f_{m_2}+z_{m_2})']B_m$$

$$(A.34)$$

$$+ [(f_{m_1}+z_{m_1})' + \zeta(f_{m_2}+z_{m_2})]P_m +k(f_{m_3}+z_{m_3})C_m$$

in the half-space: $\quad \bar{u}_2(p) = \text{Re} \int_0^\infty \bar{u}_2(\zeta)\zeta d\zeta$

$$(A.35)$$

$$\bar{u}_2(\zeta) = (\zeta F_{m_1} + F'_{m_2})B_m + (F'_{m_1} + \zeta F_{m_2})P_m + kF_{m_3}C_m$$

where

$$F_{m_1} = d_m e^{-\Gamma_2 z}, \quad F_{m_2} = e_m e^{-\Delta_2 z}, \quad F_{m_3} = g_m e^{-\Delta_2 z}$$

$$\Gamma_2 = (\zeta^2 + h_2^2)^{\frac{1}{2}}, \quad \Delta_2 = (\zeta^2 + k_2^2)^{\frac{1}{2}}, \quad h_2 = p/\alpha_2, \quad k_2 = p/\beta_2$$

α_2, β_2 being respectively the P and S velocities in the half space. The coefficients $a_m, \ldots, g_m$ are obtained from the boundary conditions at $z = 0$ and $z = H$, taking into account that the vectors B_m, P_m, C_m are linearly independent. The linear system obtained splits into a third-order system for the coefficients c_m^+, c_m^- and g_m, representing the SH-wave, and a sixth-order system for the other coefficients, representing the P-SV-waves.

A3. Ray expansion

a. Pure Shear Waves

    Combining the source with the free solution, solving the linear system determined by the boundary conditions, expanding the solution in a geometric series, and grouping conveniently the terms of this expansion, we get the m-th term of the displacement at the surface in the form:

$$\bar{u}^{(SH)}(\zeta) = [2k\kappa_m \sum_{\nu=0}^{\infty} b_\nu K^{\left[\frac{\nu+1}{2}\right]} e^{-NBH}]\underset{\sim}{C}_m \qquad (A.36)$$

where

$$b_\nu = \begin{cases} 1 & \text{if } \nu = \text{odd} \\ (-1)^{m+1} & \text{if } \nu = \text{even} \end{cases} \qquad N = \begin{cases} \nu+1 - \dfrac{d}{H} & \text{if } \nu = \text{odd} \\ \nu + \dfrac{d}{H} & \text{if } \nu = \text{even} \end{cases}$$

$$K = \frac{b\beta_1 - \beta_2}{b\beta_1 + \beta_2}, \quad b = \frac{\mu_1}{\mu_2}, \quad B = (\zeta^2 + k_1)^{\frac{1}{2}}, \quad M = \begin{cases} \mu+1 & \text{if } \mu = \text{odd} \\ \mu + \dfrac{d}{H} & \text{if } \mu = \text{even} \end{cases}$$

$$\qquad (A.37)$$

[...] meaning "the integral part of ..." and $k_1 = p/\beta_1$,
where β_1 is the S-velocity in the layer.

For a horizontal force in the x_2-direction there is
no displacement corresponding to $m = 0$. The displacement
corresponding to $m = 1$ is:

$$\bar{u}^{(SH)}(\zeta) = \frac{\bar{F}_2}{2\pi\mu_1 B} [\cos\phi \frac{J_1(\zeta r)}{\zeta r} \underset{\sim}{e}_r - \sin\phi \frac{\partial J_1(\zeta r)}{\partial(\zeta r)} \underset{\sim}{e}_\phi] \sum_{\nu=0}^{\infty} K^{\left[\frac{\nu+1}{2}\right]} e^{-NBH} \qquad (A.38)$$

and if the receiver is on the x_1-axis, $\phi = \pi/2$ and the
displacement is

$$\bar{u}^{(SH)}(\zeta) = - \frac{\bar{F}_2}{2\pi\mu_1} \sum_{\nu=0}^{\infty} \frac{1}{B} K^{\left[\frac{\nu+1}{2}\right]} J_1'(\zeta r) e^{-NBH} \underset{\sim}{e}_\phi \qquad (A.39)$$

Restoring the integration with respect to ζ and
performing the change of variable

$$\zeta = k_1 x \qquad (A.40)$$

we write the displacement of the S wave in the form

$$\underline{u}^{(SH)} = \bar{V}^{(SH)} e_\phi, \quad \text{where}$$

$$\bar{V}^{(SH)} = -\frac{\bar{F}_2}{2\pi\mu_1} \sum_{\nu=0}^{\infty} k_1 \int_0^\infty \frac{x}{\sqrt{x^2+n_1^2}} K^{\left[\frac{\nu+1}{2}\right]} J_1'(k_1 rx) e^{-Nk_1 H \sqrt{x^2+n_1^2}} dx .$$

(A.41)

For a horizontal force in the x_1-direction and a receiver on the x_1-axis, we get after similar steps:

$$\underline{u}^{(S)} = \bar{q}^{(S)} e_r \quad \text{where}$$

$$\bar{q}^{(S)} = \frac{\bar{F}_1}{2\pi\mu_1 r} \sum_{\nu=0}^{\infty} \int_0^\infty \frac{1}{\sqrt{x^2+n_1^2}} K^{\left[\frac{\nu+1}{2}\right]} J_1(k_1 xr) e^{-Nk_1 H \sqrt{x^2+n_1^2}} dx \quad (A.42)$$

with

$$n_1 = \beta_1 / \beta_2 . \qquad (A.43)$$

b. Compressional-Shear Waves

The system for the coefficients $a_m^+, a_m^-, b_m^+, b_m^-, d_m, e_m$ can be brought to the following form

$$\underset{\sim}{A}_m \underset{\sim}{u}_m = -i_m \sqrt{x^2+\epsilon_1^2} \, e^{-A(H-d)} \underset{\sim}{B}_m^{(P)} + j_m \frac{x^2+n_1^2}{x} e^{-B(H-d)} \underset{\sim}{B}_m^{(SV)} \qquad (A.44)$$

where $\underset{\sim}{A}_m$ is a (6×6) matrix, identical with that obtained taking the first six columns of the matrix (23) in Abramovici (1970),

$$\epsilon_1 = \beta_1/\alpha_1, \quad A = k_1 \sqrt{x^2+\epsilon_1^2} \qquad (A.45)$$

α_1 being the P-velocity in the layer, and

$$B_{\sim m}^{(P)} = \left((-1)^{m+1} \frac{2x^2+1}{\sqrt{x^2+\epsilon_1^2}} e^{A(H-2d)}, \ (-1)2e^{m+1\ A(H-2d)}, \frac{1}{\sqrt{x^2+\epsilon_1^2}}, -1, \frac{b(1+2x^2)}{\sqrt{x^2+\epsilon_1^2}}, -2b \right)^T$$

$$B_{\sim m}^{(SV)} = \left((-1)^{m+1} \frac{2x^2}{\sqrt{x^2+\eta_1^2}} e^{B(H-2d)}, \ (-1)^{m+1} \frac{2x^2+1}{x^2+\eta_1^2} e^{B(H-2d)}, \right. \tag{A.46}$$

$$\left. \frac{1}{\sqrt{x^2+\eta_1^2}}, -\frac{x^2}{\sqrt{x^2+\eta_1^2}}, \frac{2bx^2}{\sqrt{x^2+\eta_1^2}}, \frac{b(2x^2+1)}{x^2+\eta_1^2} \right)^T.$$

T meaning transposed. Thus, the displacement is split in a natural way into P and SV motions

$$u_{\sim m} = u_{\sim m}^{(P)} + u_{\sim m}^{(SV)} \tag{A.47}$$

with $u_{\sim m}^{(P)}$ and $u_{\sim m}^{(SV)}$ satisfying:

$$A u_{\sim m}^{(P)} = -i_m \sqrt{x^2+\epsilon_1^2}\ e^{-A(H-d)}\ B_{\sim m}^{(P)} \qquad \left.\vphantom{\frac{x^2+\eta_1^2}{x}}\right) \tag{A.48}$$

$$A u_{\sim m}^{(SV)} = j_m \frac{x^2+\eta_1^2}{x} e^{-B(H-d)}\ B_{\sim m}^{(SV)}$$

Solving these systems of equations, expanding into generalized rays and taking into account the expression (A.17) for the harmonic vectors we get the vertical, radial and angular displacement components w_m, q_m and V_m respectively for the P and SV motions as integrals with respect to x, having as integrands:

$$\bar{w}_m^{(P)} = -k_1 \sqrt{x^2 + \epsilon_1^2}\, J_m(k_1 xr) \mathrm{Re}(i_m e^{im\phi}) \sum_{\mu,\nu} R_3(\mu,\nu)^{-AMH-B\nu H}$$

$$\bar{q}_m^{(P)} = -k_1 x\, J'_m(k_1 xr) \mathrm{Re}(i_m e^{im\phi}) \sum_{\mu,\nu} S_3(\mu,\nu) e^{-AMH-B\nu H}$$

$$\bar{v}_m^{(P)} = -\frac{m}{r} J_m(k_1 xr) \mathrm{Re}(i_m e^{im\phi} i) \sum_{\mu,\nu} S_3(\mu,\nu) e^{-AMH-B\nu H}$$

$$\bar{w}_m^{(SV)} = k_1 \mathrm{Re}(j_m e^{im\phi}) \frac{\sqrt{x^2+\epsilon_1^2}\,\sqrt{x^2+\eta_1^2}}{x} J_m(k_1 xr) \sum_{\mu,\nu} R_4(\mu,\nu) e^{-A\mu H-BNH} \qquad (A.49)$$

$$\bar{q}_m^{(SV)} = k_1 \sqrt{x^2+\eta_1^2}\, \mathrm{Re}(j_m e^{im\phi}) J'_m(k_1 rx) \sum_{\mu,\nu} S_4(\mu,\nu) e^{-A\mu H-BNH}$$

$$\bar{v}_m^{(SV)} = \sqrt{x^2+\eta_1^2}\, \mathrm{Re}(j_m e^{im\phi} i)\frac{m}{xr} J_m(k_1 xr) \sum_{\mu,\nu} S_4(\mu,\nu) e^{-A\mu H-BNH}$$

where

$$R_3(\mu,\nu) = (-1)^{(m+1)(\mu+\nu+1)} R_1(\mu,\nu), \quad R_4(\mu,\nu) = (-1)^{m(\mu+\nu+1)} \frac{x^2}{\sqrt{x^2+\epsilon_1^2}\,\sqrt{x^2+\eta_1^2}}$$

$$\qquad (A.50)$$

$$\cdot R_2(\mu,\nu)$$

$$S_3(\mu,\nu) = (-1)^{(m+1)(\mu+\nu+1)} S_1(\mu,\nu), \quad S_4(\mu,\nu) = (-1)^{m(\mu+\nu+1)} S_2(\mu,\nu)$$

$R_1(\mu,\nu)$, $S_1(\mu,\nu)$ being defined in Abramovici (1970) and $R_2(\mu,\nu)$, $S_2(\mu,\nu)$ in Abramovici and Gal-Ezer (1978).

For a horizontal force in the x_2-direction, we have to take only $m = 1$. When the receiver is located on the x_1-axis, the displacement is:

$$\bar{w}^{(P)} = \bar{w}^{(SV)} = \bar{q}^{(P)} = \bar{q}^{(SV)} = 0$$

$$\bar{v}^{(P)} = - \frac{\bar{F}_2}{4\pi k_1^2 r} \sum_{\mu,\nu} \int_0^\infty \frac{x J_1(k_1 xr)}{M \sqrt{x^2 + \epsilon_1^2}} S_3(\mu,\nu) e^{-AMH - B\nu H} dx \qquad (A.51)$$

$$\bar{v}^{(SV)} = \frac{\bar{F}_2}{4\pi k_1^2 r} \sum_{\mu,\nu} \int_0^\infty \frac{\sqrt{x^2 + \eta_1^2} \, J_1(k_1 xr)}{Mx} S_4(\mu,\nu) e^{-A\mu H - BNH} dx.$$

For a horizontal force in the x_1-direction we have
again only the term m = 1. When the receiver is on the
x_1-axis, the displacement is:

$$\bar{v}^{(P)} = \bar{v}^{(SV)} = 0$$

$$\bar{w}^{(P)} = \frac{\bar{F}_1}{4\pi k_1} \sum_{\mu,\nu} \int_0^\infty \frac{x J_1(k_1 xr)}{M} R_3(\mu,\nu) e^{-AMH - B\nu H} dx$$

$$\bar{w}^{(SV)} = - \frac{\bar{F}_1}{4\pi k_1} \sum_{\mu,\nu} \int_0^\infty \frac{\sqrt{x^2 + \epsilon_1^2} \sqrt{x^2 + \eta_1^2}}{Mx} J_1(k_1 xr) R_4(\mu,\nu) e^{-A\mu H - BNH} dx \qquad (A.52)$$

$$\bar{q}^{(P)} = \frac{\bar{F}_1}{4\pi k_1} \sum_{\mu,\nu} \int_0^\infty \frac{x^2 J_1'(k_1 xr)}{M \sqrt{x^2 + \epsilon_1^2}} S_3(\mu,\nu) e^{-AMH - B\nu H} dx$$

$$\bar{q}^{(SV)} = \frac{\bar{F}_1}{4\pi k_1} \sum_{\mu,\nu} \int_0^\infty \frac{\sqrt{x^2 + \eta_1^2} \, J_1'(k_1 xr)}{M} S_4(\mu,\nu) e^{-A\mu H - BNH} dx$$

A4. The solution in the time domain
   Using the generalized Cagniard-Pekeris method

(Abramovici, 1978), each term in (A.36) and (A.49) can be inverted directly into the time domain if the time variation of the stress-discontinuity is a power of time t multiplying a step function or any linear combination of such functions. In particular, if we have a concentrated force acting in the horizontal plane (x_1, x_2) of components

$$F_1(t) = f_1 U(t) t$$

$$(A.53)$$

$$F_2(t) = f_2 U(t) t$$

where f_1, f_2 are scale factors and $U(t)$ is the unit step function, we have

$$\bar{F}_1 = \frac{f_1}{p^2}, \quad \bar{F}_2 = \frac{f_2}{p^2} \qquad (A.54)$$

and the displacement components, according to (A.41)-(A.42) and (A.51)-(A.52), for a receiver on the x_1-axis, are:

$$\bar{w} = \frac{f_1}{4\pi\mu_1 p^2} \sum_{\mu,\nu} k_1 \int_0^\infty x^2 J_1(k_1 x r) R_3(\mu,\nu) e^{-A\mu H - B\nu H} dx$$

$$(A.55)$$

$$-\frac{f_1}{4\pi\mu_1 p^2} \sum_{\mu,\nu} k_1 \int_0^\infty \sqrt{x^2 + \varepsilon_1^2} \sqrt{x^2 + \eta_1^2} J_1(k_1 x r) R_4(\mu,\nu) e^{-A\mu H - B N H} dx$$

$$\bar{q} = \frac{f_1}{4\pi\mu_1 p^2} \sum_{\mu,\nu} k_1 \int_0^\infty \frac{x^3}{\sqrt{x^2+\epsilon_1^2}} J_1'(k_1 xr) \, S_3(\mu,\nu) e^{-AMH-B\nu H} \, dx$$

$$- \frac{f_1}{4\pi\mu_1 p^2} \sum_{\mu,\nu} k_1 \int_0^\infty x\sqrt{x^2+\eta_1^2} \, J_1'(k_1 xr) \, S_4(\mu,\nu) e^{-A\mu H-BNH} \, dx \qquad \text{(A.56)}$$

$$+ \frac{f_1}{2\pi\mu_1 r p^2} \sum_{\nu=0}^\infty \int_0^\infty \frac{1}{\sqrt{x^2+\eta_1^2}} J_1(k_1 xr) K^{\left[\frac{\nu+1}{2}\right]} e^{-BNH} \, dx$$

$$\bar{V} = - \frac{f_2}{4\pi\mu_1 p^2 r} \sum_{\mu,\nu} \int_0^\infty \frac{x^2}{\sqrt{x^2+\epsilon_1^2}} J_1(k_1 xr) \, S_3(\mu,\nu) e^{-AMH-B\nu H} \, dx$$

$$+ \frac{f_2}{4\pi\mu_1 p^2 r} \sum_{\mu,\nu} \int_0^\infty \sqrt{x^2+\eta_1^2} \, J_1(k_1 xr) \, S_4(\mu,\nu) e^{-A\mu H-BNH} \, dx \qquad \text{(A.57)}$$

$$- \frac{f_2}{2\pi\mu_1 p^2 r} \sum_{\nu=0} k_1 \int_0^\infty \frac{x}{\sqrt{x^2+\eta_1^2}} J_1'(k_1 rx) \, K^{\left[\frac{\nu+1}{2}\right]} e^{-BNH} \, dx$$

The inversion into the time domain is expressed in terms of some special quantities $F_m^{n,s}$ (Abramovici, 1978) that depend on two functions and on the time variable:

$$F_m^{n,s} = F_m^{n,s} [\phi; g; t] \qquad \text{(A.58)}$$

The function ϕ is the "amplitude" of the integrands in (A(55),(56), (57)) whereas g is the argument of the exponentials. For simplicity, we shall drop here the lower index.

The time dependent displacement components for a

horizontal force are:

$$w(t) = \frac{f_1}{2\pi^2 \mu_1 \beta_1 \rho} \sum_{\mu,\nu} \left\{ F^{0,0}[x^2 R_3(\mu,\nu); M\sqrt{x^2+\epsilon_1^2} + \nu\sqrt{x^2+\eta_1^2}; t] \right.$$

(A.59)

$$\left. -F^{0,0}[\sqrt{x^2+\epsilon_1^2}\ \sqrt{x^2+\eta_1^2}\ R_4(\mu,\nu); \mu\sqrt{x^2+\epsilon_1^2} + N\sqrt{x^2+\eta_1^2};\ t] \right\}$$

$$q(t) = \frac{f_1}{4\pi^2 \mu_1 \beta_1 \rho^2} \sum_{\mu,\nu} \left\{ F^{0,1}[\frac{x^2 S_3(\mu,\nu)}{\sqrt{x^2+\epsilon_1^2}}; M\sqrt{x^2+\epsilon_1^2} + \nu\sqrt{x^2+\eta_1^2};\ t] \right.$$

$$\left. -F^{0,1}[\sqrt{x^2+\eta_1^2}\ S_4(\mu,\nu);\ \mu\sqrt{x^2+\epsilon_1^2} + N\sqrt{x^2+\eta_1^2}\ ;\ t] \right\} +$$

(A.60)

$$\frac{f_1}{2\pi^2 \mu \rho^2 \beta_1} \sum_{\nu=0}^{\infty} F^{-1,0}\left[\frac{1}{\sqrt{x^2+\eta_1^2}} K^{[(\nu+1)/2]};\ N\sqrt{x^2+\eta_1^2}\ ;\ t\right].$$

$$V(t) = -\frac{f_2}{4\pi^2 \mu_1 \beta_1 \rho^2} \sum_{\mu,\nu} \left\{ F^{-1,0}\left[\frac{x^2 S_3(\mu,\nu)}{\sqrt{x^2+\epsilon_1^2}};\ M\sqrt{x^2+\epsilon_1^2} + \nu\sqrt{x^2+\eta_1^2};\ t\right] \right.$$

$$\left. -F^{-1,0}\left[\sqrt{x^2+\eta_1^2}\ S_4(\mu,\nu);\ \mu\sqrt{x^2+\epsilon_1^2} + N\sqrt{x^2+\eta_1^2};\ t\right] \right\}$$

(A.61)

$$-\frac{f_2}{2\pi^2 \mu_1 \beta_1 \rho^2} \sum_{\nu=0}^{\infty} F^{0,1}\left[\frac{1}{\sqrt{x^2+\eta_1^2}} K^{[\frac{\nu+1}{2}]};\ N\sqrt{x^2+\eta_1^2};\ t\right]$$

where, if $\rho < \rho_1$

$$F^{n,s} = \begin{cases} 0 & \text{for } \tau < \tau_0 \\ Y^{n,s} & \tau > \tau_0 \end{cases}$$

(A.62)

and if $\rho > \rho_1$

$$F^{n,s} = \begin{cases} 0 & \text{for } \tau < \tau^* \\ X^{n,s} & \text{for } \tau^* < \tau < \tau_0 \\ Y^{n,s} & \text{for } \tau > \tau_0 \end{cases} \qquad (A.63)$$

ρ being the non-dimensional epicentral distance

$$\rho = r/H \qquad (A.64)$$

and ρ_1 the critical epicentral distance for a head wave to occur. Besides, τ is a non-dimensional time parameter, τ_0 the arrival time of the geometrical ray reflected μ times as P and ν times as S, τ^* the arrival time of the corresponding head wave. The expressions for $X^{n,s}$, $Y^{n,s}$ are given by Abramovici (1978) together with those for v_1 and x_1 appearing there, as well as the expressions for ρ_1, τ^* and τ_0.

For the particular cases needed in (A.59), (A.60), (A.61) the expressions of $X^{n,s}$ and $Y^{n,s}$ are

$$X^{0,0} = \int_{\bar{\lambda}}^{v_1} \frac{\text{Im}[\phi(iv)]}{v} G(iv, \tau) dv \qquad (A.65)$$

$$Y^{0,0} = \text{Im} \int_{\bar{\lambda}1}^{x_1} \frac{\phi(x)}{x} G(x, \tau) d\tau \qquad (A.66)$$

$$X^{0,1} = \int_{\bar{\lambda}}^{v_1} \frac{Im[\phi(iv)]}{v} \left\{ [\tau - g(iv)]G(iv,\tau) \right.$$

$$\left. + \rho^2 v^2 \ln\left[\frac{\tau - g(iv) + G(iv,\tau)}{\rho v}\right] \right\} dv \tag{A.67}$$

$$Y^{0,1} = Im \int_{\bar{\lambda}}^{v_1} \frac{\phi(x)}{x} \left\{ [\tau - g(x)]G(x,\tau) - \rho^2 x^2 \ln\left[\frac{\tau - g(x) + G(x,\tau)}{-i\rho x}\right] \right\} dx \tag{A.68}$$

$$X^{-1,0} = \int_{\bar{\lambda}}^{v_1} \frac{Im[\phi(iv)]}{v} \left\{ [\tau - g(iv)]G(iv,\tau) \ln\left[\frac{\tau - g(iv) + G(iv,\tau)}{\rho v}\right] \right\} dv \tag{A.69}$$

$$Y^{-1,0} = Im \int_{\bar{\lambda}}^{x_1} \frac{\phi(x)}{x} \left\{ [\tau - g(x)]G(x,\tau) + \rho^2 x^2 \ln\left[\frac{\tau - g(x) + G(x,\tau)}{-i\rho x}\right] \right\} dx \tag{A.70}$$

where

$$\bar{\lambda} = \min(\varepsilon_1, \varepsilon_2, \eta_1, \eta_2) \tag{A.71}$$

$$G(x,\tau) = \left\{ [\tau - g(x)]^2 + \rho^2 x^2 \right\}^{\frac{1}{2}} \tag{A.72}$$

APPENDIX B

In general, the steady-state plane wave solution to (3.3) is a constant times

$$e^{i(\vec{K}\cdot\vec{r}-\omega t)} = e^{-\vec{A}\cdot\vec{r}}\, e^{i(\vec{P}\cdot\vec{r}-\omega t)} \qquad (B.1)$$

where

$$\vec{K} = \vec{P} + i\vec{A}. \qquad (B.2)$$

$\vec{P}$ is the propagation vector and $\vec{A}$ is the attenuation vector.

From (B.2) we have

$$P^2 - A^2 = Re[K^2] \qquad (B.3)$$

and

$$2PA\cos\gamma = Im[K^2] \qquad (B.4)$$

where P and A are the amplitudes of $\vec{P}$ and $\vec{A}$ and γ is the angle between them. We now define the loss factor for P and S waves as follows:

$$Q^{-1} = \frac{Im[G]}{Re[G]} \qquad \begin{cases} G = \lambda+2\mu & \text{for P waves} \\ G = \mu & \text{for S waves.} \end{cases} \qquad (B.5)$$

Thus

$$G = m(1+i\frac{1}{Q}) \qquad (B.6)$$

and

$$K^2 = \omega^2\frac{\rho}{G} \qquad (B.7)$$

where ρ is the density and m is a constant to be determined.

145

Solving (B.3), (B.4) for P and A and taking into account
(B.6), (B.7) we get:

$$P = \omega \sqrt{\frac{\rho}{m}} \sqrt{E+F} \qquad (B.8)$$

$$A = \omega \sqrt{\frac{\rho}{m}} \sqrt{E-F} \qquad (B.9)$$

where
$$F = \frac{Q^2}{2(Q^2+1)} \qquad (B.10)$$

and
$$E = F\sqrt{1 + Q^{-2}\sec^2\gamma} \quad . \qquad (B.11)$$

But the phase velocity $c(\omega)$ is equal to $\frac{\omega}{P}$, then

$$m = c^2(\omega)\rho(E+F). \qquad (B.12)$$

Therefore using (B.6) the complex modulus G is obtained
as follows:

$$G = c^2(\omega)\rho(E+F) \left(1 + i \frac{1}{Q}\right). \qquad (B.13)$$

Futterman's model provides the phase velocity and Q as
a function of frequency.

Equation (B.2) implies that in the most general case
$\vec{P}$ and $\vec{A}$ are not parallel. When $\gamma=0$ the wave is called
homogeneous while when $\gamma\neq0$ the wave is called inhomogeneous.
In our examples we assume that the source transmits
homogeneous waves, i.e. $\gamma=0$. Care must be taken working
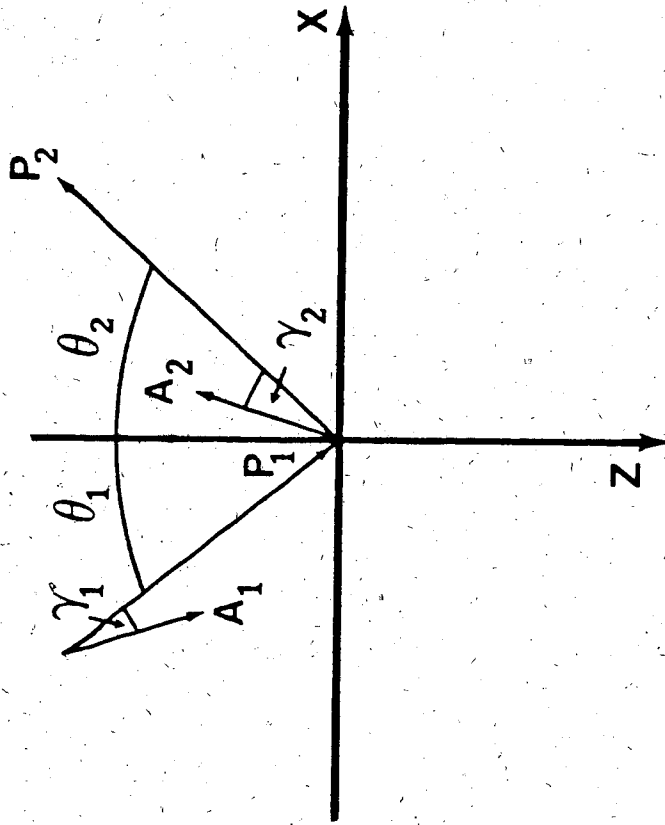
Figure 25. The notation for the angles in the case of a PP reflection from a viscoelastic interface.

out the angles of emergence for the reflecting waves.
Consider a plane P wave striking an interface and producing
reflected and transmitted P and S waves as shown in Figure
25. For simplicity the transmitted P and S waves and the
reflected S waves are not shown in Figure 25. If we know
the angle of incidence θ_1 and the attenuation angle γ_1
then the angle of emergence θ_2 and the γ_2 can be calculated
using Snell's Law, which states that the horizontal wave
number K_x is constant (Lockett 1962, Borcherdt 1977):

i.e.
$$Re[K_x] = constant$$

(B.14)

or
$$P_1 \sin\theta_1 = P_2 \sin\theta_2$$

$$Im[K_x] = constant$$

or
$$A_1 \sin(\theta_1-\gamma_1) = A_2 \sin(\theta_2-\gamma_2).$$

(B.15)

Equations (B.14), (B.15) are used to calculate θ_2 and γ_2.
Similarly, one can calculate angles of transmission and
emergence for the transmitted and reflected P and S waves.

APPENDIX C

List of Computer Programs

```
 1    C      THIS PROGRAM TAKES A GENERALIZED RAY AND
 2    C      INTRODUCES THE EFFECTS OF ANELASTICITY
 3    C      ACCORDING TO FUTTERMAN'S MODEL
 4    C      V1=P-VELOCITY IN THE LAYER
 5    C      V2=S-VELOCITY IN THE LAYER
 6    C      V3=P-VELOCITY IN THE HALF SPACE
 7    C      V4=S-VELOCITY IN THE HALF SPACE
 8    C      R1=DENSITY IN THE LAYER
 9    C      R2=DENSITY IN THE HALF SPACE
10    C      Q1Z=Q VALUE IN THE LAYER
11    C      Q2Z=Q VALUE IN THE HALF SPACE
12    C      DEPTH=DEPTH OF THE SOURCE
13    C      DIST=HORIZONTAL DISTANCE SOURCE-RECEIVER
14    C      DEL=SAMPLING RATE
15    C      FL=LOW FREQUENCY
16    C      FH=HIGH FREQUENCY
17    C      GAM=ATTENUATION ANGLE
18    C      X=GENERALIZED RAY
19    C      XR=GENERALIZED RAY WITH THE EFFECTS OF ANELASTICITY
20    C      SUBROUTINE PEL CALCULATES REFLECTION COEFFICIENTS
21    C      FOR A P INCIDENT PLANE WAVE
22    C      SUBROUTINE SEL CALCULATES REFLECTION COEFFICIENTS
23    C      FOR AN S INCIDENT PLANE WAVE
24    C      SUBROUTINE PVEL IS THE ANELASTIC VERSION OF PEL
25    C      SUBROUTINE SVEL IS THE ANELASTIC VERSION OF SEL
26    C      SUBROUTINE FASTF PERFORMS A FAST FOURIER TRANSFORM
27    C      SUBROUTINE PHAMP PUTS THE PHASE BETWEEN O AND TWOPI
28    C      SUBROUTINE LEQT1C SOLVES A SYSTEM OF FOUR EQUATIONS
29    C      WITH FOUR UNKNOWNS.
30           REAL  X(1024),XR(1024),XI(1024),AAM(1024),PPH(1024)
31           REAL  AM(1024),PH(1024)
32           REAL  VP1(1024),VP2(1024),VS1(1024),VS2(1024),QP(1024),QS(1024)
33           REAL  F(1024),Z(1024),T(1024),FG(1024)
34           COMMON /AREA1/V1,V2,V3,V4,R1,R2
35           COMMON /AREA2/VP1,VP2,VS1,VS2,QP,QS,RS1,RS2,GAM
36    C      READ THE DATA,VELOCITIES,ELASTIC PARAMETERS ETC.
37           READ(5,100)HLAY
38    100 FORMAT(6X,F9.4)
39           READ(5,100)DEPTH
40           READ(5,100)DIST
41           READ(5,100)DEL
42           READ(5,100)FL
43           READ(5,100)FH
44           READ(5,100)V1
45           READ(5,100)V2
46           READ(5,100)V3
47           READ(5,100)V4
48           READ(5,100)Q1Z
49           READ(5,100)Q2Z
50           READ(5,100)R1
51           READ(5,100)R2
52           READ(5,100)GAM
53           READ(5,101)INDEXP
54    101 FORMAT(8X,I2)
55           READ(5,101)INDEXS
56           READ(5,101)KK
57           READ(5,101)KL
58           READ(5,101)KM
59           READ(5,101)KN
60           RS1=R1
```

```
 61          RS2=R2
 62     C    READ THE GENERALIZED RAY
 63          N=512
 64          N2=N/2
 65          PI=3.141593
 66          NX=1
 67       59 CONTINUE
 68          READ(1,299,END=58)X(NX)
 69      299 FORMAT(40X,D20.9)
 70          NX=NX+1
 71          GO TO 59
 72       58 CONTINUE
 73          NX=NX-1
 74     C    TAPERING AND ADDING ZEROS
 75          ND2=(N/2)+1
 76          NTA=476
 77          NEND=N-NTA
 78          NX1=NX+1
 79          MTOT=N-NX-NTA
 80          RMTOT=FLOAT(MTOT)
 81          IC=0
 82          DO 2 I=NX1,NEND
 83          IC=IC+1
 84        2 X(I)=X(NX)*((1.0+COS(PI*FLOAT(IC)/RMTOT))*0.5)
 85          NENDS=NEND+1
 86          DO 3 I=NENDS,N
 87        3 X(I)=0.0
 88     C    FOURIER TRANSFORM OF THE RAY
 89          DO 7 I=1,N
 90          XR(I)=X(I)
 91          XI(I)=0.0
 92        7 CONTINUE
 93          CALL FASTF(XR,XI,N)
 94          DO 10 I=1,ND2
 95          AAM(I)=((XR(I)*XR(I))+(XI(I)*XI(I)))**0.5
 96       10 PPH(I)=ATAN2(XI(I),XR(I))
 97     C    KK=+1 DIRECT P OR S
 98     C    KK=-1 PP,PS,SP,SS
 99     C    KL=+1 DIRECT P
100     C    KL=-1 DIRECT S
101     C    KM=0 SP OR SS
102     C    KM=+1 PP
103     C    KM=-1 PS
104     C    KN=+1 SS
105     C    KN=-1 SP
106     C    INDEXP=+1 PP
107     C    INDEXP=+2 PS
108     C    INDEXS=+1 SP
109     C    INDEXS=+2 SS
110     C    COMPUTE THE PATH TRAVELLED AND THE ANGLE OF INCIDENCE
111          IF(KK.GT.0) GO TO 251
112          RO=((((2.0*HLAY)-DEPTH)**2)+(DIST**2))**0.5
113          VC=DIST/((2.0*HLAY)-DEPTH)
114          AN=ATAN(VC)
115          RO2=HLAY/COS(AN)
116          RO1=RO-RO2
117          GO TO 252
118      251 RO=((DIST**2)+(DEPTH**2))**0.5
119      252 CONTINUE
120     C    FUTTERMAN'S THEORY
```

```
121          EC=0.5772
122          XH=ALOG(FH/FL)
123          VP1L=V1*(1.0-(1.0/(PI*Q1Z))*(EC+XH))
124          VS1L=V2*(1.0-(1.0/(PI*Q2Z))*(EC+XH))
125          VP2L=V3*(1.0-(1.0/(PI*Q1Z))*(EC+XH))
126          VS2L=V4*(1.0-(1.0/(PI*Q2Z))*(EC+XH))
127          VP1(1)=VP1L
128          VS1(1)=VS1L
129          VP2(1)=VP2L
130          VS2(1)=VS2L
131          QP(1)=Q1Z
132          QS(1)=Q2Z
133          DO 510 I=2,ND2
134          F(I)=2.0*PI*FLOAT(I)/(FLOAT(N)*DEL)
135          Z(I)=ALOG(F(I)/FL)
136          VP1(I)=VP1L*(1.0-(1.0/(PI*Q1Z))*(EC+Z(I)))**(-1)
137          VS1(I)=VS1L*(1.0-(1.0/(PI*Q2Z))*(EC+Z(I)))**(-1)
138          VP2(I)=VP2L*(1.0-(1.0/(PI*Q1Z))*(EC+Z(I)))**(-1)
139          VS2(I)=VS2L*(1.0-(1.0/(PI*Q2Z))*(EC+Z(I)))**(-1)
140          QP(I)=Q1Z-((1.0/PI)*(EC+Z(I)))
141          QS(I)=Q2Z-((1.0/PI)*(EC+Z(I)))
142      510 CONTINUE
143  C       INTRODUCE ATTENUATION AND DISPERSION ALONG THE PATH
144  C       THE EFFECT OF INTERFACE IS ALSO CONSIDERED
145          IF(KK.LT.0) GO TO 331
146          IF(KL.LT.0) GO TO 332
147          AM(1)=AAM(1)
148          PH(1)=PPH(1)
149          DO 511 I=2,ND2
150          D1=F(I)*RO*((1.0/V1)-(1.0/VP1(I)))
151          PH(I)=PPH(I)+D1
152          AL=F(I)/(2.0*QP(I)*VP1(I))
153          EK=-AL*RO
154      511 AM(I)=AAM(I)*EXP(EK)
155          GO TO 900
156      332 AM(1)=AAM(1)
157          PH(1)=PPH(1)
158          DO 512 I=2,ND2
159          D1=F(I)*RO*((1.0/V2)-(1.0/VS1(I)))
160          PH(I)=PPH(I)+D1
161          AL=F(I)/(2.0*QS(I)*VS1(I))
162          EK=-AL*RO
163      512 AM(I)=AAM(I)*EXP(EK)
164          GO TO 900
165      331 IF(KM.EQ.0) GO TO 333
166          IF(KM.LT.0) GO TO 334
167          CALL PEL(AN,INDEXP,AME,PHE)
168          AM(1)=AAM(1)
169          PH(1)=PPH(1)
170          DO 513 I=2,ND2
171          D1=F(I)*RO*((1.0/V1)-(1.0/VP1(I)))
172          IM=I
173          CALL PVEL(IM,AN,INDEXP,AMV,PHV)
174          PH(I)=PPH(I)+D1+PHV
175          AL=F(I)/(2.0*QP(I)*VP1(I))
176          EK=-AL*RO
177      513 AM(I)=AAM(I)*EXP(EK)*AMV/AME
178          GO TO 900
179      334 AM(1)=AAM(1)
180          PH(1)=PPH(1)
```

```
181            CALL PEL(AN,INDEXP,AME,PHE)
182            DO 514 I=2,ND2
183            D1=F(I)*RO1*((1.0/V1)-(1.0/VP1(I)))
184            D2=F(I)*RO2*((1.0/V2)-(1.0/VS1(I)))
185            IM=I
186            CALL PVEL(IM,AN,INDEXP,AMV,PHV)
187            PH(I)=PPH(I)+D1+D2+PHV
188            AL1=F(I)/(2.0*QP(I)*VP1(I))
189            EK1=-AL1*RO1
190            AL2=F(I)/(2.0*QS(I)*VS1(I))
191            EK2=-AL2*RO2
192            EK=EK1+EK2
193      514  AM(I)=AAM(I)*EXP(EK)*AMV/AME
194            GO TO 900
195      333  IF(KN.LT.0) GO TO 335
196            AM(1)=AAM(1)
197            PH(1)=PPH(1)
198            CALL SEL(AN,INDEXS,AME,PHE)
199            DO 515 I=2,ND2
200            D1=F(I)*RO*((1.0/V2)-(1.0/VS1(I)))
201            IM=I
202            CALL SVEL(IM,AN,INDEXS,AMV,PHV)
203            PH(I)=PPH(I)+D1+PHV
204            AL=F(I)/(2.0*QS(I)*VS1(I))
205            EK=-AL*RO
206      515  AM(I)=AAM(I)*EXP(EK)*AMV/AME
207            GO TO 900
208      335  AM(1)=AAM(1)
209            PH(1)=PPH(1)
210            CALL SEL(AN,INDEXS,AME,PHE)
211            DO 516 I=2,ND2
212            D1=F(I)*RO1*((1.0/V2)-(1.0/VS1(I)))
213            D2=F(I)*RO2*((1.0/V1)-(1.0/VP1(I)))
214            IM=I
215            CALL SVEL(IM,AN,INDEXS,AMV,PHV)
216            PH(I)=PPH(I)+D1+D2+PHV
217            AL1=F(I)/(2.0*QS(I)*VS1(I))
218            EK1=-AL1*RO1
219            AL2=F(I)/(2.0*QP(I)*VP1(I))
220            EK2=-AL2*RO2
221            EK=EK1+EK2
222      516  AM(I)=AAM(I)*EXP(EK)*AMV/AME
223      900  CONTINUE
224     C      INVERSE FOURIER TRANSFORM
225            DO 681 I=1,ND2
226            XR(I)=AM(I)*COS(PH(I))
227            XI(I)=AM(I)*SIN(PH(I))
228      681  CONTINUE
229            DO 682 I=2,N2
230            XR(ND2+I-1)=XR(ND2-I+1)
231            XI(ND2+I-1)=-XI(ND2-I+1)
232      682  CONTINUE
233            DO 683 I=1,N
234            XI(I)=-XI(I)
235      683  CONTINUE
236            XR(ND2)=0.0
237            XI(ND2)=0.0
238            CALL FASTF(XR,XI,N)
239            DO 684 I=1,120
240            XR(I)=XR(I)/(FLOAT(N))
```

```
241        684 CONTINUE
242            WRITE(19,298)(XR(I),I=1,100)
243        298 FORMAT(40X,D20.9)
244            STOP
245            END
246            SUBROUTINE FASTF(FR,FI,N)
247     C
248     C      N IS THE NUMBER OF DATA POINTS = 2**M
249     C      FR IS THE REAL DATA SET
250     C      FI IS THE IMAGINARY PART OF THE DATA SET (= 0.0 IF ONLY REAL)
251     C      FIRST COMPUTE M
252     C
253            REAL FR(N), FI(N), GR, GI, ER, EI,EU, EZ
254            M=0
255            KD=N
256          1 KD=KD/2
257            M=M+1
258            IF(KD .GE. 2) GO TO 1
259            ND2 = N/2
260            NM1=N-1
261            L=1
262     C
263     C      SHUFFLE INPUT DATA IN BINARY DIGIT REVERSE ORDER
264     C
265            DO 4 K=1,NM1
266            IF(K .GE. L) GO TO 2
267            GR=FR(L)
268            GI=FI(L)
269            FR(L)=FR(K)
270            FI(L)=FI(K)
271            FR(K)=GR
272            FI(K)=GI
273          2 NND2=ND2
274          3 IF(NND2 .GE. L) GO TO 4
275            L=L-NND2
276            NND2=NND2/2
277            GO TO 3
278          4 L=L+NND2
279            PI=3.14159265
280     C
281     C      FIRST ARRANGE ACCOUNTING OF M STAGE
282     C
283            DO 6 J=1,M
284            NJ=2**J
285            NJD2=NJ/2
286            EU=1.0
287            EZ=0.0
288            ER=COS(-PI/NJD2)
289            EI=SIN(-PI/NJD2)
290     C
291     C      COMPUTE FOURIER TRANSFORM IN EACH M STAGE
292     C
293            DO 6 IT=1,NJD2
294            DO 5 IW=IT,N,NJ
295            IWJ=IW+NJD2
296            GR=FR(IWJ)*EU-FI(IWJ)*EZ
297            GI=FI(IWJ)*EU+FR(IWJ)*EZ
298            FR(IWJ)=FR(IW)-GR
299            FI(IWJ)=FI(IW)-GI
300            FR(IW)=FR(IW)+GR
```

```
301        5 FI(IW)=FI(IW)+GI
302          SEU=EU
303          EU=SEU*ER-EZ*EI
304        6 EZ=EZ*ER+SEU*EI
305          RETURN
306          END
307          SUBROUTINE PEL(D,INDEXP,AM,PH)
308          REAL WA(4)
309          COMPLEX HS,A(4,4),B(4,1),CABS,CSQRT
310          COMMON /AREA1/V1,V2,V3,V4,R1,R2
311          HS=SIN(D)/V1
312          A(1,1)=-V1*HS
313          A(1,2)=-CSQRT(1.0-((HS*V2)**2))
314          A(1,3)=V3*HS
315          A(1,4)=CSQRT(1.0-((HS*V4)**2))
316          A(2,1)=CSQRT(1.0-((HS*V1)**2))
317          A(2,2)=-V2*HS
318          A(2,3)=CSQRT(1.0-((HS*V3)**2))
319          A(2,4)=-V4*HS
320          A(3,1)=2.0*R1*V2*V2*HS*A(2,1)
321          A(3,2)=R1*V2*(1.0-2.0*V2*V2*HS*HS)
322          A(3,3)=2.0*R2*V4*V4*HS*A(2,3)
323          A(3,4)=R2*V4*(1.0-2.0*V4*V4*HS*HS)
324          A(4,1)=-R1*V1*(1.0-2.0*V2*V2*HS*HS)
325          A(4,2)=2.0*R1*V2*V2*HS*(-A(1,2))
326          A(4,3)=R2*V3*(1.0-2.0*V4*V4*HS*HS)
327          A(4,4)=-2.0*R2*V4*V4*HS*A(1,4)
328          B(1,1)=-A(1,1)
329          B(2,1)=A(2,1)
330          B(3,1)=A(3,1)
331          B(4,1)=-A(4,1)
332          CALL LEQT1C(A,4,4,B,1,4,0,WA,IER)
333          AM=CABS(B(INDEXP,1))
334          CALL PHAMP(B(INDEXP,1),AM,PH)
335          RETURN
336          END
337          SUBROUTINE PHAMP(POM,AMP,PHASE)
338          COMPLEX POM,CABS
339          AMP=CABS(POM)
340          REZ=REAL(POM)
341          AMZ=-AIMAG(POM)
342          IF (AMP.EQ.0) GO TO 27
343          IF (REZ.EQ.0) GO TO 28
344          IF (AMZ.EQ.0) GO TO 29
345          AR=ATAN2(AMZ,REZ)
346          IF (AR.LT.0) GO TO 30
347          PHASE=AR
348       31 RETURN
349       30 PHASE=AR+2*3.141593
350          GO TO 31
351       27 PHASE=0
352          GO TO 31
353       28 IF (AMZ.GT.0) GO TO 32
354          PHASE=3.141593*1.5
355          GO TO 31
356       32 PHASE=3.141593*0.5
357       29 IF (REZ.GT.0) GO TO 27
358          PHASE=3.141593
359          GO TO 31
360          END
```

```
361          SUBROUTINE PVEL(NW,D,INDEXP,AM,PH)
362          REAL WA(4),VP1(1024),VP2(1024),VS1(1024),VS2(1024)
363          REAL QP(1024),QS(1024)
364          REAL M1R,M1I,M2R,M2I,M3R,M3I,M4R,M4I
365          COMPLEX HS,A(4,4),B(4,1),CABS,CSQRT,CMPLX
366          COMPLEX M1,M2,M3,M4,VV1,VV2,VV3,VV4
367          COMMON /AREA2/VP1,VP2,VS1,VS2,QP,QS,RS1,RS2,GAM
368          PI=3.141593
369          GA=PI*GAM/180.0
370          S1=2.0*(1.0+(1.0/(QP(NW)**2)))
371          S2=1.0+(1.0+(1.0/(QP(NW)**2)))**0.5
372          M1R=(VP1(NW)**2)*RS1*S2/S1
373          M1I=M1R/QP(NW)
374          M1=CMPLX(M1R,M1I)
375          VV1=CSQRT(M1/RS1)
376          T1=2.0*(1.0+(1.0/(QS(NW)**2)))
377          T2=1.0+(1.0+(1.0/(QS(NW)**2)))**0.5
378          M2R=(VS1(NW)**2)*RS1*T2/T1
379          M2I=M2R/QS(NW)
380          M2=CMPLX(M2R,M2I)
381          VV2=CSQRT(M2/RS1)
382          TT1=2.0*(1.0+(1.0/(QP(NW)**2)))
383          TT2=1.0+(1.0+(1.0/(QP(NW)**2)))**0.5
384          M3R=(VP2(NW)**2)*RS2*TT2/TT1
385          M3I=M3R/QP(NW)
386          M3=CMPLX(M3R,M3I)
387          VV3=CSQRT(M3/RS2)
388          SS1=2.0*(1.0+(1.0/(QS(NW)**2)))
389          SS2=1.0+(1.0+(1.0/(QS(NW)**2)))**0.5
390          M4R=(VS2(NW)**2)*RS2*SS2/SS1
391          M4I=M4R/QS(NW)
392          M4=CMPLX(M4R,M4I)
393          VV4=CSQRT(M4/RS2)
394          X1=1.0+(1.0/(QP(NW)*COS(GA)))**2
395          X11=SQRT(X1)
396          X2=1.0+(1.0/(QP(NW)))**2
397          X22=SQRT(X2)
398          XN=1.0+X11
399          XD=1.0+X22
400          XZ=XN/XD
401          XV=SQRT(XZ)
402          PP1=XV/VP1(NW)
403          XNN=X11-1.0
404          XZZ=XNN/XD
405          XVV=SQRT(XZZ)
406          AA1=XVV/VP1(NW)
407          DD1=D-GA
408          HSR=SIN(D)*PP1
409          HSI=-SIN(DD1)*AA1
410          HS=CMPLX(HSR,HSI)
411          A(1,1)=-VV1*HS
412          A(1,2)=-CSQRT(1.0-((HS*VV2)**2))
413          A(1,3)=VV3*HS
414          A(1,4)=CSQRT(1.0-((HS*VV4)**2))
415          A(2,1)=CSQRT(1.0-((HS*VV1)**2))
416          A(2,2)=-VV2*HS
417          A(2,3)=CSQRT(1.0-((HS*VV3)**2))
418          A(2,4)=-VV4*HS
419          A(3,1)=2.0*RS1*VV2*VV2*HS*A(2,1)
420          A(3,2)=RS1*VV2*(1.0-2.0*VV2*VV2*HS*HS)
```

```
421      A(3,3)=2.0*RS2*VV4*VV4*HS*A(2,3)
422      A(3,4)=RS2*VV4*(1.0-2.0*VV4*VV4*HS*HS)
423      A(4,1)=-RS1*VV1*(1.0-2.0*VV2*VV2*HS*HS)
424      A(4,2)=2.0*RS1*VV2*VV2*HS*(-A(1,2))
425      A(4,3)=RS2*VV3*(1.0-2.0*VV4*VV4*HS*HS)
426      A(4,4)=-2.0*RS2*VV4*VV4*HS*A(1,4)
427      B(1,1)=-A(1,1)
428      B(2,1)=A(2,1)
429      B(3,1)=A(3,1)
430      B(4,1)=-A(4,1)
431      CALL LEQT1C(A,4,4,B,1,4,0,WA,IER)
432      AM=CABS(B(INDEXP,1))
433      CALL PHAMP(B(INDEXP,1),AM,PH)
434      RETURN
435      END
436      SUBROUTINE SEL(D,INDEXS,AM,PH)
437      REAL WA(4)
438      COMPLEX HS,A(4,4),B(4,1),CABS,CSQRT
439      COMMON /AREA1/V1,V2,V3,V4,R1,R2
440      HS=SIN(D)/V1
441      A(1,1)=-V1*HS
442      A(1,2)=-CSQRT(1.0-((HS*V2)**2))
443      A(1,3)=V3*HS
444      A(1,4)=CSQRT(1.0-((HS*V4)**2))
445      A(2,1)=CSQRT(1.0-((HS*V1)**2))
446      A(2,2)=-V2*HS
447      A(2,3)=CSQRT(1.0-((HS*V3)**2))
448      A(2,4)=-V4*HS
449      A(3,1)=2.0*R1*V2*V2*HS*A(2,1)
450      A(3,2)=R1*V2*(1.0-2.0*V2*V2*HS*HS)
451      A(3,3)=2.0*R2*V4*V4*HS*A(2,3)
452      A(3,4)=R2*V4*(1.0-2.0*V4*V4*HS*HS)
453      A(4,1)=-R1*V1*(1.0-2.0*V2*V2*HS*HS)
454      A(4,2)=2.0*R1*V2*V2*HS*(-A(1,2))
455      A(4,3)=R2*V3*(1.0-2.0*V4*V4*HS*HS)
456      A(4,4)=-2.0*R2*V4*V4*HS*A(1,4)
457      B(1,1)=-A(1,2)
458      B(2,1)=A(2,2)
459      B(3,1)=A(3,2)
460      B(4,1)=-A(4,2)
461      CALL LEQT1C(A,4,4,B,1,4,0,WA,IER)
462      AM=CABS(B(INDEXS,1))
463      CALL PHAMP(B(INDEXS,1),AM,PH)
464      RETURN
465      END
466      SUBROUTINE SVEL(NW,D,INDEXS,AM,PH)
467      REAL WA(4),VP1(1024),VP2(1024),VS1(1024),VS2(1024)
468      REAL QP(1024),QS(1024)
469      REAL M1R,M1I,M2R,M2I,M3R,M3I,M4R,M4I
470      COMPLEX HS,A(4,4),B(4,1),CABS,CSQRT,CMPLX
471      COMPLEX M1,M2,M3,M4,VV1,VV2,VV3,VV4
472      COMMON /AREA2/VP1,VP2,VS1,VS2,QP,QS,RS1,RS2,GAM
473      PI=3.141593
474      GA=PI*GAM/180.0
475      S1=2.0*(1.0+(1.0/(QP(NW)**2)))
476      S2=1.0+(1.0+(1.0/(QP(NW)**2)))**0.5
477      M1R=(VP1(NW)**2)*RS1*S2/S1
478      M1I=M1R/QP(NW)
479      M1=CMPLX(M1R,M1I)
480      VV1=CSQRT(M1/RS1)
```

```
481      T1=2.0*(1.0+(1.0/(QS(NW)**2)))
482      T2=1.0+(1.0+(1.0/(QS(NW)**2)))**0.5
483      M2R=(VS1(NW)**2)*RS1*T2/T1
484      M2I=M2R/QS(NW)
485      M2=CMPLX(M2R,M2I)
486      VV2=CSQRT(M2/RS1)
487      TT1=2.0*(1.0+(1.0/(QP(NW)**2)))
488      TT2=1.0+(1.0+(1.0/(QP(NW)**2)))**0.5
489      M3R=(VP2(NW)**2)*RS2*TT2/TT1
490      M3I=M3R/QP(NW)
491      M3=CMPLX(M3R,M3I)
492      VV3=CSQRT(M3/RS2)
493      SS1=2.0*(1.0+(1.0/(QS(NW)**2)))
494      SS2=1.0+(1.0+(1.0/(QS(NW)**2)))**0.5
495      M4R=(VS2(NW)**2)*RS2*SS2/SS1
496      M4I=M4R/QS(NW)
497      M4=CMPLX(M4R,M4I)
498      VV4=CSQRT(M4/RS2)
499      X1=1.0+(1.0/(QP(NW)*COS(GA)))**2
500      X11=SQRT(X1)
501      X2=1.0+(1.0/(QP(NW)))**2
502      X22=SQRT(X2)
503      XN=1.0+X11
504      XD=1.0+X22
505      XZ=XN/XD
506      XV=SQRT(XZ)
507      PP1=XV/VP1(NW)
508      XNN=X11-1.0
509      XZZ=XNN/XD
510      XVV=SQRT(XZZ)
511      AA1=XVV/VP1(NW)
512      DD1=D-GA
513      HSR=SIN(D)*PP1
514      HSI=-SIN(DD1)*AA1
515      HS=CMPLX(HSR,HSI)
516      A(1,1)=-VV1*HS
517      A(1,2)=-CSQRT(1.0-((HS*VV2)**2))
518      A(1,3)=VV3*HS
519      A(1,4)=CSQRT(1.0-((HS*VV4)**2))
520      A(2,1)=CSQRT(1.0-((HS*VV1)**2))
521      A(2,2)=-VV2*HS
522      A(2,3)=CSQRT(1.0-((HS*VV3)**2))
523      A(2,4)=-VV4*HS
524      A(3,1)=2.0*RS1*VV2*VV2*HS*A(2,1)
525      A(3,2)=RS1*VV2*(1.0-2.0*VV2*VV2*HS*HS)
526      A(3,3)=2.0*RS2*VV4*VV4*HS*A(2,3)
527      A(3,4)=RS2*VV4*(1.0-2.0*VV4*VV4*HS*HS)
528      A(4,1)=-RS1*VV1*(1.0-2.0*VV2*VV2*HS*HS)
529      A(4,2)=2.0*RS1*VV2*VV2*HS*(-A(1,2))
530      A(4,3)=RS2*VV3*(1.0-2.0*VV4*VV4*HS*HS)
531      A(4,4)=-2.0*RS2*VV4*VV4*HS*A(1,4)
532      B(1,1)=-A(1,2)
533      B(2,1)=A(2,2)
534      B(3,1)=A(3,2)
535      B(4,1)=-A(4,2)
536      CALL LEQT1C(A,4,4,B,1,4,0,WA,IER)
537      AM=CABS(B(INDEXS,1))
538      CALL PHAMP(B(INDEXS,1),AM,PH)
539      RETURN
540      END
```

```
 1     C     PHASE UNWRAPPING PROGRAM
 2     C     THIS PROGRAM IS A MODIFIED VERSION OF
 3     C     TRIBOLET'S ORIGINAL PROGRAM
 4     C     REFERENCE: TRIBOLET, J.M.(1977).
 5     C     A NEW PHASE UNWRAPPING ALGORITHM.
 6     C     IEEE VOL. ASPP-25, NO 2 P. 170-177
 7     C     X=THE INPUT SIGNAL
 8     C      INITIALIZATION
 9     C
10           L=2**12
11           M=9
12           N=2**M
13           N2=N/2
14           ND2=N2+1
15           PI=3.141596
16           TWOPI=PI*2.O
17     C         PARAMETERS FOR UNWRAPPED PHASE
18     C
19           H=TWOPI/1024
20           H1=H/L
21           THLD1=1.8*PI
22           THLD2=1.0*PI
23           ISNX=+1
24     C
25     C      TRANSFORM X(N)
26     C
27     C      LOAD CXE AND CXO ARRAYS.
28     C
29           DO 7 I=1,N
30         7 CXE(I)=X(I)
31           DO 8 I=1,N
32         8 CXO(I)=0.0
33           CALL FASTF(CXE,CXO,N)
34     C
35     C
36     C         TRANSFORM N*X(N)
37     C
38     C         LOAD YR AND YI ARRAYS
39     C
40           DO 19 I=1,N
41        19 YR(I)=I*X(I)
42           DO 20 I=1,N
43        20 YI(I)=0.0
44           CALL FASTF(YR,YI,N)
45     C
46     C   CHECK IF SIGN REVERSAL IS REQUIRED
47     C
48           IF(CXE(1).LT.O) ISNX=-1
49     C
50     C    COMPUTE LOGMAGNITUDE:STORE IN CXE
51     C    COMPUTE PHASE DERIVATIVE:STORE IN YR
52     C    COMPUTE PHASE PRINCIPAL VALUE;STORE IN YI
53     C         FOR W=(TWOPI/N)*I,I=0,1,...N2
54     C
55           DVTMN=0.
56           DO 21 I=1,ND2
57           A=CXE(I)
58           B=CXO(I)
59           C=YR(I)
60           D =YI(I)
```

```
61 -        E=A*A+B*B
62          YR(I)=-((A*C+B*D)/E)
63          DVTMN=DVTMN+YR(I)
64   C
65          CXE(I)=DLOG(E)/2
66          IF(ISNX.EQ.+1)YI(I)=DATAN2(B,A)
67      *   IF(ISNX.EQ.-1)YI(I)=DATAN2(-B,-A)
68    21 CONTINUE
69          DVTMN=(2*DVTMN-YR(1)-YR(ND2))/N
70          ELPINC=2*DVTMN*H
71   C
72   C          PHASE UNWRAPPING BY ADAPTIVE INTEGRATION
73   C
74   .       PH=O.
75          DO 22 I=2,ND2
76   C
77   C          STORE UNWRAPPED PHASE IN CXO
78   C
79          CXO(I-1)=PH
80   C
81   C
82   C              FORM PHASE ESTIMATE AT W=(TWOPI/N)*(I-1) BY
83   C              TRAPEZOIDAL INTEGRATION WITH STEP SIZE TWOPI/N
84   C
85   C
86          PHAINC=H*(YR(I)+YR(I-1))
87          IF(ABS(PHAINC-ELPINC).GT.THLD1) GO TO 23
88          PH=CXO(I-1)+PHAINC
89   C
90   C          CHECK CONSISTENCY OF ESTIMATE
91   C
92          AO=(PH-YI(I))/TWOPI
93          A1=IFIX(AO)*TWOPI+YI(I)
94          A2=A1+SIGN(TWOPI,AO)
95          A3=ABS(A1-PH)
96    .     A4=ABS(A2-PH)
97          IF(A3.GT.THLD2.AND.A4.GT.THLD2) GO TO 23
98   C
99   C              PHASE ESTIMATE WAS CONSISTENT
100  C
101         PH=A1
102         IF(A3.GT.A4)PH=A2
103         IF(ABS(PH-CXO(I-1)).GT.PI) GO TO 23
104         GO TO 22
105  C
106  C              PHASE ESTIMATE WAS NOT CONSISTENT:
107  C                    ADAPT STEP SIZE
108  C
109  C              INITIATE SOFTWARE STACK
110  C
111    23 SP=1
112         ISK(1)=N+1
113         SK1(1)=YI(I)
114         SK2(1)=YR(I)
115  C
116  C              INITIATE REGISTERS
117  C
118         IB=1
119         B1=CXO(I-1)
120  C
```

```
121          B2=YR(I-1)
122    C
123    C                    IF SOFTWARE STACK DIMENSION DOES NOT
124    C                       ALLOW FURTHER STEP REDUCTION,STOP
125    C
126    24 IF((ISK(SP)-IB).GT.1) GO TO 25
127       STOP 999
128    C
129    C            DEFINE INTERMEDIATE FREQUENCIES (I.F)
130    C                    W=(TWOPI/N)*(I-2+(K-1)/N)
131    C
132    25 K=(ISK(SP)+IB)/2
133    C
134    C            COMPUTE DFTS OF X(N) AND N*X(N) AT I.F.
135    C
136       AO=TWOPI*(I-2.+(K-1)/FLOAT(L))/FLOAT(N)
137       C1=(0.,0.)
138       C2=(0.,0.)
139       DO 26 J=1,N
140       ARG=AO*(J-1)
141       CO=CMPLX(COS(ARG),-SIN(ARG))*X(J)
142       C1=C1+CO
143    26 C2=C2+CO*(J-1)
144    C
145    C    COMPUTE PHASE DERIVATIVE AND THE
146    C        PRINCIPAL VALUE OF THE PHASE AT I.F.
147    C
148       SP=SP+1
149       ISK(SP)=K
150       A=REAL(C1)
151       B=AIMAG(C1)
152       C=REAL(C2)
153       D=AIMAG(C2)
154       IF(ISNX.EQ.+1) SK1(SP)=DATAN2(B,A)
155       IF(ISNX.EQ.-1) SK1(SP)=DATAN2(-B,-A)
156       SK2(SP)=-(A*C+B*D)/(A*A+B*B)
157    C
158    C            EVALUATE ESTIMATE AT I.F.
159    C
160    27 DELTA=H*(ISK(SP)-IB)
161       PHAINC=DELTA*(B2+SK2(SP))
162       IF(ABS(PHAINC-DELTA*2*DVTMN).GT.THLD1) GO TO 24
163       PH=B1+PHAINC
164    C
165    C            CHECK CONSISTENCY OF ESTIMATE AT I.F.
166    C
167       AO=(PH-SK1(SP))/TWOPI
168       A1=IFIX(AO)*TWOPI+SK1(SP)
169       A2=A1+SIGN(TWOPI,AO)
170       A3=ABS(A1-PH)
171       A4=ABS(A2-PH)
172       IF(A3.LT.THLD2.OR.A4.LT.THLD2) GO TO 28
173    C
174    C      ESTIMATE WAS NOT CONSISTENT:REDUCE STEP SIZE
175    C
176       GO TO 24
177    C
178    C         ESTIMATE WAS CONSISTENT: UPDATE REGISTERS
179    C
180    28 PH=A1
```

```
181          IF(A3.GT.A4)PH=A2
182          IF(ABS(PH-B1).GT.PI) GO TO 24
183          IB=ISK(SP)
184          B1=PH
185          B2=SK2(SP)
186          SP=SP-1
187    C
188    C        WHEN SOFTWARE STACK IS EMPTY ,THE UNWRAPPED
189    C        PHASE AT W=TWOPI*(I-1)/N IS HELD IN THE
190    C            B1 REGISTER
191    C
192          IF(SP.NE.0) GO TO 27
193          PH=B1
194    C
195    C        END OF STEP SIZE ADAPTATION
196    C
197      22 CONTINUE
198          IF(ISNX.EQ.-1)GO TO 191
199          GO TO 192
200     191 CONTINUE
201          DO 193 I=1,N2
202     193 CXO(I)=CXO(I)-PI
203     192 CONTINUE
204          STOP
205          END
```